

Engineering Liposomes Using Microfluidic Devices to Model Cancer-Derived Extracellular Vesicles (EV)

by

Chaymaa ZOUGGARI BEN EL KHYAT

THESIS PRESENTED TO ÉCOLE DE TECHNOLOGIE SUPÉRIEURE IN
PARTIAL FULFILLEMENT FOR A MASTER'S DEGREE WITH THESIS
IN ENGINEERING IN HEALTHCARE TECHNOLOGY
M.A.Sc

MONTREAL, AUGUST 17, 2022

ÉCOLE DE TECHNOLOGIE SUPÉRIEURE
UNIVERSITÉ DU QUÉBEC

© Copyright 2022 reserved by Chaymaa Zouggari Ben El Khyat

© Copyright reserved

It is forbidden to reproduce, save or share the content of this document either in whole or in parts. The reader who wishes to print or save this document on any media must first get the permission of the author.

BOARD OF EXAMINERS

THIS THESIS HAS BEEN EVALUATED

BY THE FOLLOWING BOARD OF EXAMINERS

Mr. Vahé Nerguizian, Thesis Supervisor
Department of Electrical Engineering at École de technologie supérieure

Mrs. Julia Valdemarin Burnier, PhD, Thesis Co-supervisor
Department of Pathology at McGill University

Mrs. Lyne Woodward, President of the Board of Examiners
Department of Electrical Engineering at École de technologie supérieure

Mrs. Sophie Lerouge, Member of the jury
Department of Mechanical Engineering at École de technologie supérieure

THIS THESIS WAS PRESENTED AND DEFENDED

IN THE PRESENCE OF A BOARD OF EXAMINERS AND PUBLIC

MONTREAL, AUGUST 8, 2022

AT ÉCOLE DE TECHNOLOGIE SUPÉRIEURE

ACKNOWLEDGMENT

I would like to express my gratitude to Rubén Rodrigo López Salazar, whose leadership (and patience) guided me through this project, to Vahé Nerguizian, whose words of encouragements never faltered, and to Julia Valdemarin Burnier, who was always there for us.

Thank you to my lab mates: Tadhg, Yunxi, Alexandra, Thupten, Prisca, Fatemeh and Amélie.

Thank you to my family and friends, who never stopped supporting me, even from thousands of miles away.

Thank you to the Proteomics and Immunophenotyping platforms, especially Ed and Marie-Hélène.

Thank you to the New Frontiers in Research Fund, who have made this project possible.

Développement de liposomes qui imitent les vésicules extracellulaires dérivées de cellules cancéreuses en utilisant un dispositif microfluidique

Chaymaa ZOUGGARI BEN EL KHYAT

RÉSUMÉ

Les liposomes sont des nanoparticules synthétiques polyvalentes qui peuvent transporter une variété de cargos: du matériel génétique tel que l'ARN, comme les plus récents vaccins Covid-19, ainsi que des protéines et autres molécules d'intérêt. Ce système d'administration a été inspiré par les vésicules extracellulaires (VE) naturelles, qui proviennent de tous types de cellules, y compris les cellules cancéreuses. Il a été démontré que les VE contribuent au processus de métastase en transportant des facteurs pro-tumoraux vers différents organes, préparant ainsi le terrain pour la croissance du cancer. Cependant, l'étude et l'utilisation des VE à d'autres fins est une tâche compliquée en raison de leur faible rendement lorsqu'on les isole des cellules. L'objectif est donc de fournir un protocole fiable pour produire des liposomes synthétiques qui imiteront les paramètres physicochimiques des VE cancéreuses, en particulier leur moyenne Z (diamètre) et leur potentiel Zeta (charge de surface).

Les liposomes ont été produits à l'aide d'un dispositif microfluidique développé par Lopez (López et al., 2020). Cette puce utilisait la dynamique d'écoulement de Dean pour contrôler le processus de mélange des lipides et fabriquer des liposomes dans des conditions rigoureusement contrôlées. Afin de mieux comprendre comment les liposomes sont formés, une approche par plan d'expérience (DoE) a été utilisée. Sur la base d'un plan composite central rotatif, l'espace expérimental impliquant les différents facteurs qui affectent le potentiel Zeta et la moyenne Z des liposomes a été exploré. Une série de modèles couvrant un large spectre de taille et de potentiel Zeta ont été obtenus en utilisant la méthodologie de surface de réponse. Cette approche statistique nous a permis de fabriquer avec succès des liposomes de la taille et du potentiel Zeta ciblés qui imitent les VE à l'étude. Enfin, une série d'expériences a été réalisée pour étudier le comportement des hépatocytes (cellules du foie) et des fibroblastes (tissu conjonctif) lorsqu'ils sont exposés à des liposomes mimant les VE cancéreux.

L'approche de microfabrication des liposomes présentés dans ce travail a le potentiel d'être développée davantage en les utilisant comme moyen de transport en créant un système de livraison sur mesure, permettant d'étudier davantage la communication intercellulaire et le processus de métastase.

Mots-clés : liposomes, vésicules extracellulaires, micromélangeur, plan d'expérience

Engineering Liposomes Using Microfluidic Devices to Model Cancer-Derived Extracellular Vesicles (EV)

Chaymaa ZOUGGARI BEN EL KHYAT

ABSTRACT

Liposomes are synthetic multivalent nanoparticles that can transport a variety of cargos, from genetic material such as RNA, like the most recent Covid-19 vaccines, to proteins and other molecules of interest. This delivery system was inspired by the naturally occurring extracellular vesicles (EVs), which are derived from all types of cells, including cancer cells. It has been shown that EVs contribute to the process of metastasis by transporting pro-tumor factors to different organs, setting the stage for cancer growth. However, studying EVs is a complicated task due to their poor yield when isolating them from cells. The objective is therefore to provide a reliable protocol to produce synthetic liposomes that will mimic the physicochemical parameters of cancerous EVs, particularly their Z-average (diameter) and Zeta Potential (surface charge).

Liposomes were produced using a microfluidic device developed by Lopez (López et al., 2020). This chip uses Dean Flow Dynamics to control the mixing process of lipids and fabricate liposomes under rigorously controlled conditions. In order to further understand how liposomes are formed, a design of experiment (DoE) approach was used. Based on a Rotatable Central Composite Design, the experimental space involving the different factors that affect the Zeta Potential and Z-average of liposomes were explored. A series of models spanning a broad spectrum of size and Zeta Potential were obtained using Response Surface Methodology. This statistical approach has allowed us to successfully fabricate liposomes of the targeted size and Zeta Potential that mimic the naturally occurring cancer EVs that were previously characterized. Finally, a series of experiments were carried out to study the behavior of hepatocytes (liver cells) and fibroblasts (connective tissue) when exposed to liposomes mimicking the cancerous EVs.

The liposome synthesis approach presented in this work has the potential to be further developed by loading the liposomes and creating a tailored delivery system, allowing to further study cell-to-cell communication and metastasis and act as an optimized delivery system.

Keywords: liposomes, extracellular vesicles, micromixer, design of experiment

TABLE OF CONTENTS

	Page
INTRODUCTION	1
CHAPTER 1 LITTERATURE REVIEW	3
1.1 Introduction	3
1.2 Fabrication methods of liposomes: from thin film hydration to micromixing	3
1.2.1 Thin film hydration.....	4
1.2.2 Injection method	5
1.2.3 Micromixing	5
1.3 Formulation of liposomes	7
1.4 Liposomes as a delivery system	9
1.5 Conclusion	11
CHAPTER 2 MATERIALS AND METHODS	13
2.1 Liposome production	13
2.1.1 Micromixing setup.....	13
2.1.2 Lipids preparation.....	16
2.1.3 Micromixer	19
2.2 Liposome characterization.....	20
2.2.1 Z-average and polydispersity index (PDI).....	21
2.2.2 Zeta Potential	23
2.2.3 Concentration of particles.....	25
2.3 Statistical tests and approach	26
2.3.1 Design of Experiment (DoE).....	26
2.3.2 <i>P</i> -value.....	27
2.3.3 Analysis of variance	28
2.4 Cell culture	28
2.5 Extracellular Vesicle's isolation	29
2.6 Uptake experiments	30
2.6.1 Confocal Microscopy	30
2.6.2 Flow cytometry.....	31
2.7 Conclusion	32
CHAPTER 3 FABRICATION OF ANIONIC LIPOSOMES: RESULTS AND DISCUSSION.....	33
3.1 Effect of DHP% on liposome's Zeta Potential (surface charge)	34
3.2 Two-factor Response Surface Methodology	36
3.3 Three-factor Response Surface Methodology	41
3.4 Three-factor Vs Two-factor anionic model	48
3.5 Effect of PBS on liposomes' Z-average and Zeta Potential	49
3.6 Dialyzed three-factor Central Composite Design.....	51
3.7 Conclusion	56

CHAPTER 4	FABRICATION OF CATIONIC LIPOSOMES: RESULTS AND DISCUSSION.....	57
4.1	Effect of DOTAP% on liposome's Zeta Potential.....	58
4.2	Cationic three-factor response surface model.....	60
4.3	Three-factor model dialyzed.....	64
4.4	Conclusion	70
CHAPTER 5	CELLULAR UPTAKE OF LIPOSOMES: RESULTS AND DISCUSSION.....	71
5.1	Cellular uptake mechanisms	71
5.2	Confocal microscopy	72
	5.2.1 EV-mimicking liposomes	74
	5.2.2 Liposomes of different Zeta Potentials.....	75
5.3	Flow cytometry	77
	5.3.1 EV-mimicking liposomes	80
5.4	Conclusion	85
CONCLUSION.....		87
ANNEX A	Z-AVERAGE OF ANIONIC AND CATIONIC LIPOSOMES.....	87
LIST OF BIBLIOGRAPHICAL REFERENCES.....		93

LIST OF TABLES

	Page
Table 1.1	Information on the three mRNA vaccines against COVID-19 and Onpattro Adapted from Schoenmaker et al. (2021).....8
Table 2.1	Lipids used and their formulation. Retrieved from Millipore Sigma17
Table 3.1	Objectives, Strategies and Factors at play of anionic liposomes' production33
Table 3.2	CCCR design results for the 29 runs. The factors are FRR and TFR (with coded values in parenthesis), the responses are Z-average, PDI and Zeta Potential38
Table 3.3	R-squared values for the model. R-squared adjusted accounts for the runs of the experiment, while R-square predicted determines how well the model will predict the Z-average in the future.....39
Table 3.4	P-value and F-value for the Z-average and the respective independent variables39
Table 3.5	Cubic and axial values of the three factors at study.....41
Table 3.6	CCCR design results for the 47 runs. The factors are FRR, TFR and DHP% (with coded values in parenthesis), the responses are Z-average, PDI and Zeta Potential.....42
Table 3.7	R-squared, R-squared adjusted and predicted for the 3-factor response surface model44
Table 3.8	P-value and F-value for all three factors and responses44
Table 3.9	Factors input in the two models, respectively.....48
Table 3.10	2-factor model Vs 3-factor model Z-average response to targeting 150nm48
Table 3.11	Results of an experiment comparing different formulations of liposomes' Z-average, PDI and Zeta Potential, before and after dialysis50
Table 3.12	Dialyzed three-factor anionic CCCR design responses: Z-average, Zeta Potential and PDI51
Table 3.13	P-value and F-value of Zeta Potential and Z-average responses53

Table 3.14	R-squared adjusted and predicted for the dialysed responses: Zeta Potential, Z-average and PDI.....	53
Table 4.1	Objectives and strategies used for the synthesis of tailored cationic liposomes	57
Table 4.2	CCCR cationic design results for the 47 runs. The factors are FRR, TFR and DOTAP% (with coded values in parenthesis), the responses are Z-average, PDI and Zeta Potential	60
Table 4.3	R-squared, adjusted and predicted for the Z-average, Zeta Potential and PDI responses.....	61
Table 4.4	P-value and F-value of the different factors involved in the Zeta Potential and Z-average responses.....	62
Table 4.5	Dialyzed three-factor cationic CCCR design responses Z-average, Zeta Potential and PDI.....	64
Table 4.6	R-squared, adjusted and predicted for the Z-average, Zeta Potential and PDI	65
Table 4.7	P-value and F-value of the responses for the dialyzed response surface model.....	66
Table 5.1	Anionic, neutral, and cationic formulations, liposomes were produced at TFR=23.22ml/h, FRR=5.97 and T=25°C	76
Table 5.2	Percentage of events detected in quadrant 2 for IHH and BJ cells.....	83

LIST OF FIGURES

	Page
Figure 1.1	Formation of a liposome3
Figure 1.2	Thin film hydration method Adapted from “Liposome Preparation via Thin Film Hydration”, by BioRender.com (2022) Retrieved from https://app.biorender.com/biorender-templates4
Figure 1.3	Hydrodynamic focusing.....6
Figure 1.4	a) Periodic Disturbance Mixer (PDM) and b) Staggered Herringbone Micromixer7
Figure 2.1	Liposome Production Process schematic showing all the steps involved in producing liposomes14
Figure 2.2	LypoSynthesis software14
Figure 2.3	Liposome fabrication set-up15
Figure 2.4	Phospholipid structure16
Figure 2.5	Periodic Disturbance Mixer From López et al. (2020)19
Figure 2.6	Liposome characterization process20
Figure 2.7	Schematic of Rayleigh and Mie light scattering21
Figure 2.8	Correlogram (left) and size distribution by intensity measurement (right) of an anionic liposome measured on Zetasizer Nano. Size: 201.1nm and PDI: 0.01622
Figure 2.9	Cartoon showing an anionic liposome and the electric double layer (EDL) Adapted from Bhattacharjee (2016)24
Figure 2.10	Capillary cells used for microelectrophoresis (DTS1070, Malvern Panalytical)25
Figure 2.11	CCCR design. All the experimental points are at the same distance Axial (red stars) and cubic (blue squares) points have been repeated three times and the central point (yellow circle) has been repeated five times.....27
Figure 2.12	Graphical explanation of the p-value28

Figure 2.13	Confocal microscopy simplified scheme	31
Figure 2.14	Simple schematics of flow cytometry	32
Figure 2.15	Materials and methods summary	32
Figure 3.1	Zeta Potential measurement for all 18 samples, three replicates per different lipid composition. The percentage of DHP is increased progressively in intervals of 2% molar ratio from 0% to 10%.....	35
Figure 3.2	Mean Zeta Potential per increasing molar ratio of DHP, average of three replicates	35
Figure 3.3	CCCR design. All the experimental points are at the same distance Axial (red stars) and cubic (blue squares) points have been repeated three times and the central point (yellow circle) has been repeated five times.....	37
Figure 3.4	Surface plot and contour plot of the Z-average in function of TFR & FRR.....	40
Figure 3.5	CCCR design with three factors: six axial points (red stars) and four cubic points (blue squares), repeated three times and a central point repeated five times (yellow circle).....	42
Figure 3.6	Three-factor Response Surface Model. Contour and surface plot of the Zeta Potential in function of FRR and DHP%.....	46
Figure 3.7	Three-factor Response Surface Model. Contour and surface plot of the Z-average response in function of FRR and TFR.....	47
Figure 3.8	Ionic strength influences the formation of homogenous liposomes	49
Figure 3.9	Comparison between dialyzed and non-dialyzed responses of Zeta Potential	54
Figure 3.10	Comparison between dialyzed and non-dialyzed responses of Z-average	55
Figure 4.1	Effect of DOTAP% on the Zeta Potential of liposomes	58
Figure 4.2	Effect of DOTAP% on the Zeta Potential of liposomes, mean average of the three replicates.....	59
Figure 4.3	Surface plot (up) and contour plot (down) of the Zeta Potential response to the three-factor cationic model	63

Figure 4.4	Contour and surface plot of the dialyzed Z-average response in function of FRR and TFR.....	67
Figure 4.5	Contour and surface plot of the dialyzed Zeta Potential response in function of DOTAP% and FRR.....	68
Figure 4.6	Comparison of the dialyzed and non-dialyzed response of Zeta Potential	69
Figure 5.1	Endocytosis of liposomes	72
Figure 5.2	Images of the different cell structures of IHHs captured by each channel of the confocal microscope over 12 hours.....	73
Figure 5.3	Immortalized Human Hepatocytes (IHH) absorbing EV-like liposomes	74
Figure 5.4	IHHs time lapse pictures absorbing liposomes vs control.....	75
Figure 5.5	Confocal microscopy images of IHH and BJ cells vs control, anionic, neutral and cationic liposomes (24 hours of incubation). ZP stands for Zeta Potential.....	76
Figure 5.6	Forward vs Side scattering gating The region containing intact cells is selected.....	77
Figure 5.7	Quadrants and thresholds for signal detection in red and blue channels, theoretical controls schematics	79
Figure 5.8	Flow cytometry results of IHH uptake of anionic liposomes Sizes are between 89.5nm to 157nm, and Zeta Potential is ~ -25mV.....	81
Figure 5.9	Flow cytometry results of IHH uptake of anionic liposomes Size is ~160nm, and Zeta Potential ranges -12.46mV to -46.87mV	81
Figure 5.10	Flow cytometry results of BJs uptake of anionic liposomes. Sizes are between 89.5nm to 157nm, and Zeta Potential is ~ -25mV.....	82
Figure 5.11	Flow cytometry results of BJ uptake of anionic liposomes Size is ~160nm, and Zeta Potential ranges -12.46mV to -46.87mV	83
Figure 5.12	Quantitative uptake of liposomes of different sizes and similar Zeta Potential in IHH and BJ.....	84
Figure 5.13	Quantitative uptake of liposomes of different Zeta Potentials and similar size in IHH and BJ.....	84

LIST OF ABBREVIATIONS

ANOVA	Analysis of variance
APD	Avalanche Photo Diode
CHOL	Cholesterol
DHP	Dihexadecyl phosphate
DMPC	1,2-dimyristoyl-sn-glycero-3-phosphocholine
DNA	Deoxyribonucleic acid
DoE	Design of experiment
DOPE	1,2-dioleoyl-sn-glycero-3-phosphoethanolamine
DOTAP	1,2-dioleoyl-3-trimethylammonium-propane
DSPC	1,2-distearoyl-sn-glycero-3-phosphocholine
EV	Extracellular Vesicles
FRR	Flow Rate Ratio
IHH	Immortalized Human Hepatocytes
NTA	Nanoparticle Tracking Analysis
PBS	Phosphate Buffered Saline
PDI	Polydispersity Index
PDM	Periodic Disturbance Mixer
PEG-2000DMG	1,2-Dimyristoyl-rac-glycero-3-methoxypolyethylene glycol-2000
RCF	Raw Correlation Function
RNA	Ribonucleic acid
TFR	Total Flow Rate

INTRODUCTION

Liposomes have been a subject of great interest due to the race for the vaccine against COVID-19. They have the ability to protect important and delicate molecules such as messenger RNA and deliver them successfully in targeted organs and tissues in the body. These nanoparticles are spherical, with a width of 30-300 nm, and can be made with different lipid formulations using various methods. Interestingly, this delivery system was inspired by nature itself: extracellular vesicles (EVs) are naturally produced lipid nanoparticles that are made of a variety of lipids and proteins and carry a myriad of biomolecules through the body. They are secreted by nearly all types of cells and have been recently shown to play a key role in cell-cell communication in the cancer microenvironment, particularly in metastasis. EVs derived from cancer cells deliver protumor factors to distant organs and set the stage for tumor growth, meaning that they actively contribute to the process of metastasis (Tsering et al., 2020). EVs are heterogenous nanoparticles produced at different rates depending on the type of cell but collecting and isolating them is a complicated process with low yield (EVs in solution with low concentrations). Moreover, the exact parameters influencing how cells specifically uptake (absorb) these naturally occurring nanoparticles are still unknown (Chang, Cerione et Antonyak, 2021).

Knowing that EVs could be reverse engineered, the goal of this work is to develop liposomes that mimic cancer-derived EVs, using a uveal melanoma (ocular cancer) cell line: MP41. A microfluidic mixer and different lipid compositions are used to modulate the physicochemical properties of liposomes to imitate the EV Zeta Potential (surface charge) and Z-average (hydrodynamic diameter). Mimicking these parameters will allow us to further study how they affect intercellular transport. This work's main contribution is the development of a translational approach to the synthesis of lipid nanoparticles using Design of Experiment that enabled us to create EV-mimicking liposomes to study the behavior of cells

Chapter 1 investigates the literature on the key players of this projects: liposomes and EVs. The materials and methods in Chapter 2 detail the fabrication protocol and the characterization process of liposomes, as well as the different steps of the experiments involved.

EVs have different sizes and surface charges depending on the cells they are secreted from; therefore, a Design of Experiment approach was used to build a statistical model (Circumscriber Central Composite Design) based on Response Surface Methodology that relates the different production parameters on the microfluidic mixer to the physicochemical properties of liposomes. This model is presented in Chapter 3 and spans a vast array of Z-average and Zeta Potential combinations, allowing us to fabricate liposomes that could mimic a variety of cancer-derived EVs.

This methodology was applied to the fabrication of cationic liposomes in Chapter 4, which are widely used for the delivery genetic material in different types of cells, since the electrostatic interaction between the cationic lipids of the nanoparticle encourage the encapsulation of the negatively charged DNA and RNA fragments and facilitate the transfection in cells.

Finally, in Chapter 5, the resulting models were used to produce tailored liposomes to use in the uptake experiments to explore how different types of cells (mainly Immortalized Human Hepatocytes and BJ fibroblasts) absorbed the EV-mimicking liposomes.

CHAPTER 1

LITTERATURE REVIEW

1.1 Introduction

Liposomes were first discovered by Dr Alec Bangham in the 1960s (Bangham et Horne, 1964) at the Babraham Institute in Cambridge, UK, and were called *banghosomes*. Since then, the field of liposomes has evolved to use them as efficient drug delivery systems for a multitude of purposes. These artificial vesicles made of a lipid bilayer have been the tool used to deliver the most recent mRNA vaccines and is currently applied in many other fields, such as cancer research. This literature review begins by describing the fabrication methods of liposomes involving nanoprecipitation, then the importance of lipid formulation is discussed and finally the role of liposomes in cancer therapeutics are investigated.

1.2 Fabrication methods of liposomes: from thin film hydration to micromixing

The lipid bilayer of liposomes is obtained by assembling the lipids in an organized and stable manner. Phospholipids are extensively used for this purpose: because of their dual polarity which is manifested in a hydrophilic head and a hydrophobic tail, they reorganize when they enter in contact with polar molecules, such as water. This process is called nanoprecipitation: the lipids aggregate and precipitate, forming a double layer, as depicted in Figure 1.1.

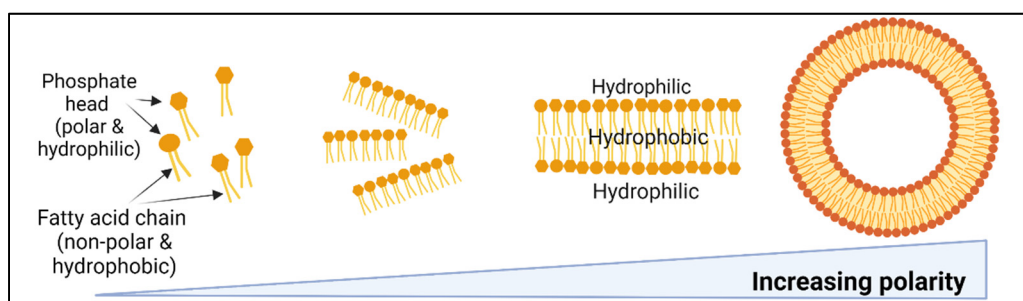


Figure 1.1 Formation of a liposome

The lipids are usually suspended in an organic solvent, such as ethanol, and when they become in contact with a polar solvent (water, buffers, etc), the lipids aggregate and form a lipid bilayer that becomes organized in the form of a spherical double layer with an empty lumen, as first described by Fessi et al. (Fessi et al., 1989). The nanoprecipitation can take place in various ways, but this literature review will focus on the following methods: thin film hydration, injection method and passive micromixing.

1.2.1 Thin film hydration

The first liposomes developed by Bangham used the thin film hydration method to trigger the self-assembly of the lipids into a bilamellar vesicle. The lipids were mixed while in suspension in an organic solvent that would be later evaporated, leaving a thin lipid layer at the bottom of the flask. These lipids are re-hydrated using a polar solvent and sonicated to reduce the size of the liposomes (see Figure 1.2). This mixing process relies heavily on the formation of a homogenous and thin lipid layer, which is complicated to control, and an agitation step that yields non-homogenous populations (Bangham, Standish et Weissmann, 1965).

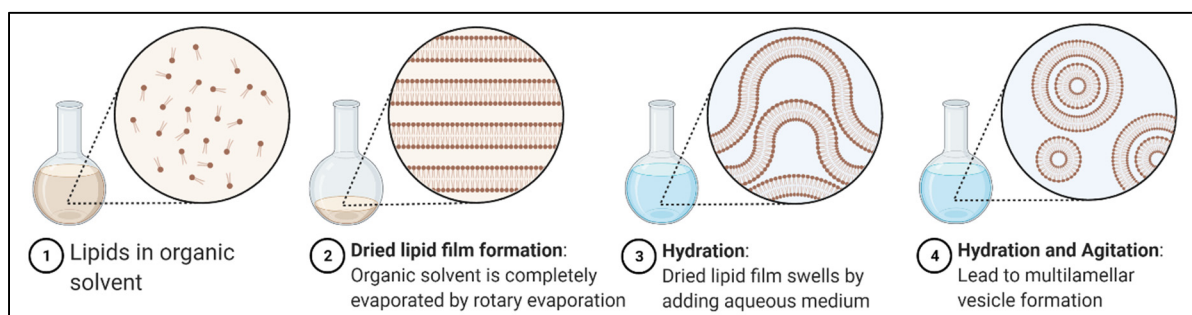


Figure 1.2 Thin film hydration method

Adapted from “Liposome Preparation via Thin Film Hydration”, by BioRender.com (2022)

Retrieved from <https://app.biorender.com/biorender-templates>

1.2.2 Injection method

The injection method was first described in 1973 by Batzri and Korn and was extensively used as an alternative to the thin film hydration method: the lipids are injected in a controlled manner into a polar solvent (Batzri et Korn, 1973). This method was further refined by adding a nozzle that releases droplets of lipids, which are suspended in ethanol, into a buffer with different ions present in its composition (Pons, Foradada et Estelrich, 1993). Moreover, Pons and collaborators were using different concentrations of lipids and osmolality (presence of ions in the buffer) and observed the sizes of liposomes. They determined that size was highly dependant on the injection velocity (the speed at which the lipids are dropped in the solvent) and the lipid concentration (which is the number of molecules being dropped in the solvent), shedding light on the interaction of lipids and how they form: the more molecules of lipids available, the bigger the liposomes, and vice versa. Nonetheless, this method has very little control over the mixing process itself and the formation of liposomes (Stano et al., 2004).

1.2.3 Micromixing

The most widely used method to produce liposomes is based on microfluidics. The passive micromixers involve a microfluidic chip and some sort of pumping system to inject the lipids and the solvents. The mixing of the organic and aqueous phases happens within the channels of the micromixer chips under rigorously controlled conditions that yield homogenous populations of liposomes. Microfluidic chips have significantly improved the liposome production process because they have allowed to fully control the volumes of fluids being mixed via hydrodynamic focusing, described in Figure 1.3. The schematic of this figure shows a chip with three inlets that converge to a central channel. The liquid inserted in inlet 2 is mixed with the one inserted in inlets 1 and 3, in a laminar flow: the speed is homogenous across the three “layers” of fluids.

For the purpose of liposome production, the lipids are inserted via inlet 2 and the polar solvent via inlets 1 and 3 (Jahn et al., 2004). The liposomes would form at the interface between both solvents via the mechanism of diffusion (Figure 1.3).

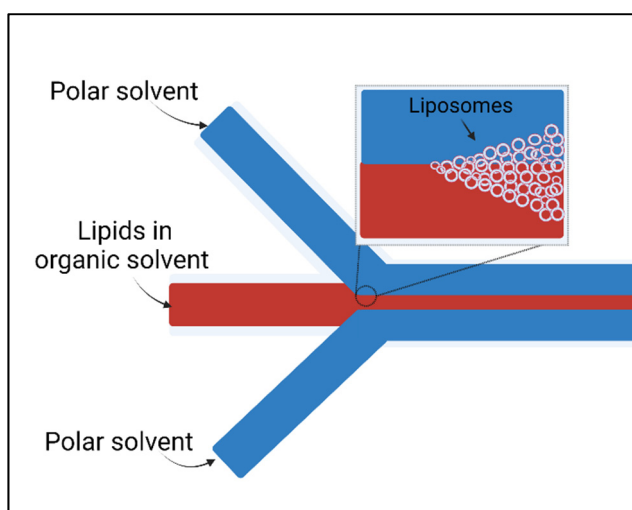


Figure 1.3 Hydrodynamic focusing

Diffusion is described as the movement of particles across the concentration gradient: the particles move from the more concentrated regions to the lower concentration regions. In Figure 1.3, the molecules of lipids in suspension in the red fluid would reorganize and assemble into liposomes when entering in contact with the polar solvent (blue).

A publication from Prof. Langer's laboratory at the Massachusetts Institute of Technology in 2012 had already foreseen the potential of microfluidics in nanomedicine (Valencia et al., 2012). Fast-forward a decade, and the most recent microfluidic chips now include different geometries within the microfluidic channels to enhance the mixing process: these structures are obstacles that encourage the interaction of polar (water) and apolar (lipids) molecules without disrupting the laminar flow in the chip. Two examples are shown in Figure 1.4:

- The periodic disturbance mixer fabricated by Lopez et al. has semicircular lateral structures (López et al., 2020).

- The NanoAssemblr microfluidics mixer from the Vancouver-based company Precision Nanosystems Inc. has a herringbone structure similar to the one shown below (Chiesa et al., 2019).

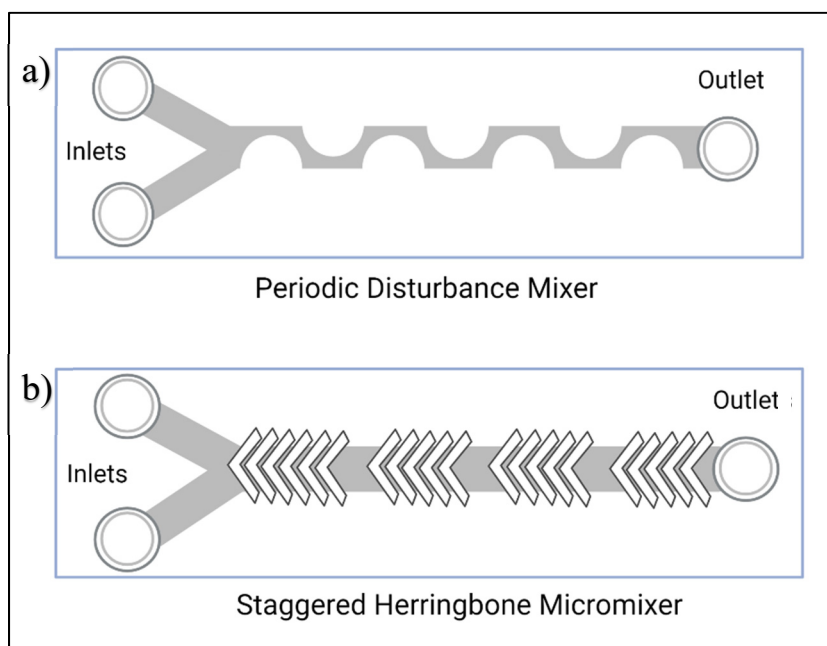


Figure 1.4 a) Periodic Disturbance Mixer (PDM) and b) Staggered Herringbone Micromixer

1.3 Formulation of liposomes

Liposomes' formulation depends ultimately on their purpose. Even though liposomes were first developed to study the cellular membrane and imitate it in the 1960s (Bangham et Horne, 1962), they have been used as a delivery system since the 1990s (Akinc et al., 2019).

Liposomes must interact with the cellular membrane to successfully deliver their cargo, therefore cationic lipids (positively charged, such as 1,2-dioleoyl-3-trimethylammonium propane, DOTAP, and 1,2-di-O-octadecenyl-3-trimethylammonium propane, DOTMA) were used to increase their electrostatic interactions with the negatively charged membranes. Moreover, genetic materials such as RNA and DNA are also negatively charged and form a

complex called lipoplex with the positively charged lipids that facilitates their endocytosis (absorption) by cells (Ostróžka-Cieślik et Sarecka-Hujar, 2017). However, positively charged lipids have raised toxicity concerns since the early beginnings of the field because they trigger the immune system and activate an inflammation response in the body (Sze et al., 2003), which have led to the development of different strategies regarding the composition of liposomes.

For instance, to improve the circulation time of liposomes in the body (making it long enough to reach the target organs) and avoid being detected and discarded, PEG lipid (for example PEG-2000DMG lipid) has been used in very small percentages (1-2%) to produce stealth-cationic liposomes (Perli et al., 2019) and the latest mRNA vaccines (see Table 1.1). PEGylation also improves the therapeutic effects of the cargo molecule in the liposomes and reduces their toxicity (Milla, Dosio et Cattell, 2012). More recently, ionizable lipids, such as SM-102, ALC-0315, ALC-0159 and DLin-MC3 (all proprietary information), have stolen the show and are the main components of the Moderna and Pfizer-BioNTech Comirnaty COVID-19 vaccines (Table 1.1). Ionizable lipids are protonated at low pH, which allows them to bond with RNA and other negatively charged molecules, forming lipoplexes that protect them from degradation. At physiological pH (pH=7.4), ionizable lipids are neutral which reduces their cytotoxicity (Han et al., 2021).

Table 1.1 Information on the three mRNA vaccines against COVID-19 and Onpattro
Adapted from Schoenmaker et al. (2021)

	Composition	Molar lipid ratios (%)
Moderna	SM-102 : DSPC : CHOL : PEG2000-DMG	50:10:38.5:1.5
CureVac	Cationic lipid : Phospholipid : Cholesterol : PEG-lipid conjugate	50:10:38.5:1.5
Pfizer-BioNTech Comirnaty	ALC-0315 : ALC-0159 : CHOL : DSPC	46.3:9.4:42.7:1.6
Onpattro patisiran	DLin-MC3-DMA : DSPC : CHOL : PEG200-DMG	50:10:38.5:1.5

On the other hand, liposomes must be structurally stable and have a decent shelf life. “Helper” lipids found in cellular membranes such as cholesterol (CHOL) are highly present in the vaccines and therapies presented in Table 1.1, and enhance the delivery efficiency of these nanoparticles by filling the gaps in the membrane and stabilizing it. Phosphatidylcholines (PCs) such as distearoylphosphatidylcholine (DSPC) favor the formation the lipid bilayer and contributes to its stability thanks to their low melting temperature (Cheng et Lee, 2016).

Other lipids are currently used for RNA-delivery purposes but are not included in the recent vaccines against COVID-19. Phosphatidylethanolamines are found in biological membranes and 1,2-dioleoyl-sn-glycero-3-phosphoethanolamine (DOPE) is a lipid that contributes specifically to endosomal escape, which is the mechanism through which cells discard the absorbed components before they reach their cytosol. Liposomes are usually greeted by a group of cellular organelles called the endosome, in charge of degrading foreign molecules (Ball et al., 2018). Escaping from the endosome is therefore a crucial step in the drug delivery process, and it is therefore important to include lipids that will specifically help escaping the endosome. DOPE has shown to promote the effective delivery of genetic material in both *in vitro* and *in vivo* studies (Du et al., 2014).

Regarding the most famous liposome formulations presented in Table 1.1, there is a winning combination of helper lipids (CHOL, DOPE, DSPC) and ionizable lipids that is dominating the field: the only difference between the Onpattro, Moderna and Curevac formulation is the type of ionizable/cationic lipid used, but the rest of the components and the molar proportions are identical. This combination of lipids has proven to successfully deliver genetic cargos, but the underlying mechanisms of the biological processes involved are yet to be understood.

1.4 Liposomes as a delivery system

Given that the formulation possibilities are virtually infinite, a biocentric approach is necessary to develop an efficient liposome delivery system. However, the exact mechanisms involved in the specific targeting are still under study. It is hypothesized that the following parameters will

dictate the fate of liposomes: the lipid formulation, the surface moieties (proteins and other molecules placed on the shell of the liposomes), the size and the surface charge.

A study from Cheng et al (2020) investigated the role of the surface charge of the liposomes in the delivery of the CRISPR-Cas, a gene editing protein, and developed a selective organ targeting strategy (named SORT). They fabricated the liposomes using a method similar to ethanol injection. By adding a lipid with a particular charge to the formulation of the liposomes (the SORT molecule), they were able to target specifically a variety of organs and cell types. This successful strategy can be employed to effectively deliver a variety of molecules to the spleen, liver, lungs, kidneys, and heart of mice, opening new avenues for targeted gene therapy.

Another strategy to create an effective delivery system would be to imitate the naturally existing ones. Extracellular vesicles, such as exosomes, are released by cells and mediate intercellular communication. They carry a variety of cargos and, in the case of cancer cells, they have recently been identified as transporters of pro-tumor factors that set the stage for cancer growth (Tsering et al., 2020). Sakai-Kato (2020) imitated the naturally occurring extracellular vesicles released from HepG2 (a liver cancer cell) by fabricating liposomes with a similar lipid composition, stiffness, and surface charge. The liposomes were made using the thin film hydration method. They subsequently studied how HeLa cells (epithelial cells originated from cervical cancer) were responding and absorbing these liposomes.

The lipid composition was particularly important, unveiling that integrin proteins present on the surface of HeLa cells were binding to the phosphatidylserine lipids of the liposomes' shell. Integrins are expressed in all cell types, except erythrocytes (red blood cells), they are key mediators in cell to cell communication and their signaling ability is tightly controlled (De Franceschi et al., 2015). Moreover, the lipid composition also determined the stiffness of the liposomes, which could be added as a sub-parameter of liposomes. However, this study disregarded the size of the liposomes when analyzing the uptake, which is contradictory to previously published studies (Blanco, Shen et Ferrari, 2015; Harashima et al., 1994) and only used one type of cell, the cancerous HeLa cells, as receptor cells for their EV-mimicking liposomes.

1.5 Conclusion

Liposomes have proven successful as a delivery system but the underlying mechanisms that influence the cellular response are still under study. Liposomes can be made using a myriad of techniques, certain techniques will allow for a better control over their physicochemical properties, which is necessary to pinpoint exactly which parameters influence the cellular behavior and ultimately their potential as a delivery system. At the moment, the only study that has successfully mimicked extracellular vesicles failed to model an effective communication between cancerous and non-cancerous cells. Our contribution is aiming to advance the current knowledge on both cell-to-cell communication and liposome production by:

- Synthesizing EV-like liposomes that have the same physicochemical parameters (mainly the Zeta Potential and Z-average)
- Evaluating how these liposomes are uptaken by cells and how the Z-average and Zeta Potential affect it.

CHAPTER 2

MATERIALS AND METHODS

In this chapter, the materials and methods used to produce liposomes and experiment with the physicochemical parameters will be detailed. Moreover, the characterization procedure as well as the cell culture protocols involved in the variety of experiments presented in this thesis will be explained.

2.1 Liposome production

Liposomes are formed by nanoprecipitation. This phenomenon happens when the lipids aggregate and precipitate, forming a double layer, as detailed by Fessi et al. (1989). Nanoprecipitation can be controlled using microfluidic devices that are going to determine both the speed and the volume of each component during the mixing procedure. This work has used a Periodic Disturbance Mixer (PDM), developed by Lopez et al. (2019) that will be further explained in this chapter.

2.1.1 Micromixing setup

The setup is composed of two syringe pumps (Pump 11 Elite and Pump 11 Pico Elite, from Harvard Apparatus), a Periodic Disturbance Micromixer (developed by Lopez et al., 2019) and a hot plate (EchoTherm HS40 Programmable Digital Stirring Hot Plate, 115V, Torrey Pines). The pumps and the hot plate are controlled by the LipoSynthesis software (Version 2.2.1, developed by Luz-Maria Sanchez). Figure 2.1 shows a cartoon of the fabrication set-up while Figure 2.2 and Figure 2.3 show the software's main page and the real fabrication set-up, respectively.

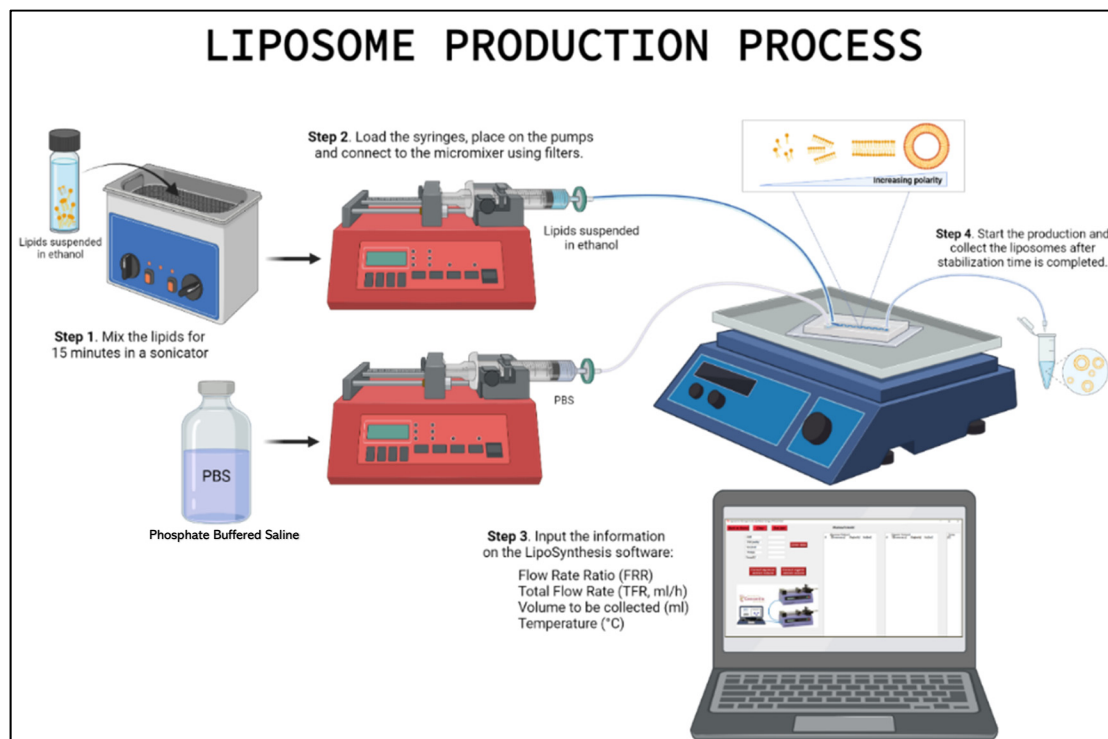


Figure 2.1 Liposome Production Process schematic showing all the steps involved in producing liposomes

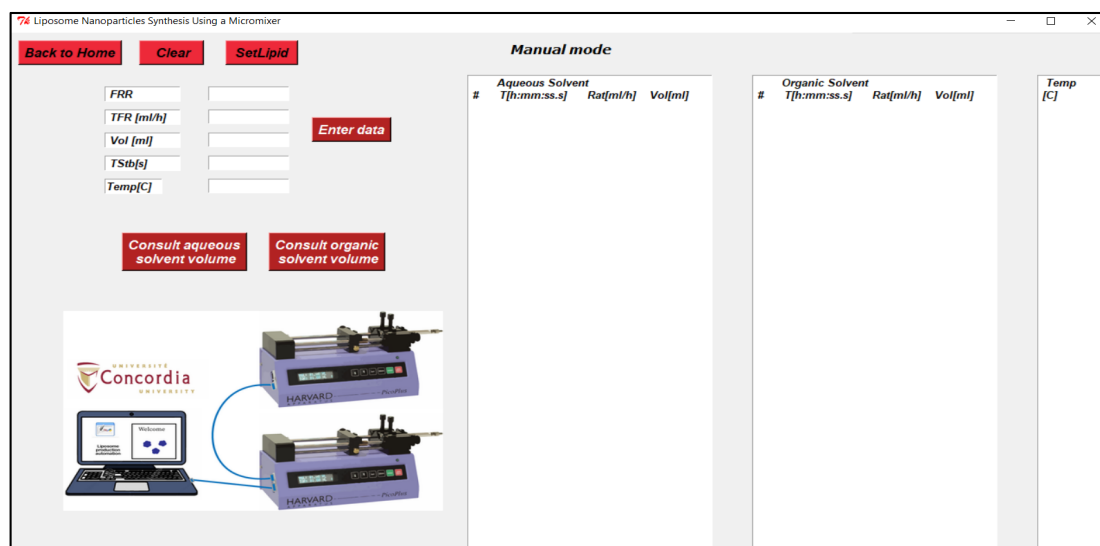


Figure 2.2 LipoSynthesis software

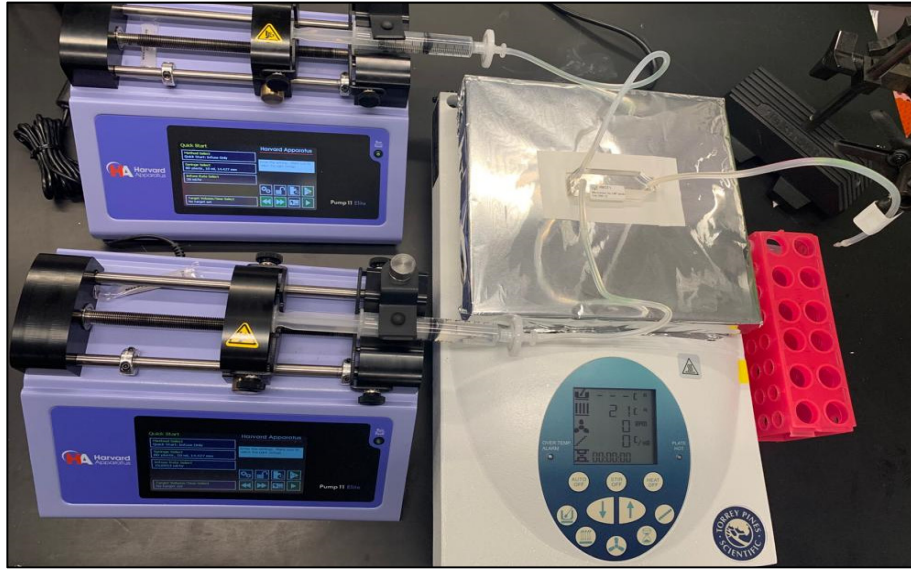


Figure 2.3 Liposome fabrication set-up

Information such as Total Flow Rate (TFR, in ml/h), Flow Rate Ratio (FRR), Temperature (in °C), stabilization time and volume (ml) of sample to be collected are input in the software. TFR can be defined as the fluid's speed at the outlet of the microfluidic chip and the FRR is the ratio between aqueous and organic solvents' flow. Both fluids are mixed under very controlled conditions inside the microfluidic device. The program starts the pumps, but the sample is not collected until the stabilization time is completed, ensuring that the sample is produced within a laminar flow. The TFR and FRR are calculated as follows:

$$Q_{aq} = \frac{FRR * TFR}{(1 + FRR)} \quad (2.1)$$

$$Q_{org} = \frac{TFR}{(1 + FRR)} \quad (2.2)$$

Where Q_{org} stands for the organic solvent with the diluted lipids' flow (ml/h), and Q_{aq} stands for aqueous solvent flow (ml/h). Each syringe pumps will be pushing the content of a 10mL BD syringe into the micromixer: on one side the mixture of lipids suspended in an organic

solvent (ethanol) and on the other side the polar solvent required to form the liposomes (Phosphate or Citrate Buffer). Each syringe is connected to the system through a 0.22 μ m filter (Millipore Express PLUS Membrane Filter 0.22 μ m) and a tube (Masterflex® Chemital tube).

A dialysis step using Millipore Sigma Pur-A-Lyzer® Dialysis Kit and following the manufacturer's instructions is introduced to standardize the concentration of ions in the solvent. Liposomes' size and Zeta Potential are actively affected by the presence of buffer in the colloid. To standardize the production and characterization of liposomes, the sample's solvent, usually containing a mixture of ethanol and buffer, with a 4% phosphate buffer saline (PBS) solution.

2.1.2 Lipids preparation

Lipids are an essential component of the cellular membrane. They are the main component of extracellular vesicles and are soluble in organic, non-polar solvents such as ethanol and chloroform. There are several types of lipids, depending on their structure and composition. This section will focus on the lipids used to fabricate EV-mimicking liposomes.

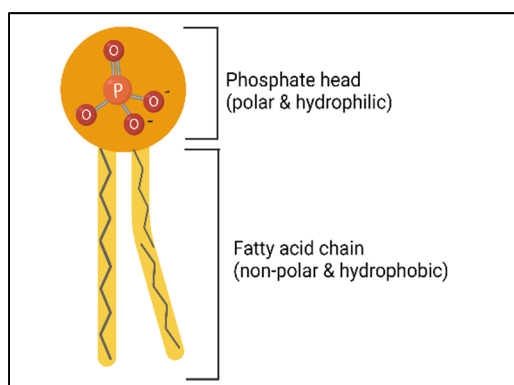


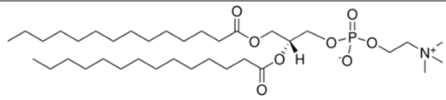
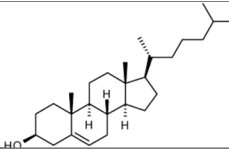
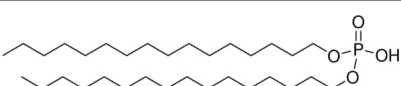
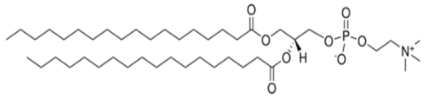
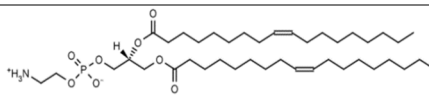
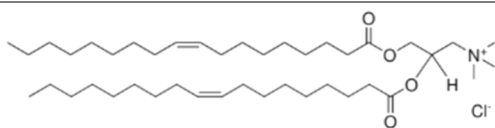
Figure 2.4 Phospholipid structure

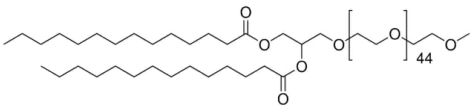
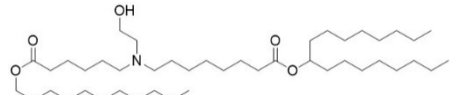
Phospholipids are the main building blocks of lipid bilayers; they have a polar phosphate head that is hydrophilic and a hydrophobic fatty acid tail (Figure 2.4).

The lipids used are shown in Table 2.1. Most of them are phospholipids and have different charges in their polar heads. The exception is Cholesterol (CHOL). CHOL is not a phospholipid, but a sterol (a modified steroid) and it is an integral component in the structure of lipid membranes, regulating its fluidity (Ikonen, 2008; Meyer et Smit, 2009). CHOL, 1,2-dimyristoyl-sn-glycero-3-phosphocholine (DMPC), 1,2-dioleoyl-sn-glycero-3-phosphoethanolamine (DOPE) and 1,2-distearoyl-sn-glycero-3-phosphocholine (DSPC) are structural lipids that contribute to the stability and morphology of liposomes. DOPE has an important role in the transfection of nucleic acid (Degors et al., 2019; Mochizuki et al., 2013), which is the process through which genetic molecules are introduced in cells using nanoparticles as carriers.

Lipids like Dihexadecyl phosphate (DHP) and 1,2-dioleoyl-3-trimethylammonium-propane (DOTAP) carry a negative and a strong charge, respectively. DHP has been used to make anionic liposomes and DOTAP for cationic liposomes.

Table 2.1 Lipids used and their formulation. Retrieved from Millipore Sigma

Lipid	Name	Formula
DMPC (14:0 PC)	1,2-dimyristoyl-sn-glycero-3-phosphocholine	
CHOL	Cholesterol	
DHP	Dihexadecyl phosphate	
DSPC (18:0 PC)	1,2-distearoyl-sn-glycero-3-phosphocholine	
DOPE (18:1 PE)	1,2-dioleoyl-sn-glycero-3-phosphoethanolamine	
DOTAP (18:1 TAP)	1,2-dioleoyl-3-trimethylammonium-propane	

Lipid	Name	Formula
PEG-2000	1,2-Dimyristoyl-rac-glycero-3-methoxypolyethylene glycol-2000	
SM-102	Proprietary information	

Lipids purchased from Avanti Polaris Inc. and Echelon Biosciences are usually suspended in chloroform and need to be dried using a speed vacuum at 45°C (reference of the speed vac) for up to 3 hours and then placed in the vacuum desiccator overnight. The lipids were then resuspended in ethanol at a 10mM concentration. Moreover, the lipids purchased in powder format were diluted in ethanol directly. To guarantee a homogenous suspension of the lipids in ethanol, they are sonicated during 15 min at 45C (Ultrasonic Cleaner, Cole Parmer) prior to use for liposome production.

Different formulas have been used to explore the fabrication of liposomes with different physicochemical parameters. Anionic liposomes (with negative Zeta Potential) were made using 50% DMPC, 40 to 50% Cholesterol and 0 to 10% DHP.

Cationic liposomes were made using DSPC:Cholesterol:DOPE:DOTAP in variable ratios. For neutral liposomes, they were either made with DMPC: CHOL 1:1 or using the Moderna formulation: SM-102:Cholesterol:DSPC:PEG-2000 with ratios 50:38.5:10:1.5% (Schoenmaker et al., 2021). The lipids are stored in ethanol at a 10mM concentration. The amount needed of a particular lipid is calculated as follows:

$$\text{Mass}_{\text{lipid}} = R * C_f * V_T * M_w \quad (2.3)$$

Where R is the molar ratio (%) of the lipid in question, C_f is the final concentration of lipids (10mM usually), V_T is the total volume and M_w is the molecular weight of the lipid at study.

For example, DMPC has a $M_w=677.93\text{gr/mol}$ and is present in the anionic formulation at $R=50\%$. To make a volume of 2mL with a concentration of 10mM of lipids, the total mass needed of DMPC is calculated as follows:

$$\text{Mass}_{\text{DMPC}}(\text{gr}) = 50\% * 10\text{mM} * 2\text{mL} * 677.93 \text{ gr/mol} \quad (2.4)$$

The mass of DMPC needed is $6,78\text{mgr}$.

2.1.3 Micromixer

The micromixer developed by Lopez et al. (2019) has a 1 to 1 aspect ratio, with a width and height of $300\mu\text{m}$. It is fabricated using a standard soft-lithography procedure: the PDMS chip is made from a SU-8 mold and subsequently plasma bonded to a $75 \times 25\text{mm}$ glass slide. The microfluidic chip has two inlets and one outlet, and a series of semicircular structure that encourage the mixing of both solvents and the nanoprecipitate of liposomes. This takes place within a laminar flow, by passive molecular diffusion and advection. The advection is caused by the obstacles within the microfluidic chip that move the fluid thanks to the centrifugal force, but the speed remains the same throughout the process.

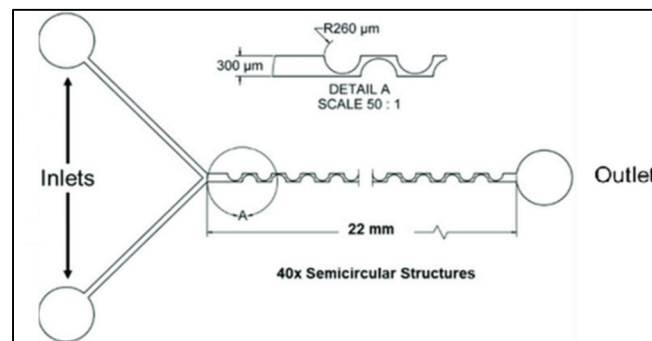


Figure 2.5 Periodic Disturbance Mixer
From López et al. (2020)

The ratio between centrifugal forces and inertial forces is described by the Dean Number, which measures the formation of Dean Vortices (López et al., 2020):

$$De = Re \sqrt{\frac{D_H}{2R_c}} \quad (2.5)$$

Where D_H is the hydraulic diameter, Re is the Reynolds number, R_c is the ratio of curvature of the channel. The micromixer developed by Lopez et al. is specifically tailored to Dean Flow Dynamics.

2.2 Liposome characterization

Liposomes have been characterized by their Z-average (hydrodynamic diameter in nm), their Zeta Potential (mV), their size distribution and their concentration. Dynamic Light Scattering (DLS), Nanotracking Analysis (NTA), Confocal Microscopy and Flow Cytometry, as shown in Figure 2.6, have been used for this purpose.

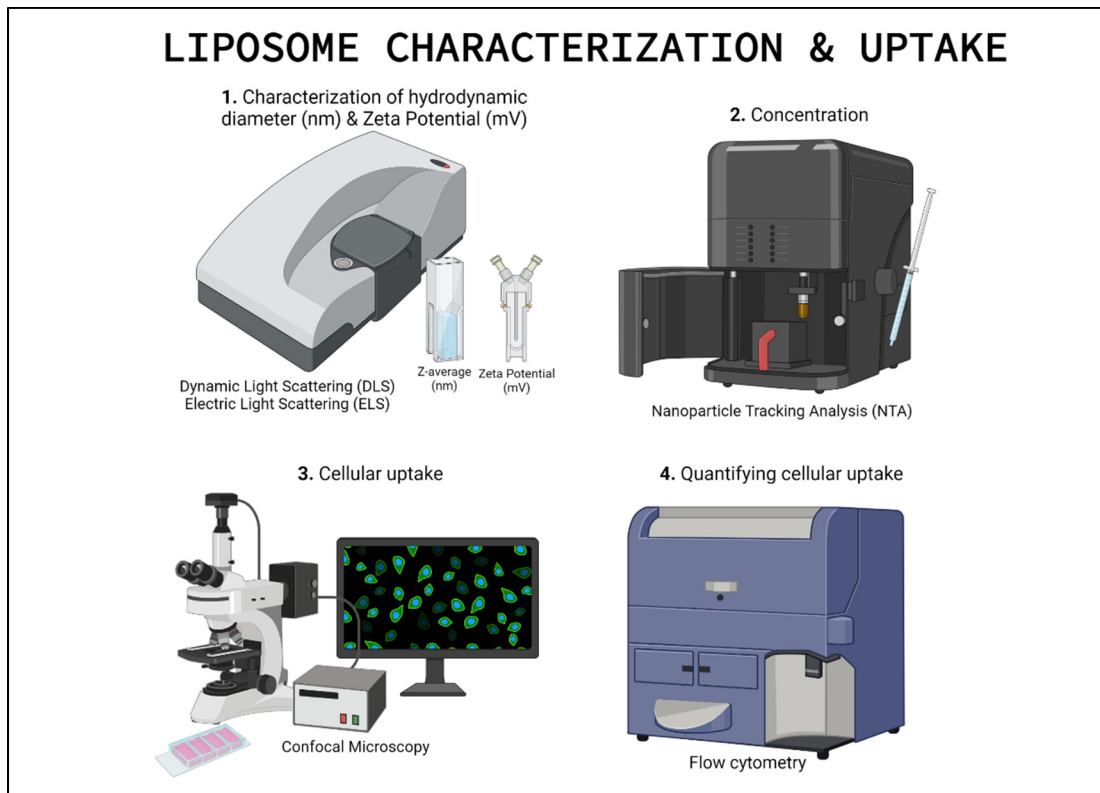


Figure 2.6 Liposome characterization process

2.2.1 Z-average and polydispersity index (PDI)

The Z average is the intensity weighted mean hydrodynamic size of the particles analyzed by DLS. Depending on the size of the particle, the incident light (Figure 2.7) will be (Finsy, 1994):

- Scattered elastically (Rayleigh scattering) if the diameter of the nanoparticle is smaller than one tenth of the wavelength ($\lambda / 10$ i.e.). In this case, there is no loss of energy.
- Scattered anisotropically (Mie inelastic scattering) when the nanoparticle's diameter is larger than one tenth of the wavelength. The scattering is therefore angle dependent.

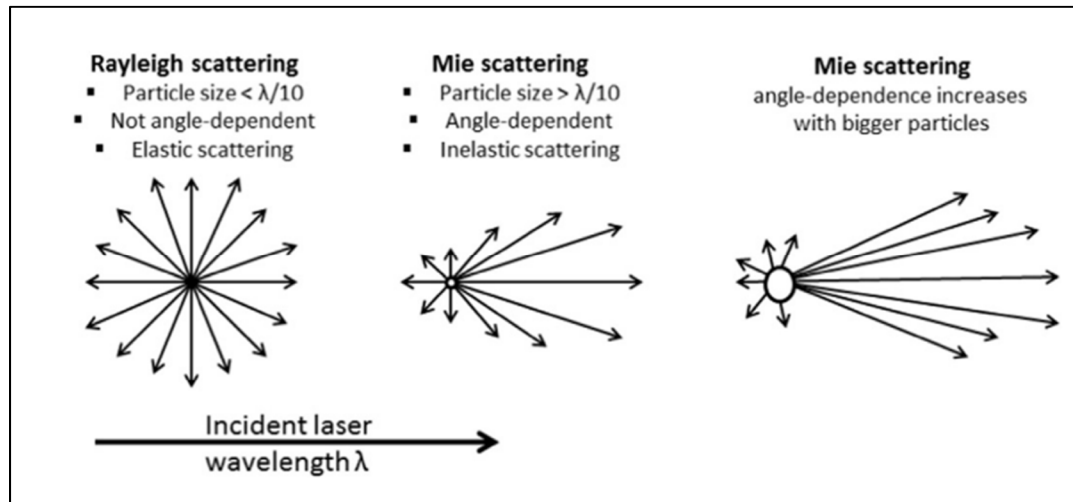


Figure 2.7 Schematic of Rayleigh and Mie light scattering

The DLS detects the intensity of the light scattered by the constantly moving nanoparticles in suspension. The Z average is then derived from the autocorrelation function that compares the signal with a delayed copy of itself, meaning that they are correlated against short decay intervals (τ). For purely monodispersed populations, the intensity autocorrelation function can be described as follows (Bhattacharjee, 2016):

$$G(\tau) = 1 + b \cdot e^{-2D_t q^2 \tau} \quad (2.6)$$

Where b is a constant that depends on the instrument's settings, D_t is the translational diffusion coefficient and q is the scattering vector, which can be expressed as (Bhattacharjee, 2016):

$$|q| = \frac{4\pi n_0}{\lambda_0 \sin \frac{\theta}{2}} \quad (2.7)$$

n_0 is the refractive index of the solvent, λ_0 is the wavelength (in vacuum) and θ is the scattering angle. The intensity measured by the DLS is a result of the constructive and destructive interferences of the scattered light, therefore the raw correlation function (RCF) is generated by the software by data fitting to calculate the hydrodynamic size of the nanoparticles as shown in Figure 2.8 (Bhattacharjee, 2016):

$$RCF = G2(\tau) - 1 = G1(\tau)^2 \quad (2.8)$$

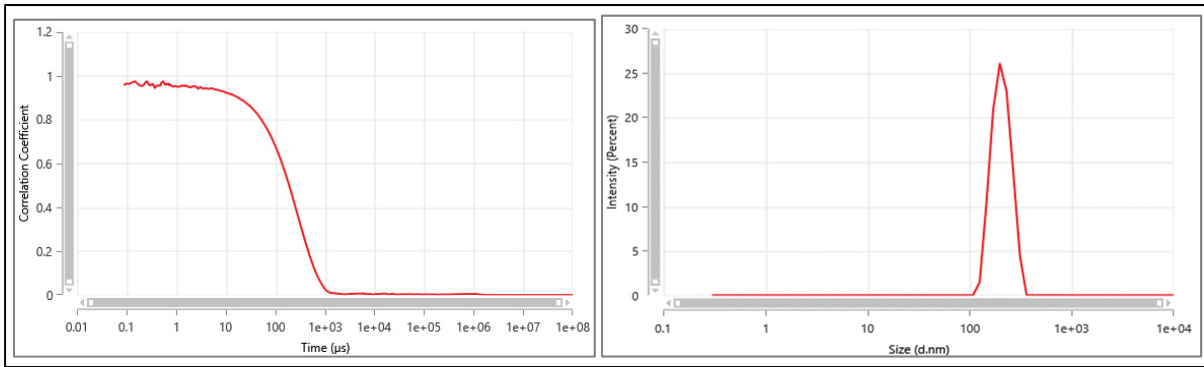


Figure 2.8 Correlogram (left) and size distribution by intensity measurement (right) of an anionic liposome measured on Zetasizer Nano. Size: 201.1nm and PDI: 0.016

The autocorrelation function $G1(\tau)$ is therefore derived from the data fitting and the size of the nanoparticle is calculated from the translational diffusion parameter, D_t , obtained from equation 2.1. D_t is itself defined as (Bhattacharjee, 2016):

$$D_t = \frac{k_B T}{6\pi\eta R_H} \quad (2.9)$$

Where k_b is the Boltzmann constant (it relates the kinetics of the particles with the thermodynamic temperature and is $1.38064852 \times 10^{-23}$ J/K), T is the temperature, η is the absolute viscosity and R_H is the hydrodynamic radius of the nanoparticle.

The Z average is measured on the Malvern Zetasizer Nano Pro. This instrument uses a red He-Ne laser with a $\lambda=633\text{nm}$ and an avalanche photo diode (APD) placed at 173° to detect backscattering light and exclude excess scattered light. Since the concentration of particles affects considerably the results obtained in DLS measurements, the samples are produced at a standardized concentration of 0.4mM (lipid concentration) which is the equivalent of 4×10^{11} particles/mL and they are placed to scratch-free disposable cuvettes (Micro cuvettes and macro references) and measured at 25°C . The viscosity and the refractive index of the solvent are input in the ZS Explorer Software. The type of particles at study are lipid nanoparticles with a refractive index of 1.45. Coloured particles can also be measured using the same protocol (Bhattacharjee, 2016).

The polydispersity index (PDI) is calculated as the $(\text{width}/\text{mean})^2$ for each peak. A PDI below 0.1 indicates a monodispersed population, a PDI between 0.1 and 0.2 indicates a lowly polydisperse population and a PDI above 0.3 indicates a polydisperse sample (Bhattacharjee, 2016).

2.2.2 Zeta Potential

The Zeta Potential, also known as the electrokinetic potential, is described as the charge at the slipping plane of a particle. The slipping plane marks the outer frontier of the Stern layer that mainly contains ions and molecules of opposite charge to the nanoparticle that are bound to it by electrostatic interactions (Figure 2.9). These electrostatic interactions wear off at a certain distance from the nanoparticle, which is dictated by Debye's law ($1/e$). The Zeta Potential is therefore the potential at the particle/fluid interface (Bhattacharjee, 2016).

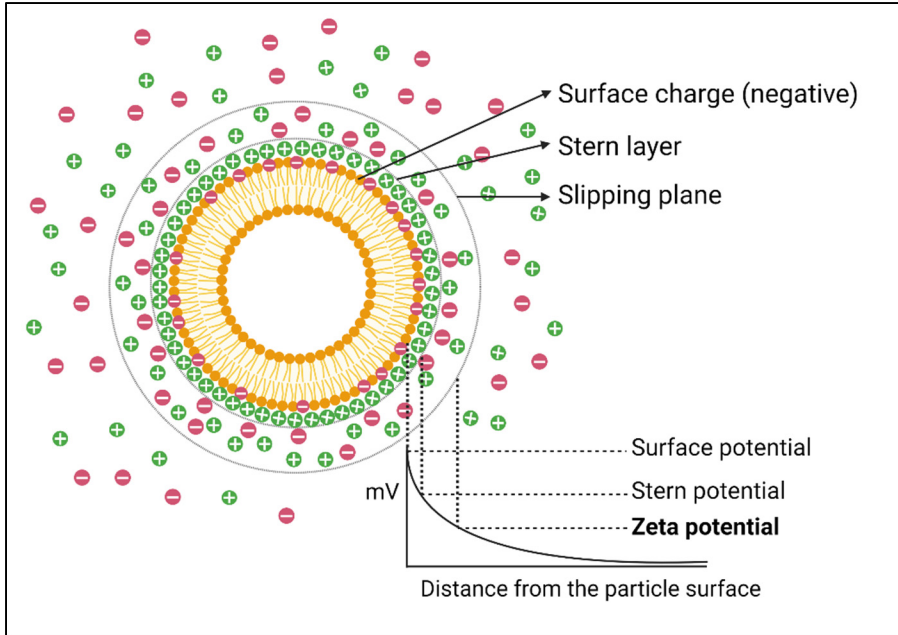


Figure 2.9 Cartoon showing an anionic liposome and the electric double layer (EDL)
Adapted from Bhattacharjee (2016)

The Zeta Potential is measured by particle electrophoresis: electrophoretic light scattering (ELS), also called Doppler Electrophoresis, is a technique based on dynamic light scattering. In the case of DLS, the particles were in movement because of the Brownian motion. For ELS, an oscillating electric field is used to trigger the movement of the particles and the electrophoretic mobility, μ (m^2/Vs), of the particles is calculated as follows:

$$\mu = \frac{v}{E} \quad (2.10)$$

Where v is the electrophoretic velocity and E is the electric field strength (Charcosset, 2016). The light scattered is measured in short decay intervals to quantify its frequency shift. The Zeta Potential (ζ , mV) is measured according to the Smoluchowski equation:

$$\zeta = \frac{\mu 4\pi\eta}{\varepsilon} \quad (2.11)$$

Where ε is the permittivity of the medium and η its viscosity. The Zeta Potential is therefore dependent on these parameters. The Zetasizer Nano Pro was used to measure both Z-average and Zeta Potential. A capillary cell containing two gold-plated electrodes (Figure 2.10) create the electric field for microelectrophoresis to take place.

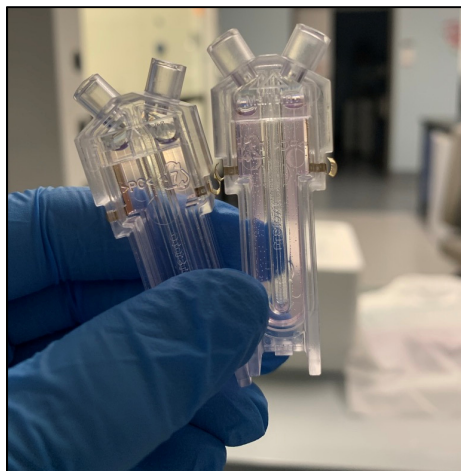


Figure 2.10 Capillary cells used for microelectrophoresis (DTS1070, Malvern Panalytical)

2.2.3 Concentration of particles

The concentration of liposomes is calculated via Nano Tracking Analysis (NTA). It is a particle-by-particle analysis that uses the diffusion equation, also known as Stokes Einstein equation, shown below to evaluate the mean size of nanoparticles and their concentration. The NTA carries out a number-based measurement and the optimal range of concentration for an accurate measurement is between 10^8 to 10^{12} particles per mL. The diffusion coefficient is described as follows by the Stokes Einstein equation (Rangamani et Iyengar, 2007):

$$D = \frac{k_B T}{6\pi\eta R_0} \quad (2.12)$$

Where k_B is the Boltzman constant, T is the temperature, η is the solvent's viscosity and R_0 the nanoparticle radius. The NTA obtains the diffusion coefficient by tracking each particle overtime and provides an accurate measurement of a sample of the population at study. The NanoSight NS3000 from Malvern Panalytical has been used throughout this work.

While this technique is particularly precise for size measurements of the liposomes, we have decided to focus on the information provided by the intensity-based measurements of the DLS to characterize our samples. The information provided by the NTA is taken into account and compared to the DLS results.

2.3 Statistical tests and approach

The statistical approach used to model the Zeta Potential and Z-average values of liposomes is based on a Design of Experiment approach. Moreover, a collection of tests involving P-value, F-value, and analysis of variance (ANOVA) tests have been used to comprehend the data presented.

2.3.1 Design of Experiment (DoE)

The Design of Experiment (DoE) approach explores a particular experimental space of the variables at study. In the case of liposome production, the variables that ultimately influence the resulting liposomes are: the total flow rate (TFR, ml/h), flow rate ratio (FRR) and lipid composition. They are the independent factors, the combinations of different FRRs, TFRs and lipid compositions are virtually infinite, it is therefore necessary to establish a limited experimental space. DoE provides the framework to create a design that will span the desired experimental space and build a subsequent regression model that will relate the independent factors to the responses. In the case of liposome production, the responses are their hydrodynamic diameter (Z-average), the PDI and the Zeta Potential.

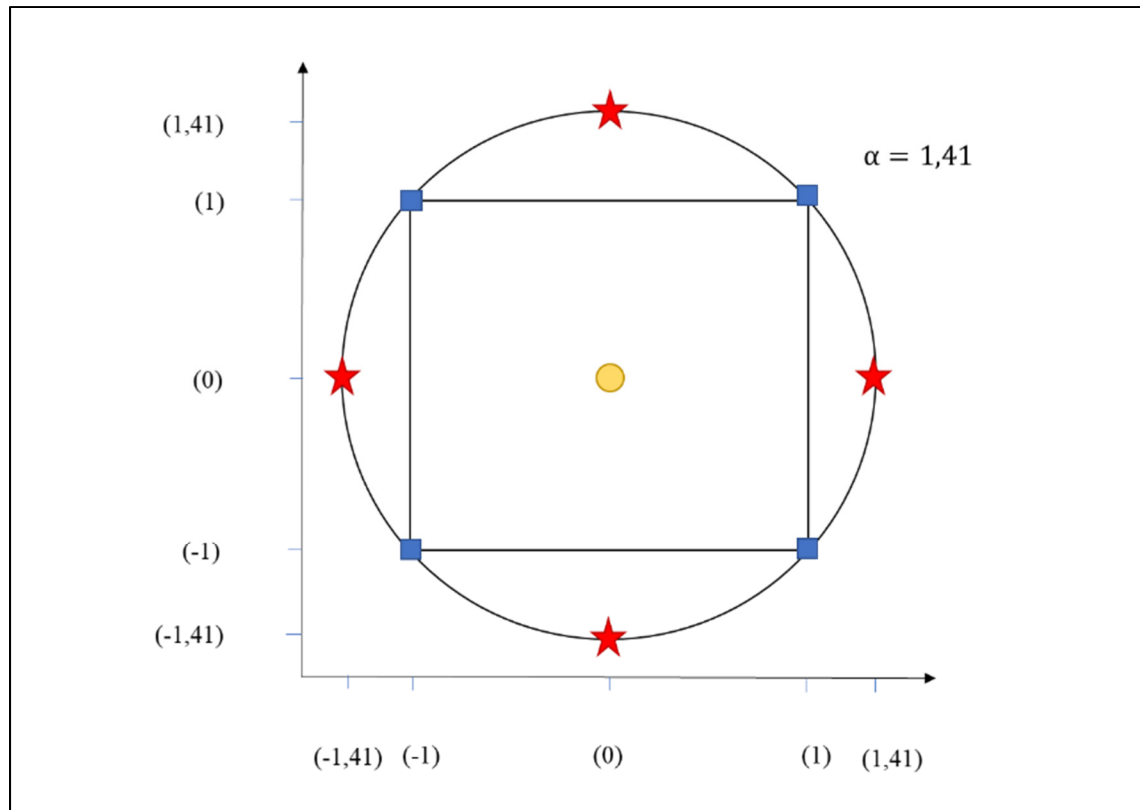


Figure 2.11 CCCR design. All the experimental points are at the same distance from the center point. Axial (red stars) and cubic (blue squares) points have been repeated three times and the central point (yellow circle) has been repeated five times

The chosen design depicted in Figure 2.11 is a circumscribed central composite design that is rotatable, meaning that all the experimental points are placed at the same distance from the center point. Figure 2.11 depicts a two-variable design but this approach has been used with three variables as well. The axes are defined by the independent variables and the axial, cubic and central points establish the combinations of factors to use when producing the liposomes.

2.3.2 *P*-value

The *p*-value comes from the student's *t*-test, which is a hypothesis test statistic. A *p*-value below the threshold α will reject the presented null hypothesis. The α marks the significance level and is set by the researcher, commonly at $\alpha=0.05$ (not to be mistaken with the DoE radius, α), see Figure 2.12 (Thisted, 1998).

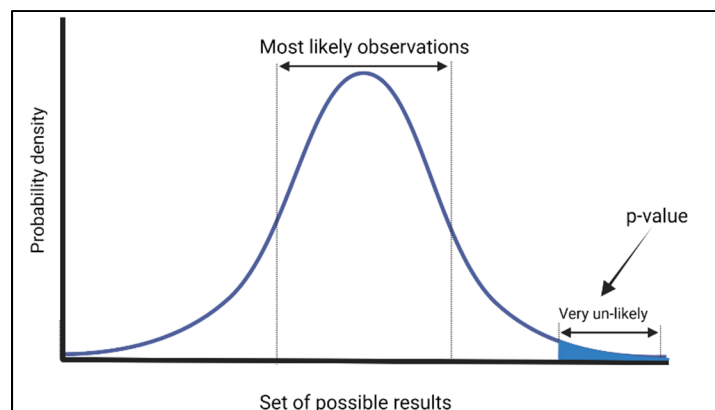


Figure 2.12 Graphical explanation of the p -value

The null hypothesis will state that there is no relationship between the two variables at study. For example, to study the influence of the Total Flow Rate (TFR, ml/h) on the size of the liposomes, a p -value below the threshold of 0.05 will allow us to conclude that the TFR has a significant impact on the size response of liposomes, meaning that changing the TFR will change the size. Vice versa, a p -value above 0.05 will indicate that there is no relationship between the variables.

2.3.3 Analysis of variance

The analysis of variance, also known as ANOVA test, studies specifically the difference between the means of two or more groups. Having a different mean will establish that the groups at study are significantly different. The yield of the ANOVA test are the F -value and the p -value. The greater the F -value, the more significant the difference between the means and vice versa with the p -value: the smaller the p -value, the more significant is the difference.

2.4 Cell culture

Cells were cultured to test the uptake of the produced liposomes in several experiments. Immortalized Human Hepatocytes (IHH) were gifted by Dr Peter Metrakos (McGill University) and highly transfectable human embryonic kidney 293 (HEK293) cells were

purchased (CRL-1573, American Type Culture Collection). Both cell lines were cultured until they reached 90% confluency with Dulbecco's Modified Eagle media (DMEM) supplemented with 1% Penicillin-Streptomycin antibiotics and 10% Fetal Bovine Serum (FBS). BJ's fibroblasts were purchased (CRL-2522, American Type Culture Collection) as well as MP41 Uveal Melanoma cancer cells (CRL-3297, American Type Culture Collection) and expanded in Roswell Park Memorial Institute media (RPMI 1640) supplemented with 10% Fetus Bovine Serum, 0.1% 10 U/mL penicillin and 10 µg/mL streptomycin, 4 mM L-glutamine and 10 µg/mL insulin, 1 mM Sodium Pyruvate. All the media components were purchased from Corning.

2.5 Extracellular Vesicle's isolation

Extracellular vesicles (EVs) are secreted by both healthy and cancerous cells and can be collected in the supernatant when culturing cells. They must be subsequently isolated using a series of ultracentrifugation steps.

Cells were grown in T75 flasks until 90% confluency was reached, then the conditioned media was replaced by medium containing EV-depleted Fetal Bovine Serum (FBS). After incubating cells for 24h with this new media, they are collected in 50ml tubes and centrifugated for 10 minutes at 500g to remove all cell debris and apoptotic bodies. The collected supernatant is centrifugated at 2000g for 20min at 4°C and the supernatant is then filtered with 0.22 µm filters and transferred to a 26mL ultracentrifuge tube (Beckman Coulter) to be centrifuged at 16,500g for 20 minutes at 4°C. The supernatant is then ultracentrifuged at 120000g (40000 rpm) for 70 minutes at 4°C using 70 Ti rotor in Optima XE ultracentrifuge machine (Beckman Coulter) to pelletize the EVs. The pellet is then resuspended in 20mL of PBS. The EVs are washed again at 120000g (40000rpm) for 70 minutes at 4°C and the pellet is collected for further characterization or stored at -80°C until use.

2.6 Uptake experiments

A series of uptake experiments were carried to evaluate how the Zeta Potential and size of liposomes affect the behavior of cells. It was evaluated according to the cellular uptake, which is a cellular process through which cells absorb different molecules in their environment. The liposomes produced were exposed to Immortalized Human Hepatocytes (HH) and fibroblast (BJs) cells. After seeding the cells for 24 hours, a certain number of liposomes was injected in the cell media. The cells were stopped from growing and fixed using paraformaldehyde and then observed under Laser Confocal Scanning Microscopy (LCSM) and further analyzed via flow cytometry to measure the uptake of liposomes.

2.6.1 Confocal Microscopy

This high-resolution optical imaging technique allows to see the cells as well as their different organelles and the liposomes. The confocal microscope used is the LSM Zeiss 900. The cells' nuclei and the liposomes are dyed using NucBlue™ (R37606, ThermoFisher) and the red dye DilC₁₈(3) (D282, ThermoFisher) respectively. A laser (red, green, or blue depending on the dye used) scans the sample at study. As illustrated in Figure 2.13, the laser source is used to stimulate the dyes and the emitted fluorescent signal dyes is received through the pinhole aperture of the microscope. This pin hole allows for the digital camera to retrieve the images of one focal place at the time. The signal is converted to an analog electrical signal by the photomultiplier. An analog-to-digital (A/D) converter yields the digital information that can be examined on the software. Each image is taken separately depending on the channel used and then superposed to see the full picture.

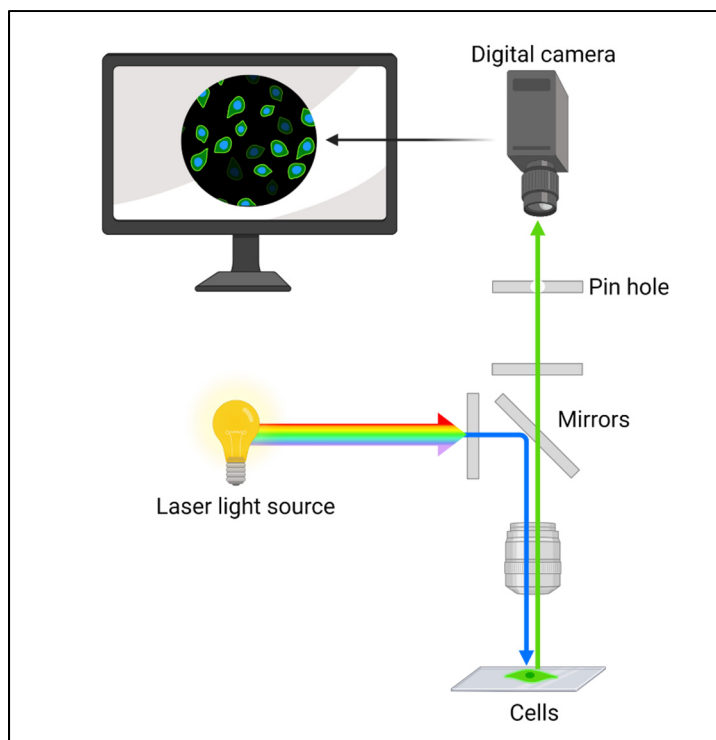


Figure 2.13 Confocal microscopy simplified scheme

2.6.2 Flow cytometry

Using the BD LSRFortessa™, we were able to count the liposomes successfully absorbed by the cells. After incubating the dyed liposomes and cells for 24 hours, the cells were washed to remove the liposomes that were not absorbed and fixed using formaldehyde. The nucleus of the cells was dyed using NucBlue. Then, cells containing liposomes were passed through the fluidic system of the BD LSRFortessa™ that exposed each sample to a laser and counted the events detected by forward and side scattering. As depicted in Figure 2.14, the scattered light is collected by a detection system and converted to a digital signal that is sent to the computer for further analysis. A single sample containing different dyes (NucBlue for the nucleus of the cells and DiIC18(3) for the liposomes) can be analyzed and the light scattered by these fluorophores can be calculated to evaluate the uptake of liposomes (identified as red) vs the presence of cells (identified via the blue dye) (Salvati et al., 2018).

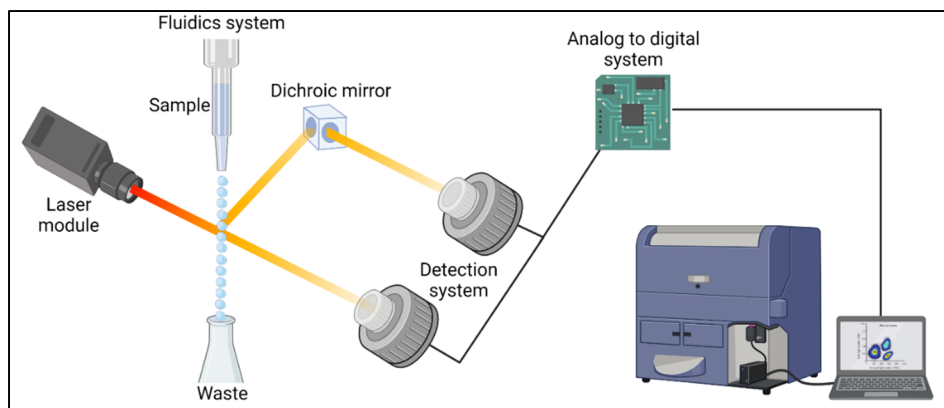


Figure 2.14 Simple schematics of flow cytometry

2.7 Conclusion

The techniques involved in the approach to design liposomes that mimic the hydrodynamic diameter (Z-average) and surface charge (Zeta Potential) of extracellular vesicles have been described. The following figure summarizes the steps involved in this approach.

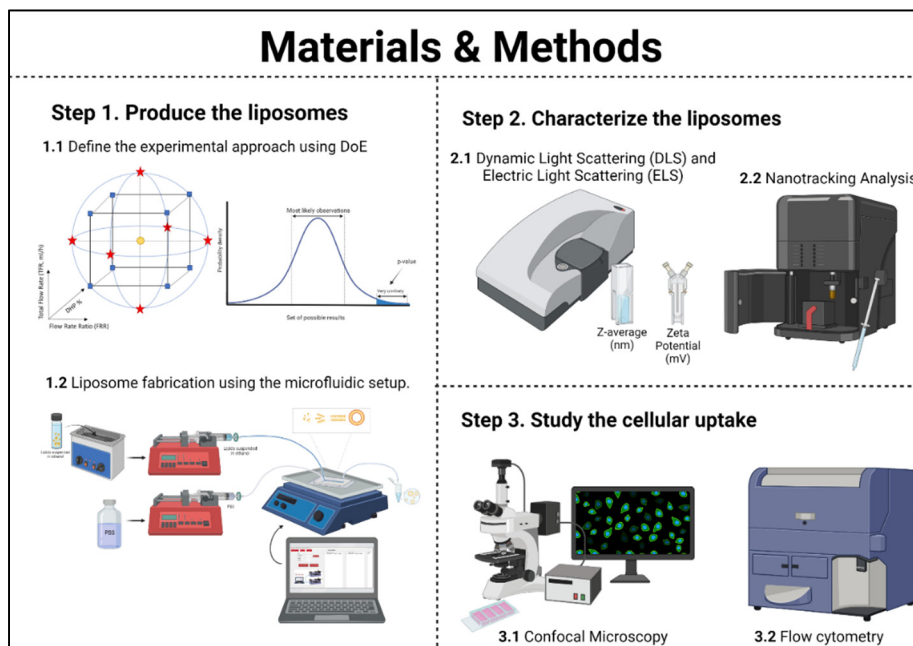


Figure 2.15 Materials and methods summary

CHAPTER 3

FABRICATION OF ANIONIC LIPOSOMES: RESULTS AND DISCUSSION

This chapter will explore the different experiments carried out to build a regression equation that allows to produce tailored liposomes in terms of size and Zeta Potential. Table 3.1 summarizes the steps followed towards completion of this objective.

Table 3.1 Objectives, Strategies and Factors at play of anionic liposomes' production

Objective	Strategy	Factors
Understanding which parameters affect the Zeta Potential (surface charge, mV)	Study the effect of DHP on liposomes	DHP%
Understanding which parameters affect the Z-average (diameter, nm)	Two-factor Response Surface Model	TFR FRR
Understanding which parameters affect both Z-average & Zeta Potential	Threefactor Response Surface Model	TFR FRR DHP%

Anionic liposomes are characterized by their negative zeta potential that usually indicates the presence of a lipid with a net negative charge. Throughout this work, anionic liposomes have been made using 1,2-dimyristoyl-sn-glycero-3-phosphocholine (DMPC), Cholesterol (CHOL) and Dihexadecyl Phosphate (DHP) in varying concentrations, but the DHP% has been used a factor in our experimental approach (DMPC% remained constant while CHOL% is reduced to accommodate the DHP%). The goal being to modulate the physicochemical parameters of liposomes, it was first demonstrated that DHP percentage (DHP%) has a considerable effect on the Zeta Potential of liposomes. The DHP molar ratio progressively increased, at the expense of the CHOL ratio%, which decreased from 50% to 40%. Once it was clear that the Zeta Potential can be controlled by the DHP%, a two-factor Circumscribed Central Composite Design was carried out to explore the effect of Total Flow Rate (TFR, ml/h) and Flow Rate Ratio (FRR) on the size of the liposomes. Finally, a third model, this time focused on three-factor Response Surface Methodology involving FRR, TFR and DHP% combined all three

factors to effectively control both the size and Zeta Potential of liposomes. Finally, the model was dialysed to circumvent technical challenges, which yielded a new set of samples and therefore a new three-factor response surface model. This statistical approach will be thoroughly explained in the following sections.

3.1 Effect of DHP% on liposome's Zeta Potential (surface charge)

Liposomes were produced following the protocol indicated in Chapter 2. The lipid mixture used was DHP 0-10% molar ratio, CHOL 40-50% molar ratio and DMPC 50% molar ratio. The DHP% was progressively increased to evaluate its effect on the Zeta Potential and the size. A total of five lipid formulations were explored, ranging from 0 to 10% molar ratio of DHP. Lipids' concentration when input in the PDMS microfluidic chip was 10mM and the aqueous solvent was phosphate-buffered saline (PBS). Flow Rate Ratio (FRR) was 1 to 1 between both fluids and the Total Flow Rate (TFR) was 18ml/h. The liposomes were collected at the outlet of the microfluidic chip and diluted in deionized water to a 0.4mM concentration of lipids for further characterization using DLS. Phosphate buffered saline (PBS) was used as the polar solvent and its final concentration in the sample was 4%. Three replicates were made per lipid formulation to discard any measurement error. Figure 3.1 and Figure 3.2 showcases the change of Zeta Potential as the DHP% increases.

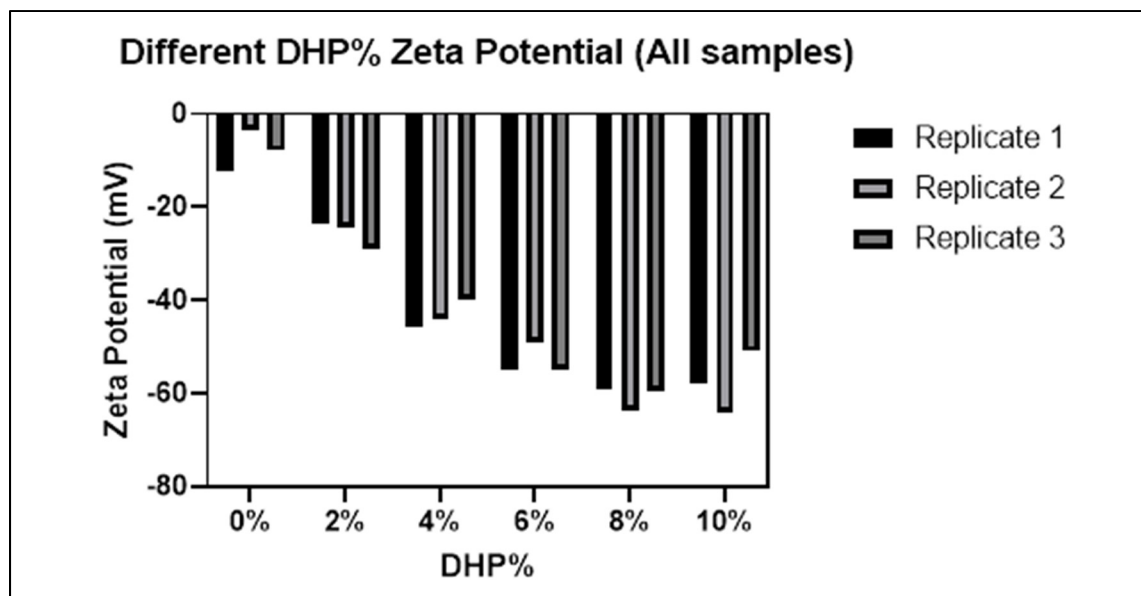


Figure 3.1 Zeta Potential measurement for all 18 samples, three replicates per different lipid composition. The percentage of DHP is increased progressively in intervals of 2% molar ratio from 0% to 10%

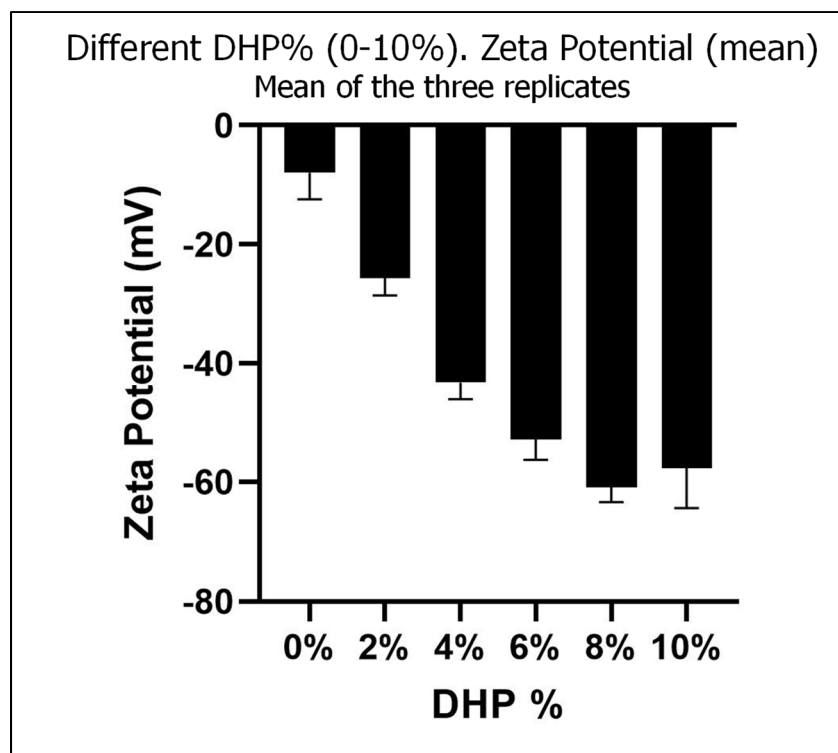


Figure 3.2 Mean Zeta Potential per increasing molar ratio of DHP, average of three replicates (n=3)

An analysis of variance showed a significant difference between the mean values of Zeta Potential obtained. The different lipid formulations, mainly DHP%, significantly affected the Zeta Potential with a $p\text{-value}=0.00008$ among the groups of replicates ($p\text{-value} < 0.05$ indicates that the factor is significant). Figure 3.1 shows each replicate while Figure 3.2 shows the mean of each group of replicates. Moreover, analysis of variance in-group, among the three repeats, yielded a $p\text{-value}=0.6532$, confirming that there were no measurement errors. Regarding the Z-average of the liposomes, the analysis of variance is inconclusive, and no correlation was observed between Z-average and DHP% (see ANNEX A).

As expected, the Zeta Potential highly depends on the formulation of liposomes. Changing the ratio of the negatively charge lipid DHP yielded a significant difference between the sample groups. Several parameters affect the Z-average and Zeta Potential of liposomes, this experiment fulfilled its role to provide a reliable factor to influence the Zeta Potential, but not the Z-average. Many experiments have proven the effect of lipid composition on Zeta Potential (Soema et al., 2015), but only for the purpose of synthesizing cationic liposomes and not with negatively charged lipids. This experiment represents the first step towards the production of tailored *anionic* liposomes.

3.2 Two-factor Response Surface Methodology

Inspired by the work of López and collaborators (López et al., 2020), a design of experiment approach was used to further study the parameters influencing the fabrication of liposomes. This model focused on evaluating how the TFR and FRR can control the Z-average of liposomes. Response Surface Methodology was used, particularly, a rotatable two-factor Circumscribed Central Composite (CCCR) design provided an experiment plan varying the TFR and FRR. For this experiment, the composition remained the same for all the samples produced: DMPC: CHOL: DHP in 50:48:2% molar ratio (based on previous experiments this ratio yields liposomes with a Zeta Potential of -25mV). The polar solvent used was phosphate buffered saline (PBS) and the samples were diluted in deionized water to obtain a final

concentration of 0.4mM. The TFR and FRR varied according to the region of best operability of the microfluidic chip, which is shown in Figure 3.3.

The Central Composite Design explores the experimental space within certain limits, provided by the axial points. The objective of this design is to obtain a quadratic model that relates the factors (TFR and FRR) to the response (Z-average and Zeta Potential). The designed experiment provides the data points to create a linear regression and fit the model to the actual response.

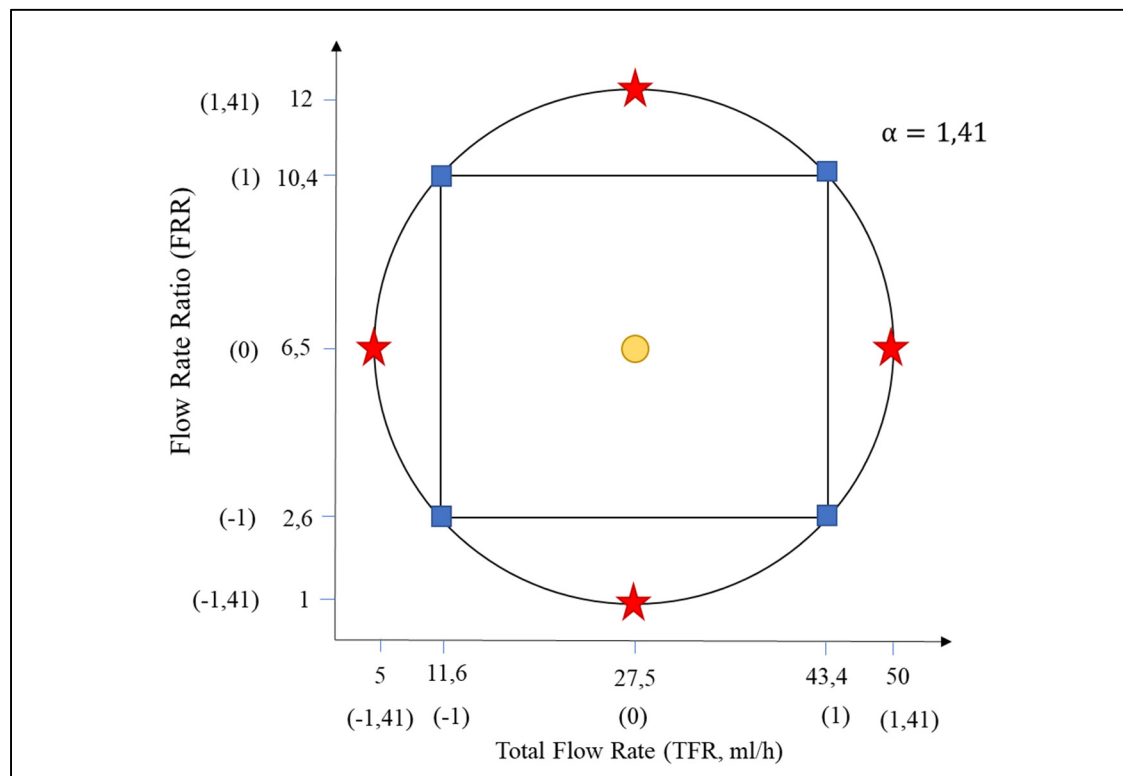


Figure 3.3 CCCR design. All the experimental points are at the same distance from the center. Axial (red stars) and cubic (blue squares) points have been repeated three times, and the central point (yellow circle) has been repeated five times.

A rotatable design ensures that all the experiment points are at the same distance from the center and can therefore predict the responses with the same accuracy. The radius was calculated according to the formula below (López et al., 2020):

$$\alpha = [2^k]^{1/4} \quad (3.1)$$

k stands for the number of factors. The radius for this model is 1,41. A total of 29 samples were produced in randomized order, three repeats per axial and cubic point and 5 repeats for the central point. Table 3.2 shows the list of samples prepared.

Table 3.2 CCCR design results for the 29 runs. The factors are FRR and TFR (with coded values in parenthesis), the responses are Z-average, PDI and Zeta Potential

EXPERIMENTAL ORDER	Factors		Responses		
	FRR	TFR (ml/h)	Z-average	PDI	Zeta Potential
1	6.50 (0)	50.00 (1,41)	109.20	0.146	-16.74
2	1.00 (-1,41)	27.50 (0)	103.70	0.110	-21.12
3	10.39 (1)	11.59 (-1)	101.00	0.107	-19.21
4	6.50 (0)	5.00 (-1,41)	101.10	0.123	-12.51
5	12.00 (1,41)	27.50 (0)	99.53	0.125	-18.97
6	2.61 (-1)	11.59 (-1)	101.50	0.113	-24.42
7	2.61 (-1)	43.41 (1)	271.40	0.165	-22.64
8	10.39 (1)	43.41 (1)	268.40	0.105	-28.29
9	6.50 (0)	27.50 (0)	266.10	0.183	-14.04
10	2.61 (-1)	11.59 (-1)	265.10	0.180	-24.46
11	10.39 (1)	11.59 (-1)	265.90	0.160	-16.75
12	6.50 (0)	50.00 (1,41)	263.30	0.139	-22.56
13	1.00 (-1,41)	27.50 (0)	156.90	0.068	-25.17
14	10.39 (1)	43.41 (1)	155.40	0.121	-9.75
15	2.61 (-1)	43.41 (1)	154.00	0.076	-18.89
16	12.00 (1,41)	27.50 (0)	155.60	0.142	-17.31
17	6.50 (0)	5.00 (-1,41)	155.20	0.093	-13.83
18	6.50 (0)	27.50 (0)	151.90	0.155	-16.6
19	6.50 (0)	27.50 (0)	194.70	0.054	-15.98
20	2.61 (-1)	11.59 (-1)	189.50	0.111	-23.04
21	10.39 (1)	11.59 (-1)	187.00	0.136	-16.49
22	6.50 (0)	50.00 (1,41)	186.30	0.097	-20.03
23	1.00 (-1,41)	27.50 (0)	186.50	0.149	-24.39
24	10.39 (1)	43.41 (1)	189.70	0.109	-14.16
25	2.61 (-1)	43.41 (1)	114.90	0.125	-12.13
26	12.00 (1,41)	27.50 (0)	113.60	0.113	-5.28
27	6.50 (0)	5.00 (-1,41)	112.30	0.127	-12.1
28	6.50 (0)	27.50 (0)	110.20	0.087	-11.1
29	6.50 (0)	27.50 (0)	111.40	0.124	-18.17

The Response Surface Model was run on Minitab® software, yielding the following results. The Z-average was shown to be highly modulable by the TFR and FRR: according to the R-squared values (in Table 3.3) the response surface model yielded from this DoE explains more than 87% of the values obtained for the Z-average, which confirms that this Z-average is dependent on the TFR and FRR. The R-squared assesses the goodness of fit of our model to the real results, the higher the R-squared the higher the control of the model over the outcome (Z-average in this case).

Table 3.3 R-squared values for the model. R-squared adjusted accounts for the runs of the experiment, while R-square predicted determines how well the model will predict the Z-average in the future

R-squared	R-squared (adjusted)	R-squared (predicted)
91,74%	90,36%	87,63%

Moreover, the p-value and F-value for each factor are depicted in the table below:

Table 3.4 P-value and F-value for the Z-average and the respective independent variables

Independent variable	Z-average (nm)	
	P-value	F-value
Flow Rate Ratio (FRR)	$< 10^{-12}$	188,59
Total Flow Rate (TFR)	$1,80 \times 10^{-6}$	39.20
FRR*FRR	$4,34 \times 10^{-6}$	34.84

The p-value is a hypothesis test used to validate the significance of the factors on the response. $1 - p\text{-value}$ is the probability that the change in the factor affects the change in response. The lower the p-value, the higher the impact of the factor on the response. In this design, it is much below the $p < 0,05$ threshold, both TFR and FRR are statistically relevant for the Z-average response.

Moreover, the F-value indicates the mean squares error. A low F-values indicates a low variability between group means and therefore a less significant difference. In this case, the F-value states that it is significant between the different groups of samples. The model described by a quadratic regression obtained is stated in equation 3.2 and illustrated as a surface plot and contour plot in Figure 3.4.

$$Z_{\text{average}} = 333,37 - 32,99 \text{ FRR} - 1,580 \text{ TFR} + 1,576 \text{ FRR}^2 \quad (3.2)$$

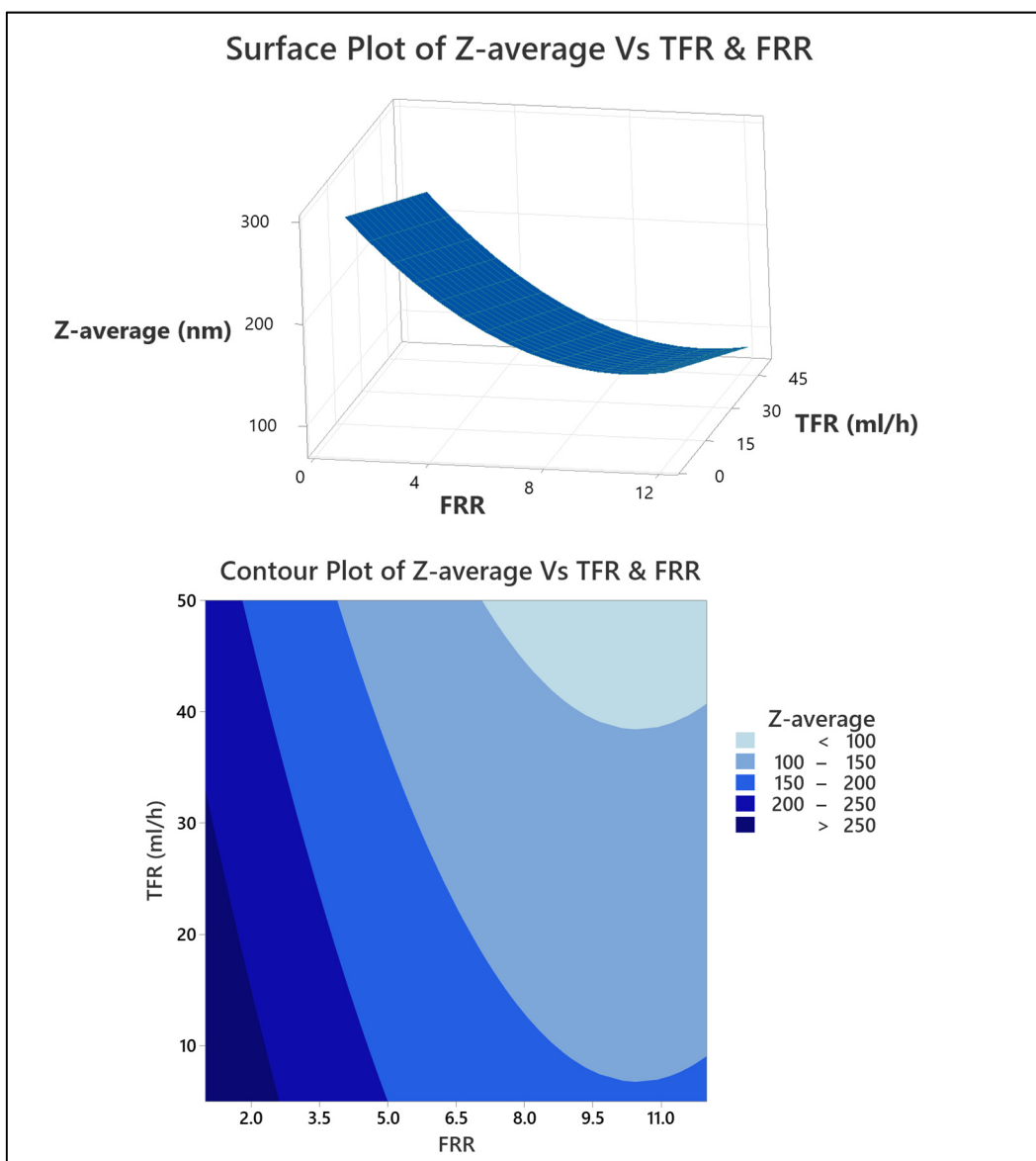


Figure 3.4 Surface plot and contour plot of the Z-average in function of TFR & FRR

Regarding the Polydispersity Index (PDI), the model failed to predict its response. The R-square predicted was 0,00% and p-value was well above 0,1 (with a very low F-values) for factors FRR and TFR. In the case of the Zeta Potential, the FRR p-value was 0,018 but R-squared was 32,38%, R-squared adjusted was 13,94% and R-squared predicted was 0,00%. This means that, even though the Zeta Potential response can not be fully explained by this model, it was still strongly influenced by the FRR but not the TFR. In conclusion, while the two-factor CCCR model successfully described the Z-average response, it failed to map the Zeta Potential. Additional factors are therefore needed to fully describe both physicochemical parameters, this result is in accordance with previous studies (López et al., 2020).

3.3 Three-factor Response Surface Methodology

Moving to a 3-factor design, this experiment included DHP% as a third independent variable. It was shown earlier that DHP% significantly influences the Zeta Potential of liposomes. A design of experiment approach using central composite design was employed but this time with three continuous factors: TFR, FRR and DHP%. This allowed to study the effects of these three factors combined on Zeta Potential and Z-average.

FRR, TFR and DHP% varied according to table information. A total of 47 samples were prepared, each of the six axial and eight cubic points were repeated three times, while the center point was repeated 5 times, in a randomized manner. According to formula 3.1, the radius is $\alpha = 8^{\frac{1}{4}}$

Table 3.5 Cubic and axial values of the three factors at study

Coded value	TFR (ml/h)	FRR	DHP%
-1,68	5	1	0
-1	14,12	3,23	2,03
0	27,50	6,50	5
1	40,88	9,77	7,97
1,68	50	12	10

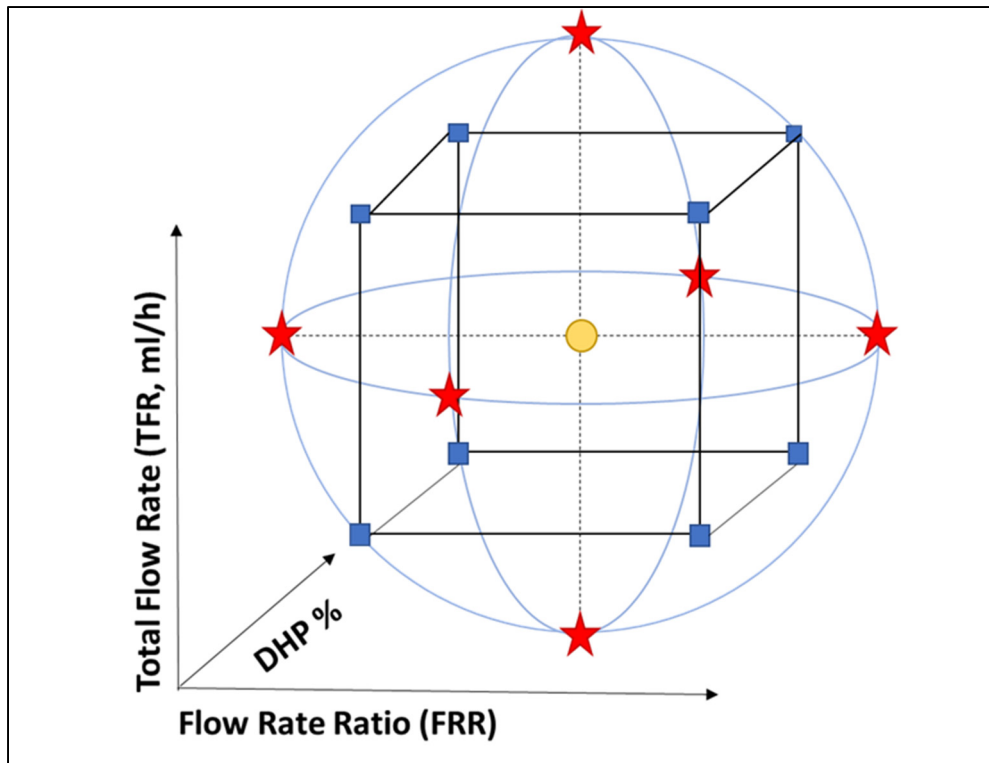


Figure 3.5 CCCR design with three factors: six axial points (red stars) and four cubic points (blue squares), repeated three times and a central point repeated five times (yellow circle)

The 47 samples were produced randomly according to the information provided by Minitab®. The table below shows 47 experimental runs required and their Zeta Potential and Z-average responses.

Table 3.6 CCCR design results for the 47 runs. The factors are FRR, TFR and DHP% (with coded values in parenthesis), the responses are Z-average, PDI and Zeta Potential

	Factors			Responses		
	FRR	TFR (ml/h)	DHP%	Z-average (nm)	PDI	Zeta Potential (Mv)
1	1.00 (-1,68)	27.50 (0)	5.00 (0)	265.43	0.15	-64.36
2	6.50 (0)	27.50 (0)	0.00 (-1,68)	151.80	0.23	-3.57
3	6.50 (0)	50.00 (1,68)	5.00 (0)	132.13	0.13	-30.84
4	9.77 (1)	14.12 (-1)	7.97 (1)	154.87	0.12	-32.71
5	12.00 (1,68)	27.50 (0)	5.00 (0)	127.32	0.12	-31.72
6	6.50 (0)	27.50 (0)	10.00 (1,68)	141.50	0.15	-45.11
7	6.50 (0)	5.00 (-1,68)	5.00 (0)	165.75	0.09	-21.48

	Factors			Responses		
	FRR	TFR (ml/h)	DHP%	Z-average (nm)	PDI	Zeta Potential (Mv)
8	9.77 (1)	40.88 (1)	7.97 (1)	127.97	0.15	-33.92
9	3.23 (-1)	14.12 (-1)	7.97 (1)	175.17	0.11	-59.52
10	6.50 (0)	27.50 (0)	5.00 (0)	151.47	0.10	-30.15
11	3.23 (-1)	40.88 (1)	7.97 (1)	159.62	0.12	-46.56
12	9.77 (1)	40.88 (1)	2.03 (-1)	92.19	0.25	-14.08
13	9.77 (1)	14.12 (-1)	2.03 (-1)	150.08	0.13	-15.95
14	3.23 (-1)	14.12 (-1)	2.03 (-1)	179.48	0.09	-21.05
15	3.23 (-1)	40.88 (1)	2.03 (-1)	151.05	0.10	-16.39
16	6.50 (0)	27.50 (0)	5.00 (0)	137.30	0.10	-30.19
17	3.23 (-1)	14.12 (-1)	7.97 (1)	151.22	0.07	-44.98
18	9.77 (1)	14.12 (-1)	7.97 (1)	152.98	0.08	-35.00
19	9.77 (1)	40.88 (1)	7.97 (1)	82.33	0.14	-31.12
20	3.23 (-1)	40.88 (1)	7.97 (1)	144.98	0.13	-43.60
21	9.77 (1)	40.88 (1)	2.03 (-1)	90.66	0.23	-14.58
22	9.77 (1)	14.12 (-1)	2.03 (-1)	134.58	0.11	-9.20
23	3.23 (-1)	14.12 (-1)	2.03 (-1)	164.03	0.10	-13.98
24	3.23 (-1)	40.88 (1)	2.03 (-1)	114.25	0.08	-24.53
25	1.00 (-1,68)	27.50 (0)	5.00 (0)	210.92	0.19	-64.73
26	6.50 (0)	27.50 (0)	0.00 (-1,68)	143.32	0.25	-5.23
27	6.50 (0)	27.50 (0)	5.00 (0)	135.80	0.11	-31.74
28	6.50 (0)	50.00 (1,68)	5.00 (0)	96.07	0.22	-31.97
29	12.00 (1,68)	27.50 (0)	5.00 (0)	124.35	0.08	-23.56
30	6.50 (0)	27.50 (0)	10.00 (1,68)	136.05	0.12	-48.52
31	6.50 (0)	5.00 (-1,68)	5.00 (0)	167.73	0.10	-25.85
32	3.23 (-1)	14.12 (-1)	7.97 (1)	156.43	0.08	-51.71
33	9.77 (1)	14.12 (-1)	7.97 (1)	134.55	0.11	-37.44
34	9.77 (1)	40.88 (1)	7.97 (1)	104.68	0.17	-46.99
35	3.23 (-1)	40.88 (1)	7.97 (1)	146.63	0.11	-36.79
36	6.50 (0)	27.50 (0)	5.00 (0)	145.83	0.11	-31.27
37	9.77 (1)	40.88 (1)	2.03 (-1)	79.55	0.40	-13.28
38	9.77 (1)	14.12 (-1)	2.03 (-1)	136.05	0.12	-15.11
39	3.23 (-1)	14.12 (-1)	2.03 (-1)	157.73	0.09	-9.55
40	3.23 (-1)	40.88 (1)	2.03 (-1)	144.17	0.10	-15.64
41	1.00 (-1,68)	27.50 (0)	5.00 (0)	259.88	0.15	-43.94
42	6.50 (0)	27.50 (0)	0.00 (-1,68)	120.95	0.08	-2.59
43	6.50 (0)	50.00 (1,68)	5.00 (0)	121.58	0.13	-26.40
44	12.00 (1,68)	27.50 (0)	5.00 (0)	119.03	0.08	-26.34
45	6.50 (0)	27.50 (0)	10.00 (1,68)	128.37	0.13	-45.31
46	6.50 (0)	5.00 (-1,68)	5.00 (0)	166.23	0.13	-35.85
47	6.50 (0)	27.50 (0)	5.00 (0)	133.38	0.10	-33.21

The following results were obtained after running the analysis on Minitab®. The R-squared for the Zeta Potential, PDI and Z-average are shown in Table 3.7.

Table 3.7 R-squared, R-squared adjusted and predicted for the 3-factor response surface model

Anionic Response Surface Model			
	R-squared	R-squared (adjusted)	R-squared (predicted)
Zeta Potential	84.44%	82.96%	79.77%
Z-average	72.81%	70.91%	65.20%
PDI	40.49%	33.23%	21.09%

The R-squared was around 80% for the Zeta Potential response, 60% for the Z-average and 20% for the PDI. The p-value and F-value of the three factors influencing these responses are shown in Table 3.8. According to the p-value, FRR and DHP% were the main factors controlling the Zeta Potential. Both FRR and TFR were influencing the Z-average, as in the two-factor model presented. Finally, the PDI was significantly influenced by the DHP% and TFR.

Table 3.8 P-value and F-value for all three factors and responses

Zeta Potential	FRR	TFR (ml/h)	DHP%
P-value	7.04×10^{-7}	0.972	10^{-12}
F-value	35.56	0,0	176.37
Z-average	FRR	TFR (ml/h)	DHP%
P-value	7.04×10^{-7}	10^{-12}	0.516
F-value	-8.30	-5.39	0.66
PDI	FRR	TFR (ml/h)	DHP%
P-value	0.139	0.02	0.038
F-value	1.51	3.30	-2.15

Since the PDI can not be accurately explained by this model (because of the low R-squared predicted), only the quadratic regression equations of the Zeta Potential and the Z-average are included:

$$\text{Zeta Potential} = -27,60 + 6,54\text{FRR} - 6,89\text{DHP}\% - 0,36\text{FRR}^2 + 0,25\text{DHP}\%^2 \quad (3.3)$$

$$\text{Z-average} = 270,5 - 24,92\text{FRR} - 1,206\text{TFR} + 2,332\text{FRR}^2 \quad (3.4)$$

Equations 3.3 and 3.4 have yielded surface and contour plots shown in Figure 3.6 and Figure 3.7. The Z-average response of this three-factor model was lower, compared to the two-factor model presented in section 3.2. The change in the DHP% greatly affected the composition of liposomes and therefore their size, but it is however not a significant factor in the Z-average response.

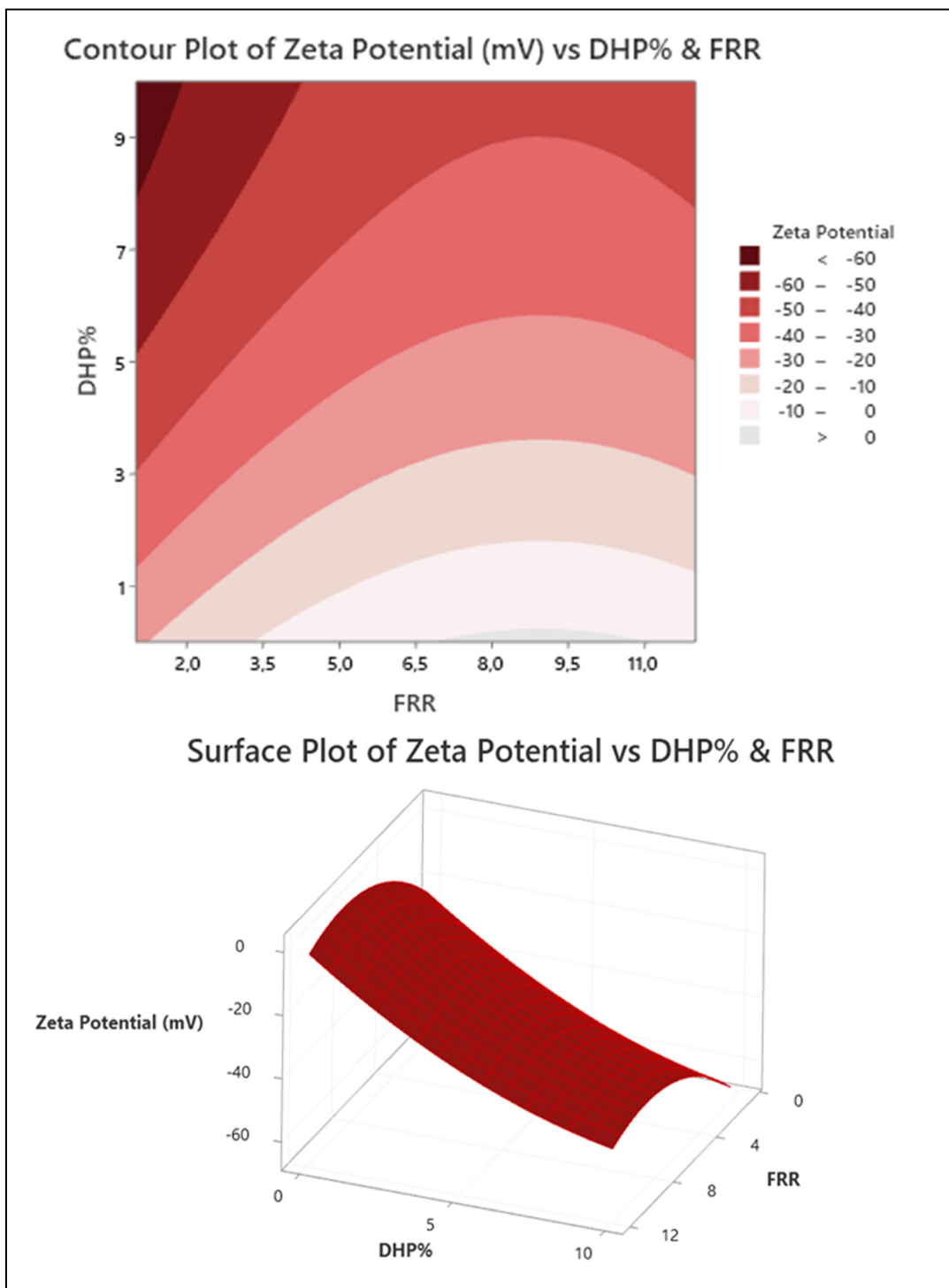


Figure 3.6 Three-factor Response Surface Model. Contour and surface plot of the Zeta Potential in function of FRR and DHP%

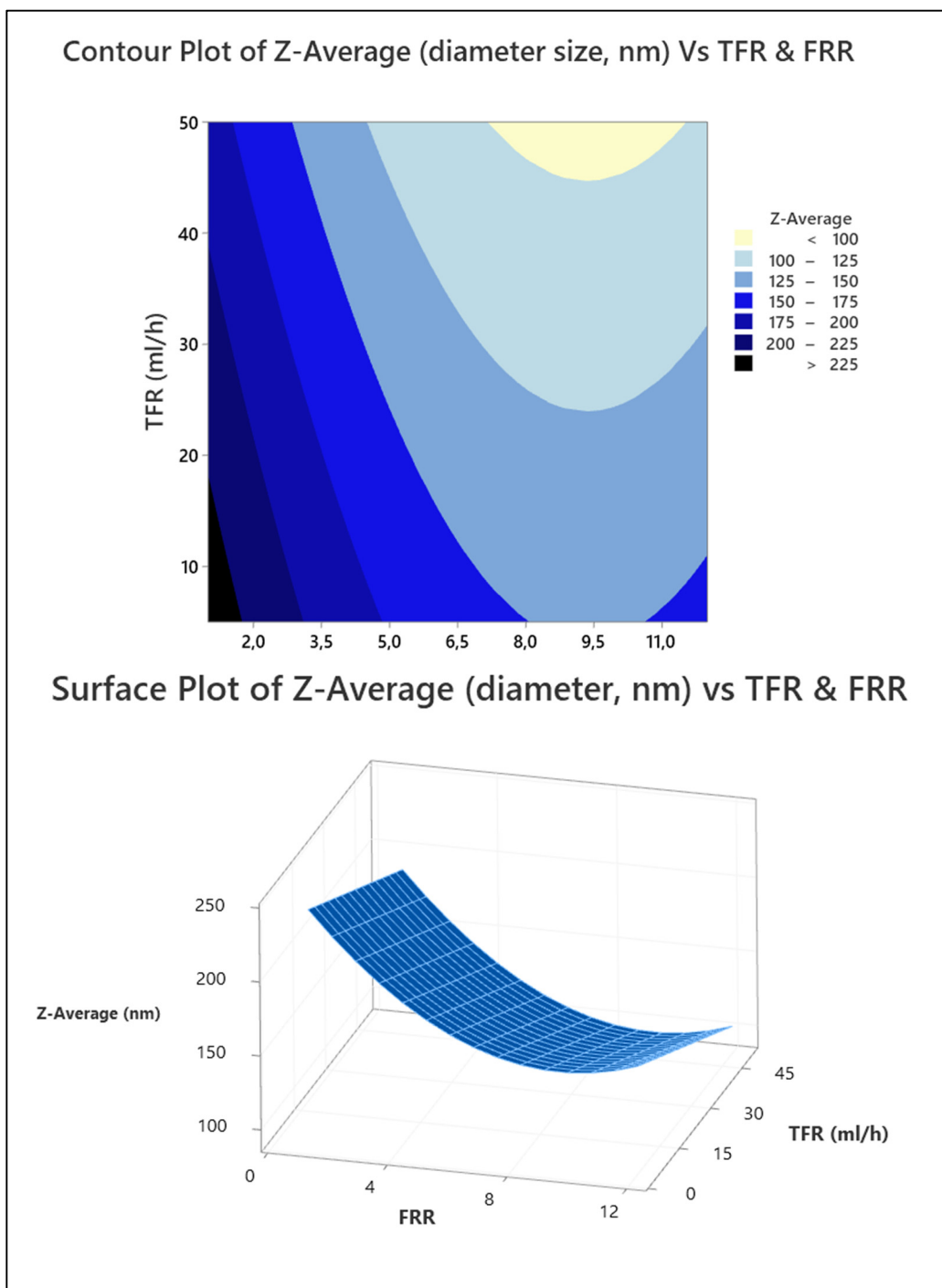


Figure 3.7 Three-factor Response Surface Model. Contour and surface plot of the Z-average response in function of FRR and TFR

3.4 Three-factor Vs Two-factor anionic model

The three-factor model presented in this section was shown to be outstanding at predicting the Zeta Potential of the liposomes, with a R^2 predicted of almost 80% and lower precision for the Z-average (R^2 predicted of 65%). Since the 2-factor model presented in section 3.2 yielded an R^2 predicted of more than 87% for the Z-average, an experiment comparing both models were carried out. The targeted physicochemical parameter was a Z-average of 150nm, which is the size of MP41 Uveal Melanoma EVs and Colorectal Cancer Cells' EVs. The factors used to target said responses are shown in Table 3.9 and the results are presented below:

Table 3.9 Factors input in the two models, respectively

<i>2-factor Model</i>		<i>3-factor Model</i>		
FRR	TFR (MI/h)	FRR	TFR (MI/h)	DHP% (molar)
5.97	23.22	12	10.93	2%

Table 3.10 2-factor model Vs 3-factor model Z-average response to targeting 150nm

<i>2-factor Model</i>				<i>3-factor Model</i>		
		Z-average (nm)	PDI			PDI
Samples	1	133,60	0,11	4	146,10	0,14
	2	135,20	0,08	5	155,80	0,12
	3	135,80	0,08	6	153,00	0,17

The percentage of DHP in both models was kept at 2%, and the results in Table 3.10 show that both models yielded monodispersed populations. Overall, the 3-factor model yielded a response closer to the targeted Z-average of 150nm, possibly because the formulation has been taken into account for the synthesis of the liposomes, versus the two-factor model which did not introduce formulation as a factor.

3.5 Effect of PBS on liposomes' Z-average and Zeta Potential

On the other hand, it was noticed that different FRR lead to different concentrations of PBS in the final sample. The PBS contains ions that significantly affect the Zeta Potential measured. The final concentration of ions is therefore dependent on the FRR employed as it dictates the ratio of organic solvent versus polar solvent. In this model, the percentage of PBS varied between 34% and 91%, meaning that the concentration of ions was not homogenous throughout the samples. The exact mechanisms behind the influence of these ions are being still debated, but a simplistic model can explain the importance of this phenomenon for our experiments: the liposomes' structure is formed in the presence of a polar solvent and the ions in the PBS salt out the formulation by increasing the electrostatic repulsion (Hyde et al., 2017) and enhancing the hydrophobicity of lipids and therefore the formation of liposomes. Without these ions altering the entropy of the solvent, the lipids tend to aggregate. This was observed by Perli and collaborators: they increase the ionic strength by increasing the concentration of ions in the polar solvent used to fabricate liposomes. They observed that higher ionic strength led to less aggregation of the lipids (Perli et al., 2019). The diagram Figure 3.8 shows the effect of low versus high ionic presence (strength).

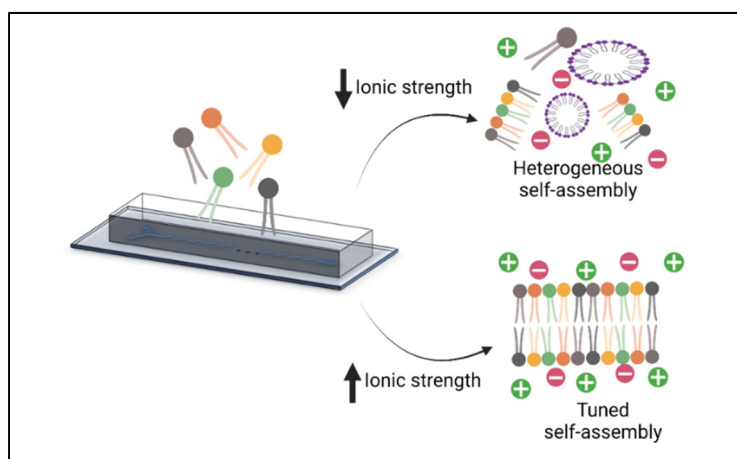


Figure 3.8 Ionic strength influences the formation of homogenous liposomes

Moreover, to evaluate the possibility of introducing a dialysis step in the fabrication protocol, a simple test was carried out to compare how it would affect the physicochemical behavior of liposomes. The results are shown in Table 3.11. A total of 8 samples of anionic, neutral, and cationic liposomes were characterized before and after dialysis. Anionic samples (1 to 6) were made of DMPC:CHOL:DHP in molar ratio of 50:48:2% or 50:46:4%, with an FRR=12 and TFR=27.5 ml/h, the goal being to target the 150nm and -25mV responses for the anionic liposomes. Neutral liposomes (sample 7) were made of CHOL:DMPC in 1:1 ratio and cationic liposomes (sample 8) were made of DSPC:DOTAP:DOPE in molar ratio of 35:40:25%. Both cationic and neutral liposomes were made with an FRR=5.97 and TFR=23.22 ml/h. All liposomes were made at 40°C using PBS as a polar solvent. The PBS% concentration was 48% for the anionic samples and 24% for the cationic and neutral liposomes. Given that FRR affect the final concentration of PBS in the sample, they were dialyzed against deionized water and 4% PBS.

Table 3.11 Results of an experiment comparing different formulations of liposomes' Z-average, PDI and Zeta Potential, before and after dialysis

Liposomes		DHP%	%PBS	Before Dialysis			After Dialysis		
				Z-average (nm)	PDI	Zeta Potential (Mv)	Z-average (nm)	PDI	Zeta Potential (Mv)
Anionic	1	2	48	99,53	0,13	-18,97	107,7	0,13	-17,86
	2	2	48	155,6	0,14	-17,31	113,5	0,08	-21,48
	3	2	48	113,6	0,11	-5,28	103,9	0,17	-17,84
	4	4	48	159,5	0,10	-7,27	144,8	0,08	-33,36
	5	4	48	161,2	0,08	-7,58	144,4	0,08	-34,6
	6	4	48	168,4	0,11	-11,17	152,8	0,17	-34,17
Neutral	7	-	24	147,2	0,18	-1,616	147,7	0,11	-5,207
Cationic	8	-	24	53,82	0,11	37,18	55,26	0,14	40,83

These results show that the presence of PBS alters both the size and the Zeta Potential of liposomes. The changes were particularly drastic for the anionic liposomes containing 2% DHP and the significant effect of dialysis was confirmed by the analysis of variance which yielded a $p\text{-value} < 10^{-6}$. Moreover, according to Cugia et al. the different ions present in PBS strongly

affect the electrophoretic mobility of liposomes (Cugia et al., 2013). They adhere to the surface of the liposomes and tend to neutralize these nanoparticles.

As explained in Chapter 2, the Zeta Potential is measured at a certain distance from the surface of the liposomes (Debye length). It is therefore important to standardize the concentration of ions to obtain reliable measurements of both Z-average and Zeta Potential.

3.6 Dialyzed three-factor Central Composite Design

Given the relevance of ion concentration in Zeta Potential measurements, the samples produced in the three-factor response surface model have been dialyzed following the instructions in section 2.1.1. This additional dialysis step replaced the liposomes' solvent containing ethanol and PBS in various concentrations by deionized water and 4% PBS solution. The goal is to standardize the presence of ions in solution in order to obtain accurate measurements of the Zeta Potential (mV). As expected, this step yielded a new response in terms of Zeta Potential and Z-average, shown in Table 3.12.

Table 3.12 Dialyzed three-factor anionic CCCR design responses:
Z-average, Zeta Potential and PDI

	Factors			Responses		
	FRR	TFR (ml/h)	DHP%	Z-average (nm)	PDI	Zeta Potential (Mv)
1	1.00 (-1,68)	27.50 (0)	5.00 (0)	231.00	0.194	-31.03
2	6.50 (0)	27.50 (0)	0.00 (-1,68)	148.00	0.238	-1.63
3	6.50 (0)	50.00 (1,68)	5.00 (0)	113.20	0.130	-29.30
4	9.77 (1)	14.12 (-1)	7.97 (1)	133.50	0.141	-44.76
5	12.00 (1,68)	27.50 (0)	5.00 (0)	114.00	0.138	-36.48
6	6.50 (0)	27.50 (0)	10.00 (1,68)	125.30	0.128	-35.11
7	6.50 (0)	5.00 (-1,68)	5.00 (0)	145.20	0.079	-32.89
8	9.77 (1)	40.88 (1)	7.97 (1)	114.30	0.172	-41.54
9	3.23 (-1)	14.12 (-1)	7.97 (1)	149.80	0.093	-44.82
10	6.50 (0)	27.50 (0)	5.00 (0)	136.00	0.930	-29.60
11	3.23 (-1)	40.88 (1)	7.97 (1)	135.90	0.114	-41.67
12	9.77 (1)	40.88 (1)	2.03 (-1)	99.50	0.286	-20.79
13	9.77 (1)	14.12 (-1)	2.03 (-1)	141.10	0.133	-18.06
14	3.23 (-1)	14.12 (-1)	2.03 (-1)	160.90	0.106	-18.64

	Factors			Responses		
	FRR	TFR (ml/h)	DHP%	Z-average (nm)	PDI	Zeta Potential (Mv)
15	3.23 (-1)	40.88 (1)	2.03 (-1)	134.20	0.091	-16.47
16	6.50 (0)	27.50 (0)	5.00 (0)	129.40	0.021	-27.46
17	3.23 (-1)	14.12 (-1)	7.97 (1)	143.90	0.090	-39.26
18	9.77 (1)	14.12 (-1)	7.97 (1)	137.30	0.073	-44.48
19	9.77 (1)	40.88 (1)	7.97 (1)	80.63	0.078	-50.78
20	3.23 (-1)	40.88 (1)	7.97 (1)	128.50	0.101	-34.10
21	9.77 (1)	40.88 (1)	2.03 (-1)	105.80	0.291	-34.11
22	9.77 (1)	14.12 (-1)	2.03 (-1)	134.20	0.141	-19.40
23	3.23 (-1)	14.12 (-1)	2.03 (-1)	148.20	0.102	-15.96
24	3.23 (-1)	40.88 (1)	2.03 (-1)	120.70	0.088	-9.60
25	1.00 (-1,68)	27.50 (0)	5.00 (0)	199.40	0.227	-35.42
26	6.50 (0)	27.50 (0)	0.00 (-1,68)	153.80	0.307	-2.74
27	6.50 (0)	27.50 (0)	5.00 (0)	124.70	0.099	-32.21
28	6.50 (0)	50.00 (1,68)	5.00 (0)	89.55	0.195	-39.53
29	12.00 (1,68)	27.50 (0)	5.00 (0)	121.50	0.064	-32.64
30	6.50 (0)	27.50 (0)	10.00 (1,68)	127.40	0.091	-46.45
31	6.50 (0)	5.00 (-1,68)	5.00 (0)	150.50	0.135	-35.87
32	3.23 (-1)	14.12 (-1)	7.97 (1)	143.80	0.097	-43.13
33	9.77 (1)	14.12 (-1)	7.97 (1)	128.60	0.119	-51.15
34	9.77 (1)	40.88 (1)	7.97 (1)	100.50	0.144	-43.91
35	3.23 (-1)	40.88 (1)	7.97 (1)	123.90	0.085	-37.03
36	6.50 (0)	27.50 (0)	5.00 (0)	128.20	0.101	-33.02
37	9.77 (1)	40.88 (1)	2.03 (-1)	66.11	0.254	-18.28
38	9.77 (1)	14.12 (-1)	2.03 (-1)	130.90	0.121	-12.38
39	3.23 (-1)	14.12 (-1)	2.03 (-1)	149.20	0.114	-11.62
40	3.23 (-1)	40.88 (1)	2.03 (-1)	135.00	0.112	-12.75
41	1.00 (-1,68)	27.50 (0)	5.00 (0)	234.60	0.219	-28.95
42	6.50 (0)	27.50 (0)	0.00 (-1,68)	120.90	0.152	1.47
43	6.50 (0)	50.00 (1,68)	5.00 (0)	116.40	0.159	-22.51
44	12.00 (1,68)	27.50 (0)	5.00 (0)	114.30	0.087	-37.30
45	6.50 (0)	27.50 (0)	10.00 (1,68)	123.40	0.112	-41.60
46	6.50 (0)	5.00 (-1,68)	5.00 (0)	148.70	0.111	-34.59
47	6.50 (0)	27.50 (0)	5.00 (0)	127.50	0.147	-30.41

To evaluate the significance of TFR, FRR and DHP % for each response, the model's p-value and F-value were again examined but only for Zeta Potential and Z-average. No factor was significant regarding the PDI of the samples, neither before nor after dialysis. Table 3.13 shows these parameters.

Table 3.13 P-value and F-value of Zeta Potential and Z-average responses

Zeta Potential	FRR	TFR (ml/h)	DHP%
P-value	0,002	0.422	10^{-12}
F-value	10,97	0,66	330,21
Z-average	FRR	TFR (ml/h)	DHP%
P-value	$2,70 \times 10^{-12}$	$0,55 \cdot 10^{-6}$	0.44
F-value	60,44	28,09	0.61

Compared to the results obtained in the non-dialyzed model, there were no significant changes: Z-average and Zeta Potential still depend on the same factors (FRR and TFR for the former and FRR and DHP% for the latter). However, regarding the F-value in the Zeta Potential response and compared to the non-dialyzed model, it was lower for the FRR (it went from 35.56 in Table 3.8 to 10.97 in Table 3.13) and higher for the DHP% (176,37 Vs 330,21). After dialysis, the difference between the group of samples became smaller when it comes to FRR, but bigger when the DHP% changes. As expected, the model has improved its R-squared for the Zeta Potential but not for the Z-average.

Table 3.14 R-squared adjusted and predicted for the dialysed responses: Zeta Potential, Z-average and PDI

Anionic Response Surface Model of the Dialyzed Response			
	R-squared	R-squared (adjusted)	R-squared (predicted)
Zeta Potential	88.79%	88.01%	86.71%
Z-average	71.90%	69.94%	64.31%
PDI	17.69%	0%	0%

The regression equations for both responses are shown below:

$$\text{Dialyzed Zeta Potential} = 3.20 - 0.695 * \text{FRR} - 8.523 * \text{DHP\%} + 0.4338 * \text{DHP\%}^2 \quad (3.5)$$

$$\text{Dialyzed Z-average} = 240.5 - 21.34 * \text{FRR} - 1.034 * \text{TFR} + 1.164\text{FRR}^2 \quad (3.6)$$

For the sake of comparison, the dialyzed responses have been plotted with their non-dialyzed counterparts (in grey), presented in section 3.3, in the following surface plots:

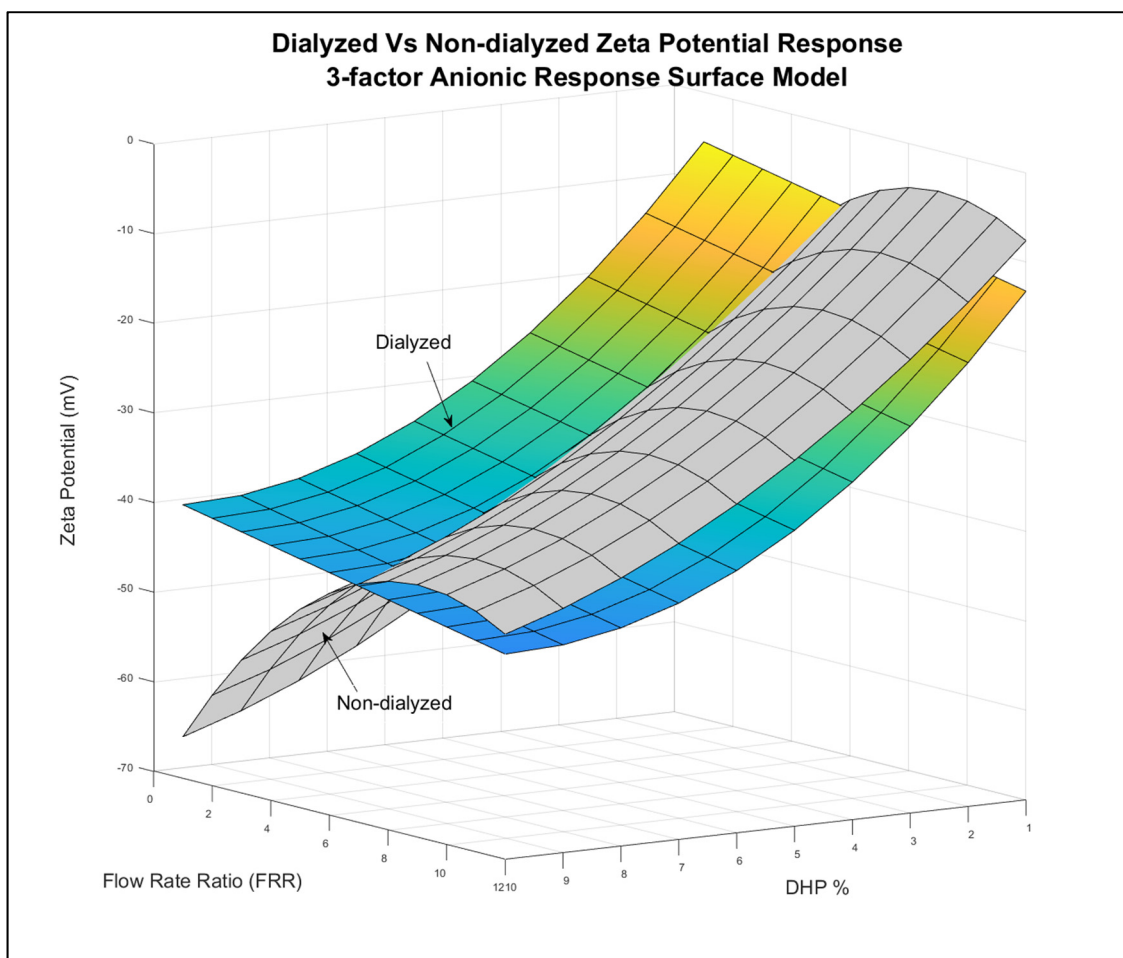


Figure 3.9 Comparison between dialyzed and non-dialyzed responses of Zeta Potential

Both the Zeta Potential and Z-average were altered by the dialysis step. Figure 3.9 showed graphically that the FRR^2 quadratic factor (present in equation 3.3 but not 3.5) was removed in the dialyzed model. As stated earlier, FRR dictates the proportion of buffer in the final sample. By lowering and standardizing the concentration of ions, it was also possible to tamper their effect on the electrophoretic mobility of the liposomes and therefore the Zeta Potential response. Moreover, the DHP% continued having a considerable effect on the Zeta Potential in the dialyzed response. Regarding the Z-average, the dialyzed model showed to yield a very similar but consistently smaller response (Figure 3.10).

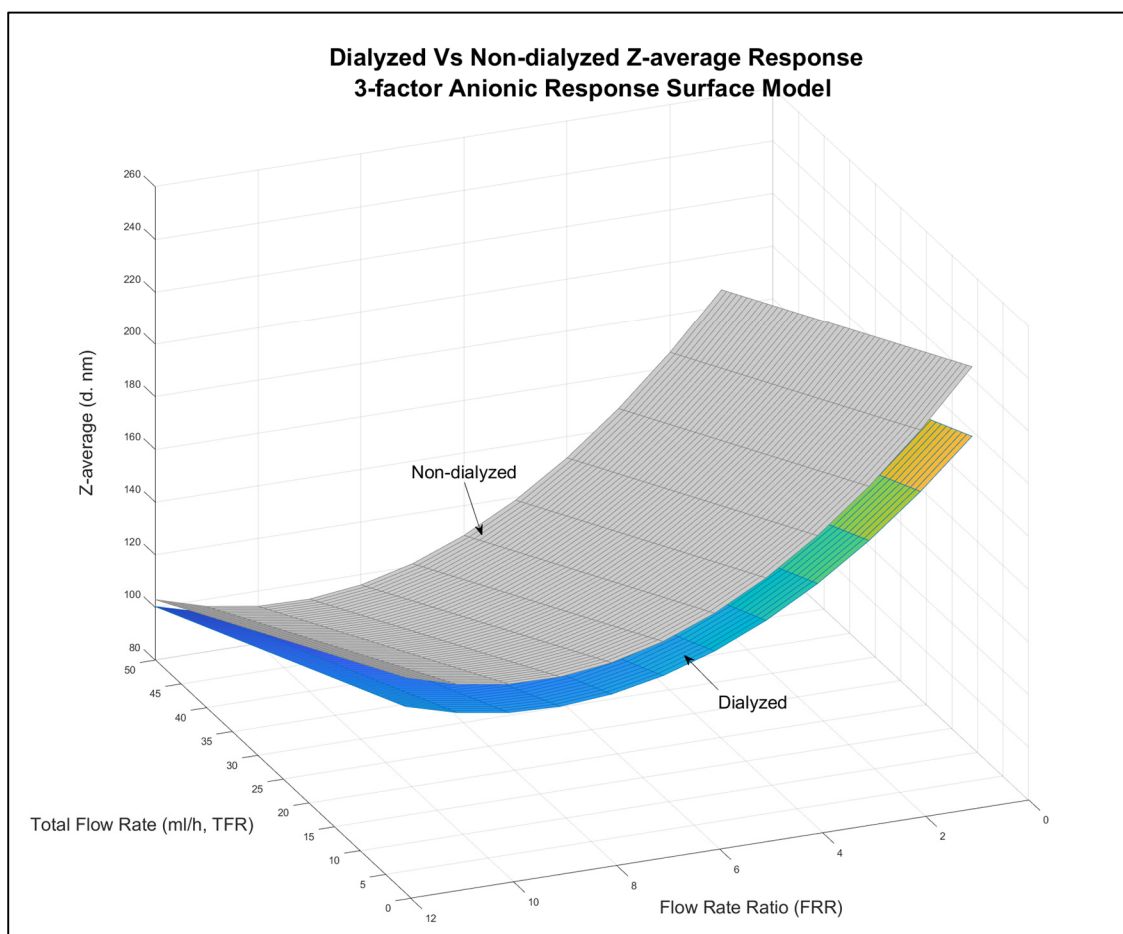


Figure 3.10 Comparison between dialyzed and non-dialyzed responses of Z-average

Conclusion

In conclusion, the models presented in this chapter have shown that FRR, TFR and DHP% have a significant impact on the Zeta Potential and Z-average. The surface charge depends on the FRR (which dictates the amount of buffer in the final sample) and DHP%, as expected. The TFR and FRR are important to predict the Z-average, as shown in both the 2-factor and 3-factor model, however, DHP% does not significantly affect the size of the liposomes. Throughout this chapter, we have focused on the development of anionic liposomes to finally yield a reliable three-factor statistical model that will allow us to produce tailored anionic liposomes. This is extremely relevant as most of the extracellular vesicles have a size and Zeta Potential that can be spanned by the dialyzed three-factor anionic response surface model. This model will be used in the following chapters to explore how these physicochemical parameters affect cellular uptake.

CHAPTER 4

FABRICATION OF CATIONIC LIPOSOMES: RESULTS AND DISCUSSION

Even though it has been proven that most of the extracellular vesicles have a negative Zeta Potential due to their surface moieties, we decided to further explore the experimental space and build a statistic model on cationic liposomes. As explained in the literature review, cationic liposomes have been used extensively for targeted drug delivery. We focused on four of the lipids described in Chapter 2: 1,2-distearoyl-sn-glycero-3-phosphocholine (DSPC), 1,2-dioleoyl-sn-glycero-3-phosphoethanolamine (DOPE), 1,2-dioleoyl-3-trimethylammonium-propane (DOTAP) and Cholesterol (CHOL).

The positively charged lipid DOTAP will be used to modulate the Zeta Potential of the cationic liposomes. The effect of DOTAP and the Zeta Potential has been widely studied in the past (Smith et al., 2017; Soema et al., 2015). A similar approach to the one presented in chapter 4 has been used:

Table 4.1 Objectives and strategies used for the synthesis of tailored cationic liposomes

Objective	Strategy	Factors
Understanding which parameters affect the Zeta Potential (surface charge, mV)	Study the effect of DOTAP on liposomes	DOTAP%
Understanding which parameters affect the Z-average (diameter, nm)	Two-factor Response Surface Model	TFR FRR
Understanding which parameters affect both Z-average & Zeta Potential	Two-factor Response Surface Model	TFR FRR DOTAP%

Since it has already been proven that the TFR and FRR cannot fully modulate the Zeta Potential of liposomes, a three-factor model was directly produced once the effect of DOTAP on different lipid compositions was studied.

4.1 Effect of DOTAP% on liposome's Zeta Potential

At first, a lipid composition of DSPC:DOPE:DOTAP in different ratios was considered. This formulation was used by Lechanteur et al. (Lechanteur et al., 2018) for RNA delivery in lung cancer cells. They found that the formulations that did not contain any Cholesterol were more efficient for the genetic cargo delivery. Therefore, the lipid formulation that was first tested was DSPC:DOPE:DOTAP in molar ratios of 50:50:0% to 50:25:25%. Four intervals of DOTAP% molar ratio were explored, from 0%, 5%, 15% and 25%, with three repeats each (Figure 4.1). The mean average (Figure 4.2).

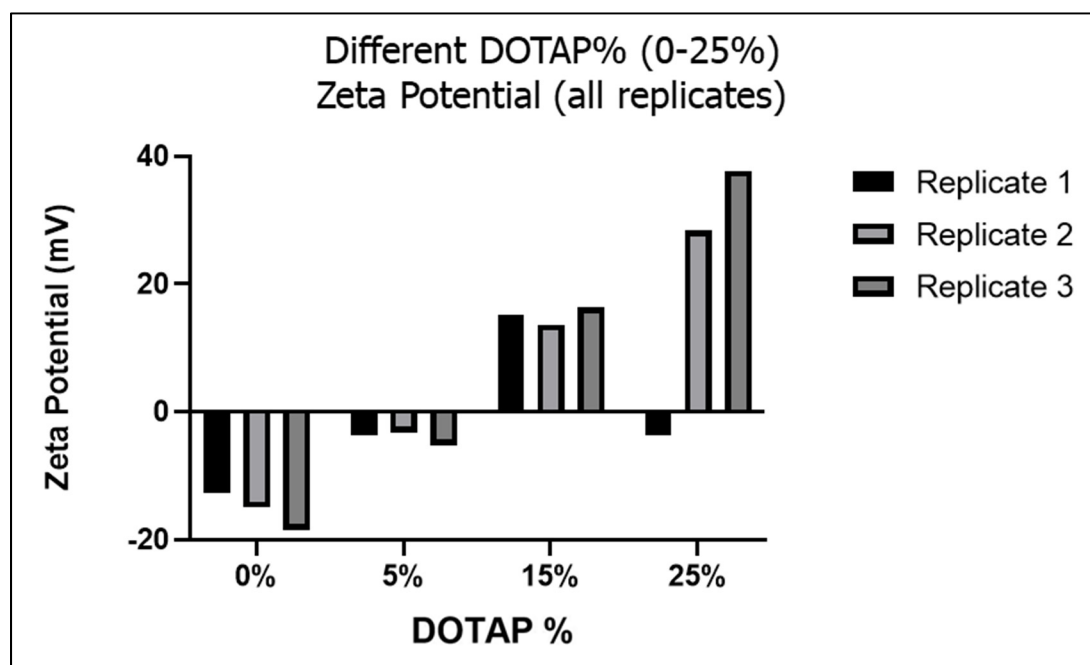


Figure 4.1 Effect of DOTAP% on the Zeta Potential of liposomes

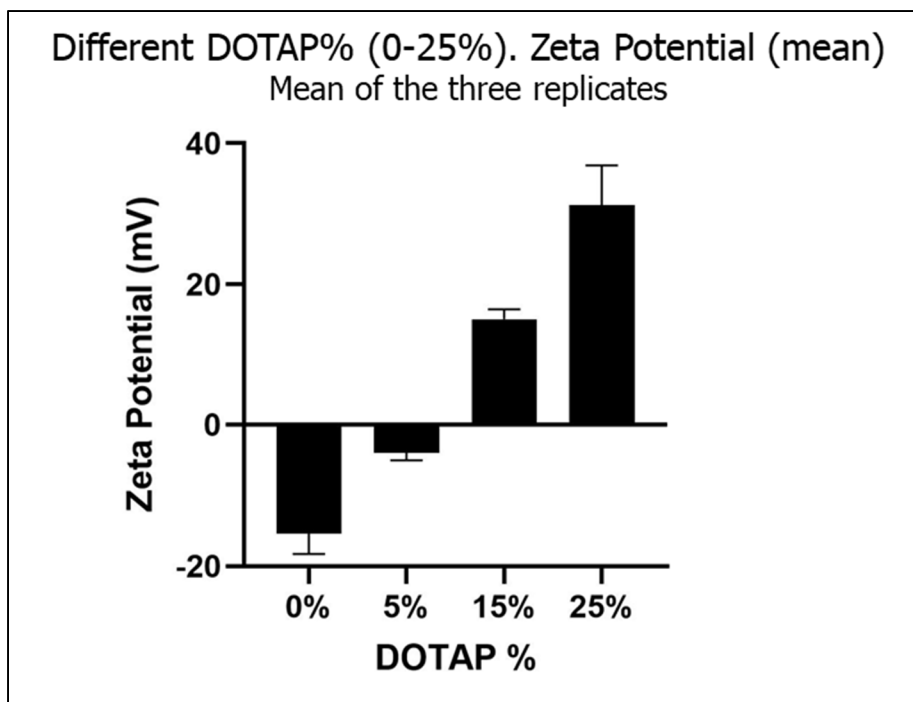


Figure 4.2 Effect of DOTAP% on the Zeta Potential of liposomes, mean average of the three replicates

An analysis of variance showed a significant difference between the means of each group, meaning that DOTAP% can modulate the Zeta Potential.

The sizes of these liposomes are presented in ANNEX A, page 89. However, the negative Zeta Potential of the 0% DOTAP samples and the precipitation issues encountered (see ANNEX I) deemed it necessary to include a second helper lipid: Cholesterol (CHOL). It has been used extensively to stabilize the lipid nanoparticles' stability in *in vivo* experiments (Cheng et Lee, 2016). The formulation used to build the cationic response surface model is therefore CHOL:DOTAP:DOPE:DSPC in molar ratios ranging from 5 to 25% DOTAP and 57.5% to 37.5% CHOL, and constant DOPE (12.5%) and DSPC (25%).

4.2 Cationic three-factor response surface model

The three-factor response surface model is based on a Rotatable Central Circumscribed Composite Design, as illustrated in Figure 3.5. The parameters are practically the same: Flow Rate Ratio (FRR), Total Flow Rate (TFR) and percentage of a charged lipid, in this case, DOTAP%. The TFR explored is between 1 and 50 ml/h and, FRR between 1 and 12 and DOTAP% between 5% and 25%, to guarantee that this model spans the positive Zeta Potential experimental space. Table 4.2 shows all 47 repetitions and the input factors. This model does not include the dialysis step.

Table 4.2 CCCR cationic design results for the 47 runs. The factors are FRR, TFR and DOTAP% (with coded values in parenthesis), the responses are Z-average, PDI and Zeta Potential

	Factors			Responses		
	FRR	TFR (ml/h)	DOTAP%	Z-average (nm)	PDI	Zeta Potential (mV)
1	6.50 (0)	25.50 (0)	25.00 (1.68)	81.580	0.064	38.240
2	12.00 (+1.68)	25.50 (0)	15.00 (0)	215.000	0.107	20.740
3	6.50 (0)	50.00 (1.68)	15.00 (0)	175.400	0.006	30.680
4	3.23 (-1)	10.93 (-1)	9.05 (-1)	251.000	0.217	22.420
5	1.00 (-1.68)	25.50 (0)	15.00 (0)	207.600	0.368	39.030
6	6.50 (0)	1.00 (-1.68)	15.00 (0)	168.100	0.234	35.110
7	6.50 (0)	25.50 (0)	5.00 (-1.68)	206.000	0.028	11.360
8	9.77 (+1)	10.93 (-1)	20.95 (1)	186.7	0.04764	27.4
9	9.77 (+1)	10.93 (-1)	9.05 (-1)	124.200	0.091	24.040
10	6.50 (0)	25.50 (0)	15.00 (0)	98.080	0.029	32.760
11	3.23 (-1)	10.93 (-1)	20.95 (1)	103.500	0.132	40.170
12	9.77 (+1)	40.07 (+1)	20.95 (1)	93.150	0.054	30.870
13	3.23 (-1)	40.07 (+1)	20.95 (1)	82.360	0.109	33.360
14	3.23 (-1)	40.07 (+1)	9.05 (-1)	122.000	0.096	26.810
15	9.77 (+1)	40.07 (+1)	9.05 (-1)	107.400	0.019	20.180
16	6.50 (0)	25.50 (0)	15.00 (0)	93.290	0.061	31.990
17	9.77 (+1)	40.07 (+1)	20.95 (1)	87.220	0.047	29.550
18	9.77 (+1)	10.93 (-1)	20.95 (1)	96.860	0.066	29.740
19	9.77 (+1)	10.93 (-1)	9.05 (-1)	129.800	0.039	18.910
20	9.77 (+1)	40.07 (+1)	9.05 (-1)	110.100	0.061	19.800
21	3.23 (-1)	10.93 (-1)	9.05 (-1)	149.000	0.104	26.790
22	3.23 (-1)	10.93 (-1)	20.95 (1)	124.300	0.249	34.190
23	3.23 (-1)	40.07 (+1)	20.95 (1)	104.200	0.081	32.200
24	3.23 (-1)	40.07 (+1)	9.05 (-1)	136.700	0.053	30.520
25	6.50 (0)	50.00 (1.68)	15.00 (0)	86.610	0.042	31.920

	Factors			Responses		
	FRR	TFR (ml/h)	DOTAP%	Z-average (nm)	PDI	Zeta Potential (mV)
26	12.00 (+1.68)	25.50 (0)	15.00 (0)	112.700	0.055	22.710
27	6.50 (0)	25.50 (0)	15.00 (0)	100.500	0.044	30.250
28	6.50 (0)	25.50 (0)	5.00 (-1.68)	145.100	0.048	16.070
29	6.50 (0)	1.00 (-1.68)	15.00 (0)	150.100	0.217	38.380
30	1.00 (-1.68)	25.50 (0)	15.00 (0)	177.400	0.164	38.850
31	6.50 (0)	25.50 (0)	25.00 (1.68)	78.420	0.111	34.350
32	9.77 (+1)	40.07 (+1)	20.95 (1)	87.320	0.153	27.050
33	9.77 (+1)	10.93 (-1)	20.95 (1)	101.100	0.078	26.130
34	9.77 (+1)	10.93 (-1)	9.05 (-1)	122.500	0.012	19.940
35	9.77 (+1)	40.07 (+1)	9.05 (-1)	126.300	0.322	22.010
36	6.50 (0)	25.50 (0)	15.00 (0)	83.220	0.052	32.750
37	3.23 (-1)	10.93 (-1)	9.05 (-1)	159.000	0.090	38.320
38	3.23 (-1)	10.93 (-1)	20.95 (1)	106.900	0.127	39.860
39	3.23 (-1)	40.07 (+1)	20.95 (1)	78.510	0.082	38.780
40	3.23 (-1)	40.07 (+1)	9.05 (-1)	144.300	0.031	27.120
41	6.50 (0)	50.00 (1.68)	15.00 (0)	93.070	0.169	35.700
42	12.00 (+1.68)	25.50 (0)	15.00 (0)	106.900	0.093	21.570
43	6.50 (0)	25.50 (0)	5.00 (-1.68)	150.800	0.002	17.120
44	6.50 (0)	1.00 (-1.68)	15.00 (0)	186.300	0.271	36.670
45	1.00 (-1.68)	25.50 (0)	15.00 (0)	294.200	0.513	37.120
46	6.50 (0)	25.50 (0)	25.00 (1.68)	88.810	0.411	41.540
47	6.50 (0)	25.50 (0)	15.00 (0)	87.370	0.106	32.590

As previously explained, the R-squared is crucial when evaluating the predictability of a model. The results obtained for this three-factor cationic model are shown in Table 4.3. While the R-squared predicted for the Zeta Potential was high (almost 80%), the Z-average is particularly low, even lower than the PDI response. This means that the statistical model will predict accurately only 10% of the Z-average responses.

Table 4.3 R-squared, adjusted and predicted for the Z-average, Zeta Potential and PDI responses

Cationic Response Surface Model			
	R-squared	R-squared (adjusted)	R-squared (predicted)
Zeta Potential	82.79%	81.59%	78.90%
Z-average	34.19%	31.20%	10.64%
PDI	41.44%	37.35%	27.22%

The factors that influence the Z-average and Zeta Potential response are listed below. FRR and DOTAP% significantly impact the Zeta Potential response, while the Z-average is only influenced by the FRR (p-value<0,05).

Table 4.4 P-value and F-value of the different factors involved in the Zeta Potential and Z-average responses

Zeta Potential	FRR	TFR (ml/h)	DOTAP%
P-value	$< 10^{-10}$	0.117	$< 10^{-10}$
F-value	102,64	2,57	101,19
Z-average	FRR	TFR (ml/h)	DOTAP%
P-value	0,005	0,098	0,136
F-value	9,01	2,87	2,32

The regression equations for each response are shown below:

$$\text{Zeta Potential} = 15.81 - 1.505\text{FRR} + 2.698\text{DOTAP\%} - 0.0625\text{DOTAP\%}^2 \quad (4.1)$$

$$\text{Z-average} = 278.5 - 46.9\text{FRR} + 3.016\text{FRR}^2 \quad (4.2)$$

The reason behind the unsatisfactory Z-average response might be related to the phase transition of the DSPC lipid (Zhao et al., 2007). As stated earlier, DSPC is a “helper” lipid that is used to stabilize the artificially produced liposomes thanks to its high melting temperature. However, it has been shown that, when combined with unsaturated cationic lipids such as DOTAP, DSPC tends to form isolated domains on the liposomes with much lower melting temperature (Koynova, Tenchov et Rapp, 1997). The technical aspects of this lipid phase transition are outside of the scope of this work. Only the Zeta Potential can be plotted against the two factors influencing it: FRR and DOTAP% (Figure 4.3)

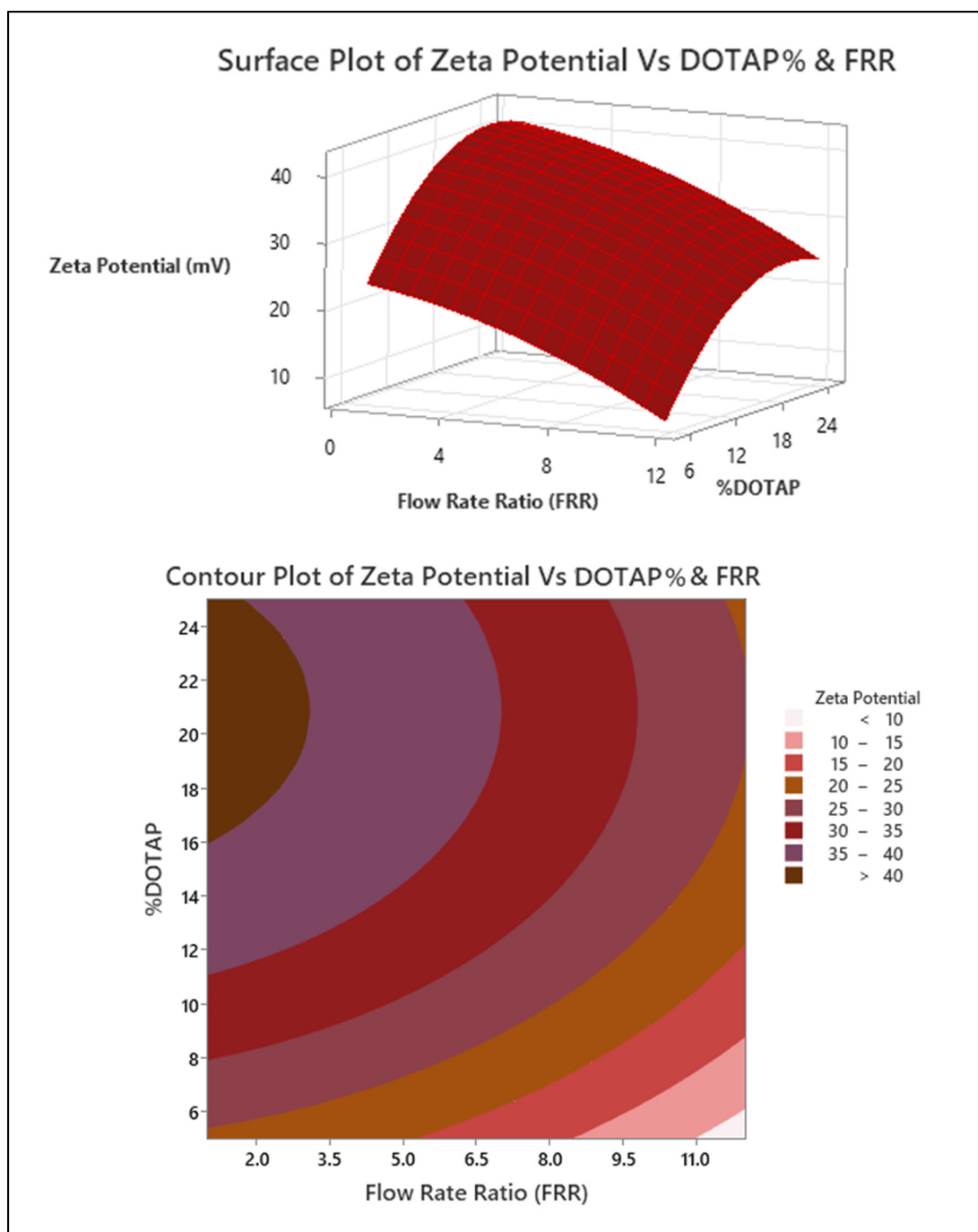


Figure 4.3 Surface plot (up) and contour plot (down) of the Zeta Potential response to the three-factor cationic model

Since Z-average only depends on FRR, neither a surface plot nor a contour plot can be drawn. This model is therefore unfit to fully predict the physicochemical parameters of liposomes. These responses could be improved by the dialysis step that yields the model presented in section 4.3.

4.3 Three-factor model dialyzed

Dialysis changes both the size and the Zeta Potential of liposomes, and therefore the response to the different factors, which are shown below:

Table 4.5 Dialyzed three-factor cationic CCCR design responses
Z-average, Zeta Potential and PDI

Factors				Responses		
	FRR	TFR (ml/h)	DOTAP%	Z-average (nm)	PDI	Zeta Potential (mV)
1	6.50 (0)	25.50 (0)	25.00 (1.68)	111.5	0.1295	41.94
2	12.00 (+1.68)	25.50 (0)	15.00 (0)	176.1	0.05871	36.23
3	6.50 (0)	50.00 (1.68)	15.00 (0)	121.8	0.046	38.44
4	3.23 (-1)	10.93 (-1)	9.05 (-1)	304.8	0.1814	29.79
5	1.00 (-1.68)	25.50 (0)	15.00 (0)	270.8	0.3953	23.67
6	6.50 (0)	1.00 (-1.68)	15.00 (0)	179	0.2191	44.63
7	6.50 (0)	25.50 (0)	5.00 (-1.68)	172	0.1048	22.36
8	9.77 (+1)	10.93 (-1)	20.95 (1)	186.7	0.04764	27.4
9	9.77 (+1)	10.93 (-1)	9.05 (-1)	151.5	0.009298	31.6
10	6.50 (0)	25.50 (0)	15.00 (0)	117.8	0.09888	40.27
11	3.23 (-1)	10.93 (-1)	20.95 (1)	126.8	0.1641	41.03
12	9.77 (+1)	40.07 (+1)	20.95 (1)	149.8	0.02072	40
13	3.23 (-1)	40.07 (+1)	20.95 (1)	96.41	0.146	39.81
14	3.23 (-1)	40.07 (+1)	9.05 (-1)	135.7	0.09007	29.17
15	9.77 (+1)	40.07 (+1)	9.05 (-1)	129.6	0.05401	38.09
16	6.50 (0)	25.50 (0)	15.00 (0)	112.7	0.1154	40.34
17	9.77 (+1)	40.07 (+1)	20.95 (1)	163.6	0.03054	44.06
18	9.77 (+1)	10.93 (-1)	20.95 (1)	146.8	0.06948	44.17
19	9.77 (+1)	10.93 (-1)	9.05 (-1)	154.6	0.01412	39.64
20	9.77 (+1)	40.07 (+1)	9.05 (-1)	137.4	0.01913	37.3
21	3.23 (-1)	10.93 (-1)	9.05 (-1)	165.4	0.09673	32.69
22	3.23 (-1)	10.93 (-1)	20.95 (1)	130.5	0.195	36.72
23	3.23 (-1)	40.07 (+1)	20.95 (1)	119.2	0.1087	34.94
24	3.23 (-1)	40.07 (+1)	9.05 (-1)	162.8	0.09715	25.22
25	6.50 (0)	50.00 (1.68)	15.00 (0)	107.4	0.02661	41.82
26	12.00 (+1.68)	25.50 (0)	15.00 (0)	124.1	0.0482	40.07
27	6.50 (0)	25.50 (0)	15.00 (0)	117	0.04125	41.8

Factors				Responses		
	FRR	TFR (ml/h)	DOTAP%	Z-average (nm)	PDI	Zeta Potential (mV)
28	6.50 (0)	25.50 (0)	5.00 (-1.68)	174.7	0.05809	22.23
29	6.50 (0)	1.00 (-1.68)	15.00 (0)	174.8	0.3371	50.81
30	1.00 (-1.68)	25.50 (0)	15.00 (0)	223.9	0.3238	27.25
31	6.50 (0)	25.50 (0)	25.00 (1.68)	137.2	0.07492	43.02
32	9.77 (+1)	40.07 (+1)	20.95 (1)	132.9	0.1608	47.84
33	9.77 (+1)	10.93 (-1)	20.95 (1)	147.8	0.08878	42.75
34	9.77 (+1)	10.93 (-1)	9.05 (-1)	147.8	0.05675	34.65
35	9.77 (+1)	40.07 (+1)	9.05 (-1)	151.3	0.2775	41.97
36	6.50 (0)	25.50 (0)	15.00 (0)	100.8	0.06318	35.26
37	3.23 (-1)	10.93 (-1)	9.05 (-1)	192.2	0.1451	30.04
38	3.23 (-1)	10.93 (-1)	20.95 (1)	129.3	0.1888	36.82
39	3.23 (-1)	40.07 (+1)	20.95 (1)	106.2	0.23	38.55
40	3.23 (-1)	40.07 (+1)	9.05 (-1)	147.7	0.09825	36.08
41	6.50 (0)	50.00 (1.68)	15.00 (0)	124.7	0.1692	49.43
42	12.00 (+1.68)	25.50 (0)	15.00 (0)	114.1	0.04908	41.5
43	6.50 (0)	25.50 (0)	5.00 (-1.68)	173.1	0.1159	27.73
44	6.50 (0)	1.00 (-1.68)	15.00 (0)	190.9	0.329	50.39
45	1.00 (-1.68)	25.50 (0)	15.00 (0)	326.2	0.4295	30.99
46	6.50 (0)	25.50 (0)	25.00 (1.68)	141.4	0.1205	50.86
47	6.50 (0)	25.50 (0)	15.00 (0)	106.3	0.07935	43.09

Analyzing the response surface model allows it to calculate the R-squared (Table 4.6), which improved slightly for the Z-average (from 10.64% to almost 37%) but was lower for the Zeta Potential (from 78,9% to 54,67%). However, the dialysis step revealed that all three factors (DOTAP%, FRR and TFR) are significant factors for the size response (whereas in section 4.2, Z-average only depended on FRR, p-value<0,05).

Table 4.6 R-squared, adjusted and predicted for the Z-average, Zeta Potential and PDI

Cationic Dialyzed Response Surface Model			
	R-squared	R-squared (adjusted)	R-squared (predicted)
Zeta Potential	63,64%	60,10%	54,67%
Z-average	54.39%	48.83%	36.53%
PDI	50.08%	41,67%	24,11%

Table 4.7 show the p-value and f-value statistical tests for both responses, and the resulting regression equations for each response (4.3 and 4.4).

Table 4.7 P-value and F-value of the responses for the dialyzed response surface model

Zeta Potential	FRR	TFR (ml/h)	DOTAP%
P-value	0,002	0.422	10^{-12}
F-value	10,97	0,66	330,21
Z-average	FRR	TFR (ml/h)	DOTAP%
P-value	0,003	0.004	0,014
F-value	10,11	9,31	6,52

$$\text{Zeta Potential} = 11.78 - 0.5\text{FRR} + 2.9\text{DOTAP\%} - 0.1(\text{FRR})^2 - 0.1\text{DOTAP\%}^2 \quad (4.3)$$

$$\text{Z-av} = 415.8 - 47.4\text{FRR} - 1.1\text{TFR} - 8.7\text{DOTAP\%} + 2.1\text{FRR}^2 + \text{FRR} * \text{DOTAP\%} \quad (4.4)$$

A surface plot and contour plot were drawn for each response. These plots graphically relate the factors and the responses. Even though the dialyzed Z-average response depends on (DOTAP%, FRR and TFR), the surface and contour plot shown in Figure 4.4 are in function of TFR and FRR. Figure 4.5 shows the contour and surface plot of the dialyzed Zeta Potential response.

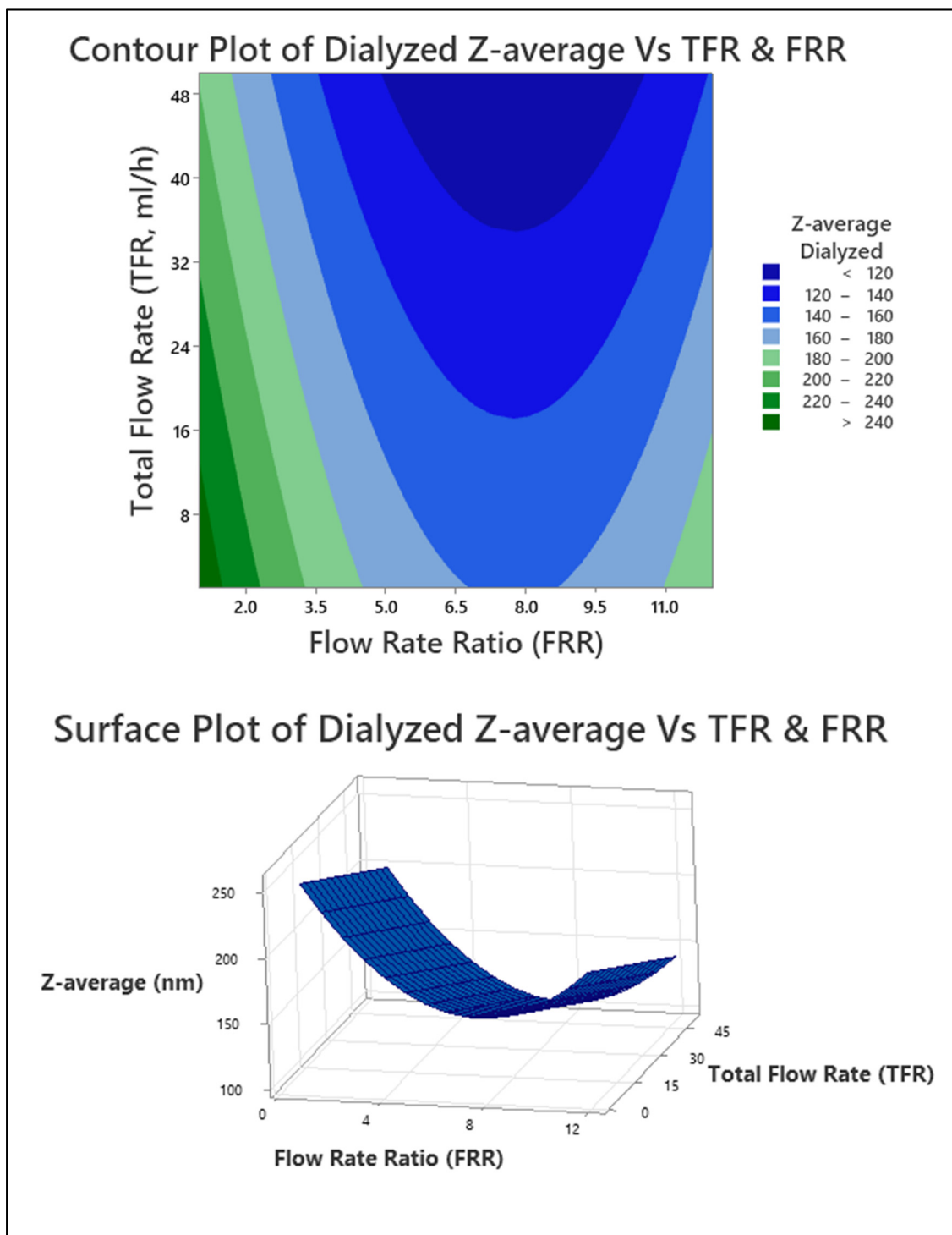


Figure 4.4 Contour and surface plot of the dialyzed Z-average response in function of FRR and TFR

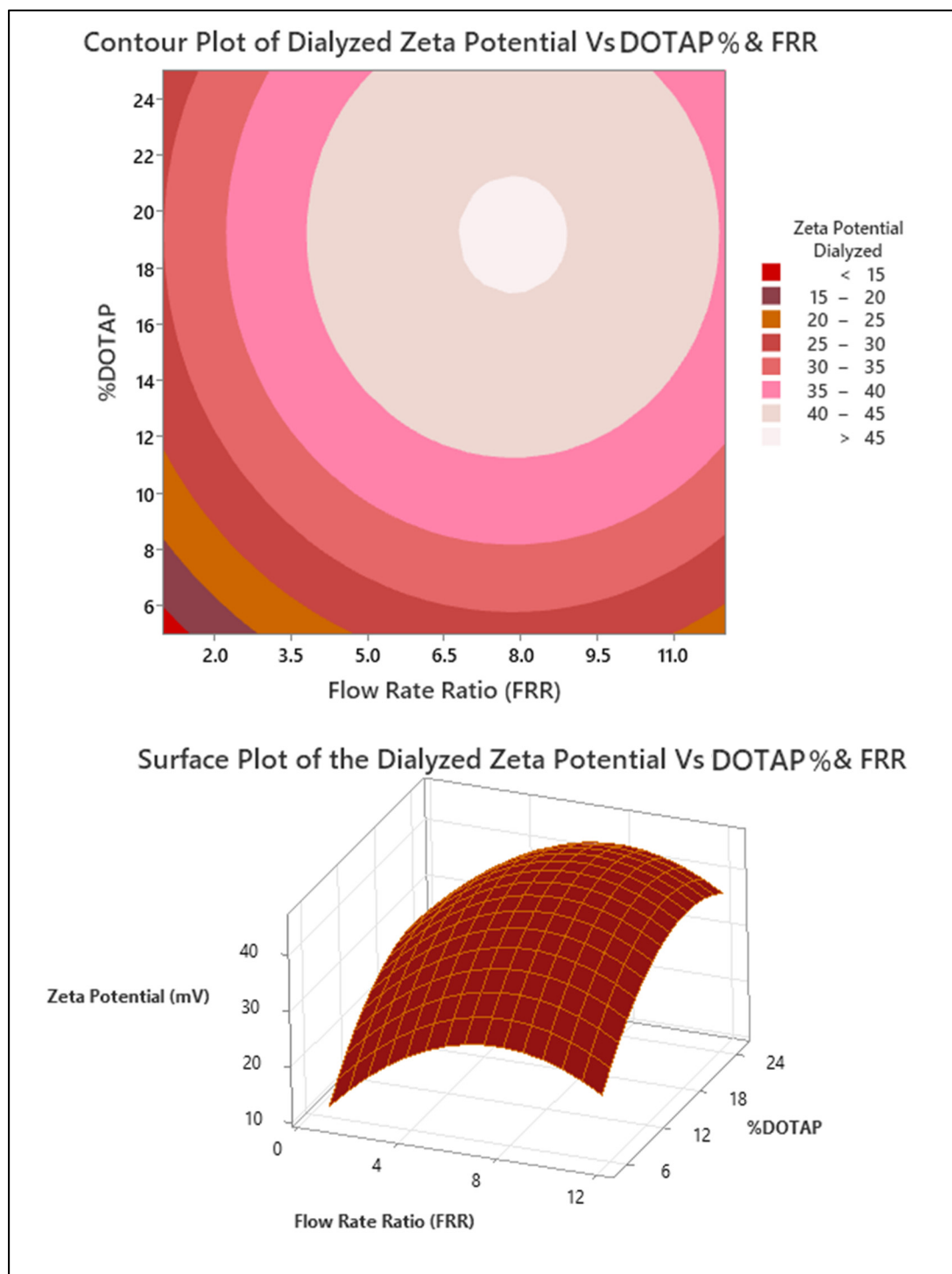


Figure 4.5 Contour and surface plot of the dialyzed Zeta Potential response in function of DOTAP% and FRR

The Zeta Potential and Z-average responses were not satisfactory, and it has been hypothesized that this might be caused by the DSPC%. Most cationic lipid formulations have fixed the DSPC% to 10% (Hou et al., 2021). DSPC% was fixed to 25 % in this formulation with the hope of developing liposomes that could be absorbed preferentially by the cells thanks to its composition. DSPC is a saturated lipid, meaning that it does not have a double bond in its hydrophobic tail. However, both DOPE (12.5%) and DOTAP (5-25%) are unsaturated lipids with a double bond in their hydrophobic tail. These differences in structures lead to different phase behaviors (Brown et Wrenn, 2013). By mixing these lipids in a microfluidic chip and using the nanoprecipitation method to fabricate liposomes, the distribution of lipids in each liposome can not be controlled. Even though most of the liposome populations presented in Table 4.2 and Table 4.5 are monodispersed (with a PDI below 0.2), it can not be confirmed that the lipids are evenly distributed, yielding an unreliable response surface model. The underlying mechanisms influencing the formation of cationic lipid membranes are out of scope. Finally, the Zeta Potential response before and after dialysis have been compared in Figure 4.6.

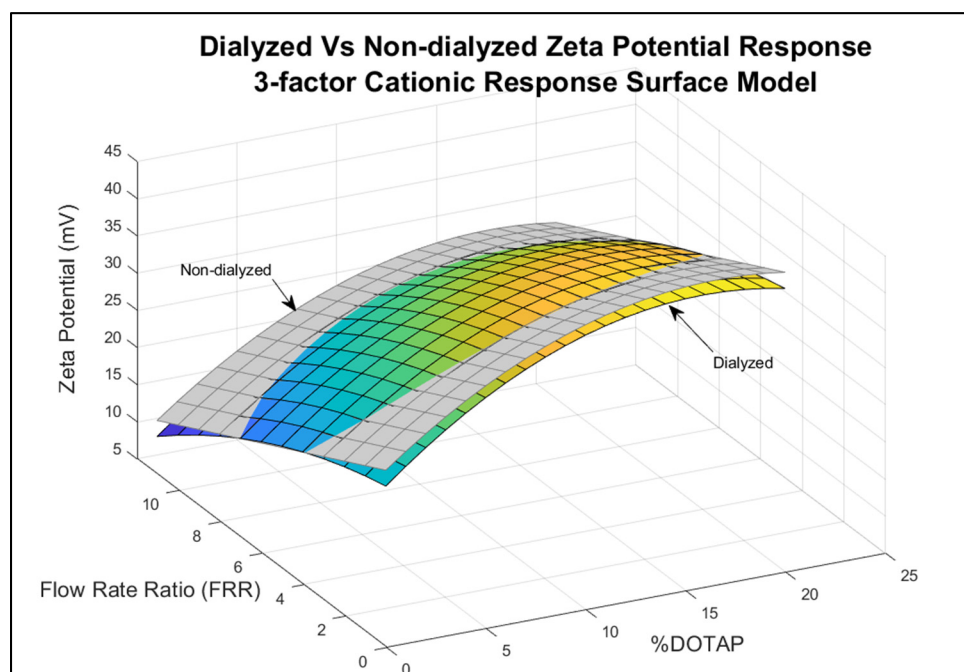


Figure 4.6 Comparison of the dialyzed and non-dialyzed response of Zeta Potential

4.4 Conclusion

The cationic three-factor response surface model using a Circumscribed Central Composite Rotatable design did not yield satisfactory results. The Zeta Potential R-squared (predicted) before and after dialysis was ~78% and ~54% respectively. For the Z-average, the R-squared predicted was below 40% in both cases. Given that the dialysis step is essential for the removal of ethanol and the homogenization of the liposomes' physicochemical parameters, the response of the cationic model was improved in the second model. This was due to the choice of lipids: a deeper investigation regarding the physicochemical properties of lipids and their different combinations must be carried out and falls out of the scope of this work. Nonetheless, it was possible to fabricate cationic liposomes of various sizes and charges to evaluate the cells responses to them.

CHAPTER 5

CELLULAR UPTAKE OF LIPOSOMES: RESULTS AND DISCUSSION

The uptake of anionic, cationic and neutral liposomes of various sizes was evaluated and the results are presented in this chapter. Thanks to the models developed in previous chapters, we were able to produce liposomes with various sizes and zeta potentials to mimic EVs for uptake measurements. In particular, the EVs collected from MP41 uveal melanoma cancer cells were isolated using the protocol described in Chapter 2 and the Zeta Potential and Z-average were measured using the Malvern Zetasizer™ DLS. After describing how liposomes can be fabricated to target specific sizes and Zeta Potentials, the specific parameters of these EVs were targeted. Since uveal melanoma spreads frequently to the liver, immortalized human hepatocytes (IHH) were exposed to EV-mimicking liposomes to evaluate their uptake. Fibroblast cells were used as a control in part of the experiments presented. This chapter starts by explaining how cells uptake liposomes, then confocal microscopy has been used to observe how liposomes are absorbed by cells and the uptake is finally evaluated using flow cytometry.

5.1 Cellular uptake mechanisms

The cellular membrane is the entry point to the cell. For successful delivery, the liposomes must be internalized by the cells and this process can happen in two forms: passive transport or active transport. The cell membrane is also made of a lipid bilayer. Passive transport does not involve any perturbation of the membrane; rather it is the movement of molecules across the concentration gradient, neutral molecules such as oxygen or carbon dioxide diffuse across the cell membrane, from the highly concentrated external medium to the low concentration medium within the cells (Foroozandeh et Aziz, 2018). Active transport, on the other hand, is used for charged or polar molecules, such as liposomes. Cells engulf and absorb them via endocytosis, as shown below:

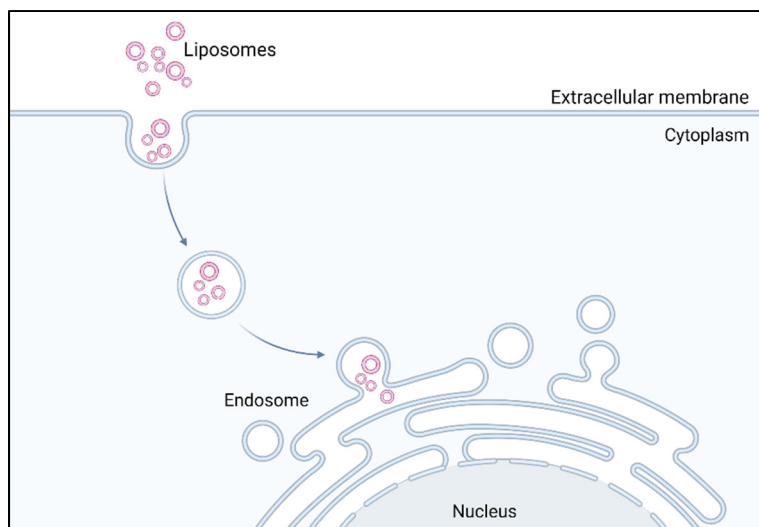


Figure 5.1 Endocytosis of liposomes

When a molecule is internalized by a cell, it can follow a myriad of pathways. The cellular membrane contains proteins that can detect certain molecules and encourage endocytosis, such as integrin receptors.

To evaluate how liposomes are absorbed by cells, they have been dyed using fluorescent reagents. The dyed cells have been observed under the confocal microscope. High resolution images of the cells have allowed us to assess qualitatively the cellular uptake, which is further analyzed quantitatively using Flow Cytometry.

5.2 Confocal microscopy

Immortalized Human Hepatocytes (IHH) and fibroblasts (BJ) were exposed to a variety of liposomes, but mainly focusing on exploring the cells response to the anionic liposomes produced using the three-factor Response Surface Model presented in Chapter 3. Using the information provided by this model, we fabricated liposomes that mimic Uveal Melanoma extracellular vesicles' parameter. The concentration of liposomes was standardized to $\sim 10^5$ liposomes/cell throughout the experiments. Moreover, other formulations that do not mimic the naturally occurring EVs have also been explored.

The confocal microscope has been configured to collect images in the following channels:

- Green (PKH67 dye) for the cellular membrane. This dye was not used in every experiment as it stained all the membranous structures in the cells.
- Red (DiIC₁₈₍₃₎) for the liposomes.
- Blue (NucBlue™) for the cell's nuclei.
- The bright field microscope captures a gray-scale image of the cells' structure.

The confocal microscope captures each image successively. Figure 5.2 shows each of the images taken: since each dye requires a different laser source, the sample is scanned by each laser consecutively. Then, bright field illumination is used to retrieve a full picture of the cells. The images collected are finally superposed for further analysis. Figure 5.2 shows the separate images taken at 0, 3, 6, 12 hours of treatment of each dyed structure and the cells in the bright field.

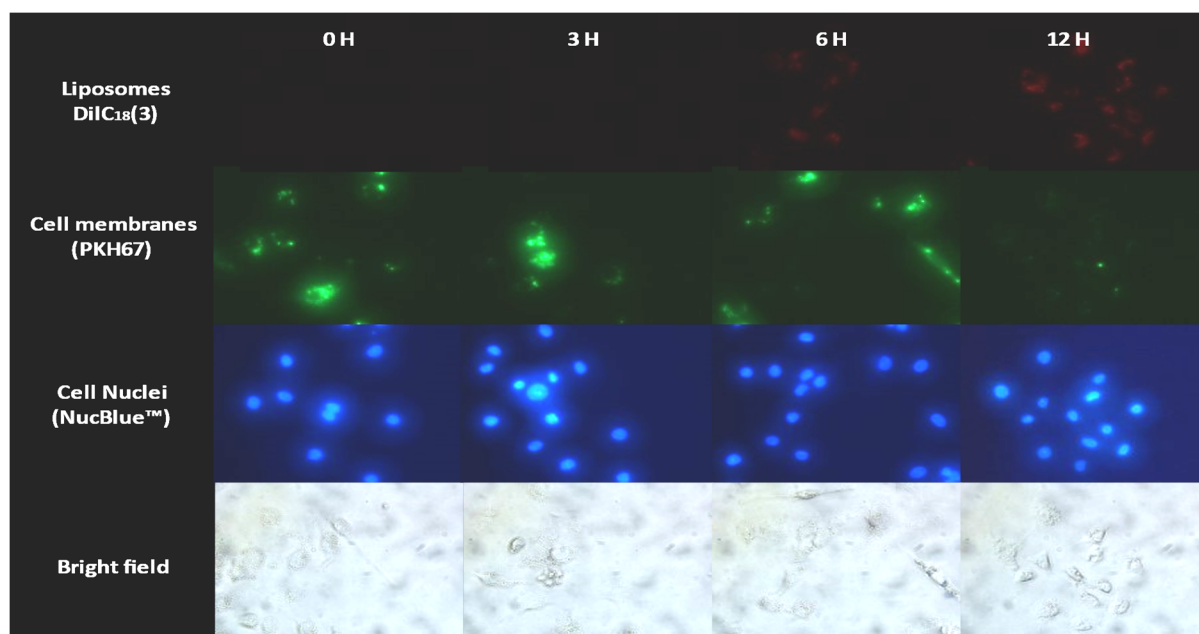


Figure 5.2 Images of the different cell structures of IHHs captured by each channel of the confocal microscope over 12 hours

5.2.1 EV-mimicking liposomes

Six different samples of anionic liposomes have been made using the three-factor response surface model presented in Chapter 3. We have explored the parameters around the Zeta Potential and the size of the naturally occurring EVs of MP41 (uveal melanoma) cancer cells. IHHs have been exposed to these particular EV-like liposomes because uveal melanoma has a great risk of metastasizing to the liver (Grossniklaus, 2013). In this way, the IHHs represent the liver microenvironment. The green dye was not used to stain the cellular membrane in all the experiments. In Figure 5.3 in particular, a clear image was necessary to qualitatively understand the uptake of the liposomes. The intense green color would have hindered the analysis. However, Figure 5.3 shows the uptake of MP41 EV-like liposomes across 12 hours of incubation and has all three dyes. Figure 5.4 confirms that liposomes of a size $\sim 150\text{nm}$ and -12.2mV are preferred by the cells. However, a quantitative analysis (flow cytometry) will be necessary to fully validate this result.

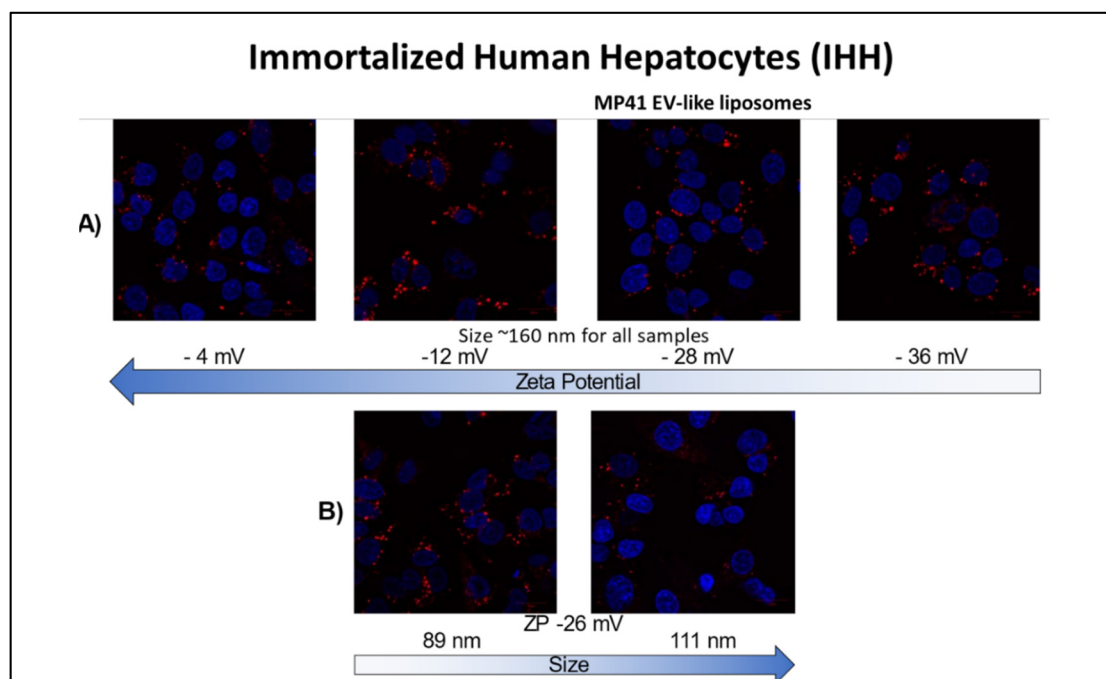


Figure 5.3 Immortalized Human Hepatocytes (IHH) absorbing EV-like liposomes

Figure 5.3A) shows 4 different samples of liposomes spanning a Zeta Potential from -4mV to -36mV with a size of 160nm approximately for all of them. Qualitatively, a greater signal is observed from the -12mV liposomes.

Figure 5.3B) shows two samples of liposomes with the same Zeta Potential ~ 26 mV and different sizes. The hepatocytes have responded more favorably to the smaller liposomes (89nm) than the slightly bigger ones (111nm) Figure 5.4 shows a time lapse of the preferentially uptaken liposomes (~ -12 mV and ~ 150 nm) versus control.

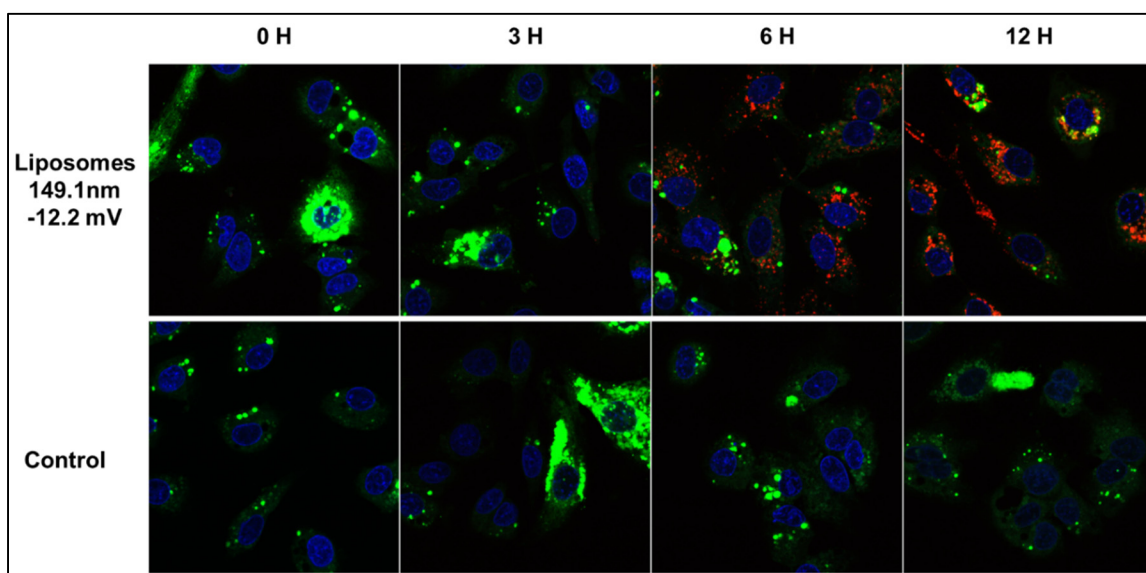


Figure 5.4 IHHs time lapse pictures absorbing liposomes vs control

5.2.2 Liposomes of different Zeta Potentials

Zeta Potential has been measured by electric light scattering and describes the surface charge of the liposomes. It is a highly volatile parameter that will depend mainly on the presence of ions in the medium. The uptake of anionic liposomes was compared to neutral and cationic liposomes and their confocal microscopy images are shown below for two types of cells. For the sake of comparison, the green dye (PKH67) was not used.

Two cell lines were compared: IHH (top) and BJ (bottom). Table 5.1 shows the lipid formulations used for each type of liposomes with the molar ratio. The TFR, FRR and temperature parameters were consistent for all three formulations, for the sake of simplicity. This yielded liposomes of varying sizes and zeta potentials.

Table 5.1 Anionic, neutral, and cationic formulations, liposomes were produced at TFR=23.22ml/h, FRR=5.97 and T=25°C

	Formulation	Ratio (mol/mol %)
Anionic	DMPC:CHOL:DHP	50:46:4%
Neutral	DMPC:CHOL	1:1
Cationic	DSPC:DOTAP:DOPE	35:40:25%

The uptake is shown in Figure 5.5. In this case BJ fibroblasts have been used as a control to evaluate the cellular response after 24 hours of incubation. Even though the size of the liposomes is different and could impact the uptake, the strong electrostatic interaction between cells and highly charged cationic liposomes have led to a more noticeable uptake of both IHH and BJ cells. Cationic liposomes interact with the negatively charged cellular membrane and can end up biting it off and destroying the cells (Hafez, Maurer et Cullis, 2001).

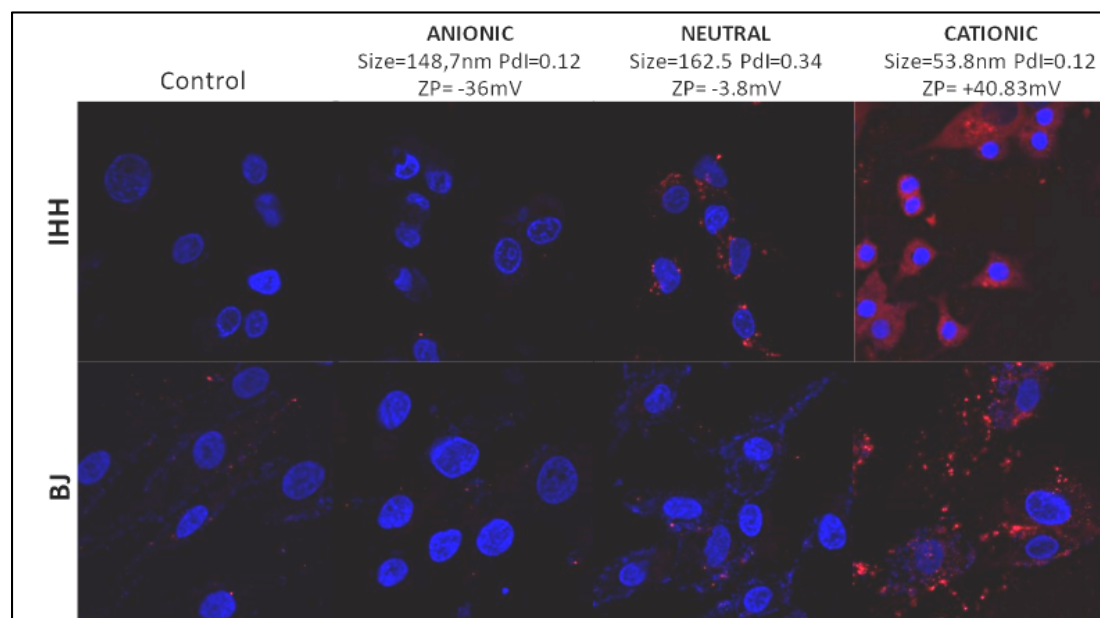


Figure 5.5 Confocal microscopy images of IHH and BJ cells vs control, anionic, neutral and cationic liposomes (24 hours of incubation). ZP stands for Zeta Potential

5.3 Flow cytometry

Flow cytometry was used to quantify the uptake of the aforementioned liposomes. Since the liposomes were dyed in blue (NucBlue™) and the liposomes in red (the green dye was not used in the following experiments), the FortessaBD Flow cytometer counted the events that are detected by each laser channel, which scan the sample simultaneously (and not consecutively). The dyes and liposomes are identical to the ones used for the confocal microscopy analysis. The flow cytometer detects the dyed structures and qualifies them as events. For this experiment, the cells were seeded in a 6-well plate at 100000 cells/well and cultured for 24h before incubating them with liposomes for another 24h. Afterwards, the cells with internalized liposomes were washed with PBS, collected, and fixed using formaldehyde. The first step of this quantitative analysis was therefore to remove the cellular debris and other structures that could hinder the results. For this purpose, the FlowJo™ Software was used to gate our samples, meaning that a specific region of the signal was selected for the analysis.

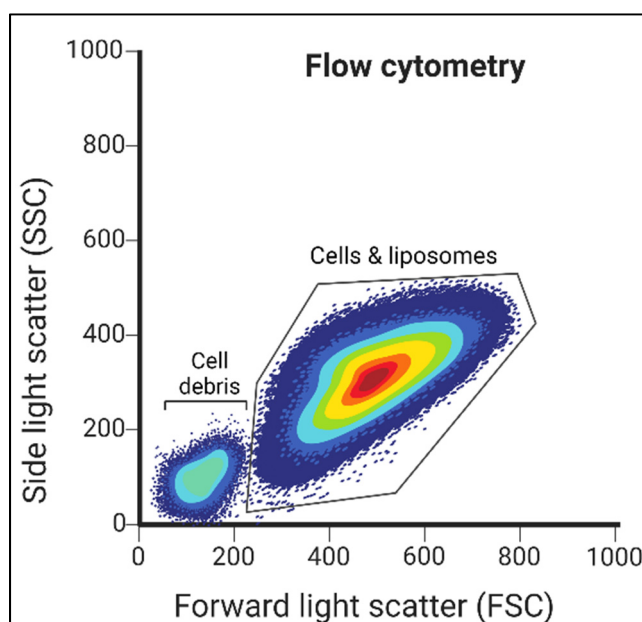


Figure 5.6 Forward vs Side scattering gating
The region containing intact cells is selected

To gate the sample to be studied, the axis selected are forward versus side scatter (FSC vs SSC). Forward scatter measures the size of the elements whereas the side scattering measures their granularity. When preparing the sample, it's very common to collect cellular debris and other elements that could distort the data. The FSC vs SSC gating allows the user to select only the cells that show the size and granularity expected and gate the region of interest containing cells and liposomes, as selected in Figure 5.6.

Once the debris have been filtered out of the events detected, we set the respective threshold for each dye used. These thresholds are set according to the controls: for each flow cytometry experiment, a negative control for each different dye used, plus a negative control with no dye. For establishing the quadrants, the forward and side scatter axis are replaced by the channels used to detect each dye. On the y-axis we selected the red channel (PE-A) for the liposomes and on the x-axis, the BV241 channel for the blue dye that accounts for the cells, see Figure 5.7.

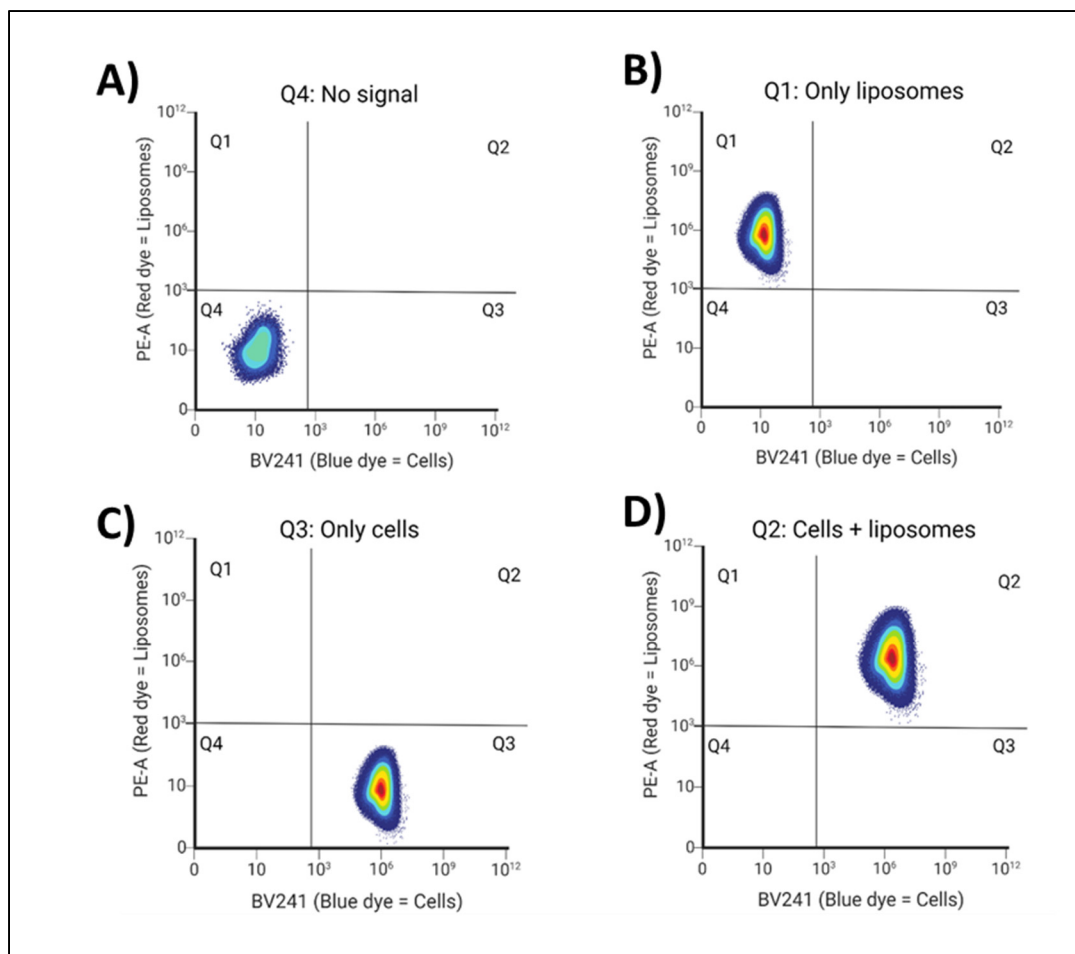


Figure 5.7 Quadrants and thresholds for signal detection in red and blue channels, theoretical controls schematics (colors indicate concentration of events)

Depending on the sample at study, a stronger or weaker uptake of liposomes will translate into a bigger or lower number of events detected, respectively. This will be assessed by first setting a threshold for each channel (PE-A for the red dyed liposomes and BV241 for the blue nuclei of the cells), yielding the four quadrants shown in Figure 5.7. If the cloud of events is detected in a particular quadrant, it will be quantified by the FlowJo™ Software.

The thresholds have been selected and they are present in each of the scatter plots presented in Figure 5.7. Figure 5.7 A) show a signal in quadrant Q4, below both the red and blue channel thresholds. Figure 5.7 B) shows a signal in Q1, below the blue channel threshold but above the red channel threshold, meaning that only liposomes are detected (the sample is therefore a control in which the cells have not been dyed with NucBlue™, but they are present). Figure

5.7 C) shows a signal in Q3, above the blue channel threshold but below the red channel threshold, therefore only cells are detected (this is another control, the cells have not been exposed to liposomes). Finally, Figure 5.7 D) shows the sample in which both cells and liposomes are detected will show up in Q2. The uptake will be quantified by assessing the number of events in Q2.

The flow cytometry experimental results will be showcased in the following section using the quadrants presented in Figure 5.7. A variety of combinations of liposome sizes and charges have been exposed to IHHs and BJ cells to evaluate their uptake.

5.3.1 EV-mimicking liposomes

As introduced in section 5.2.1 the uptake of EV-mimicking liposomes has been analyzed qualitatively via confocal microscopy imaging. In this section, quantitative analysis via flow cytometry is presented.

Anionic liposomes that mimic the properties of MP41 uveal melanoma-derived EVs have been compared to liposomes with the same Zeta Potential and different sizes below. Out of the 100000 cells seeded, only ~15000 were retrieved for the final flow cytometry analysis. After selecting the thresholds and defining the quadrants, Figure 5.8 compares how 4 different samples of IHHs have uptaken liposomes of different sizes (ranging from 89.5nm to 157nm) but same Zeta Potential (~ -25mV).

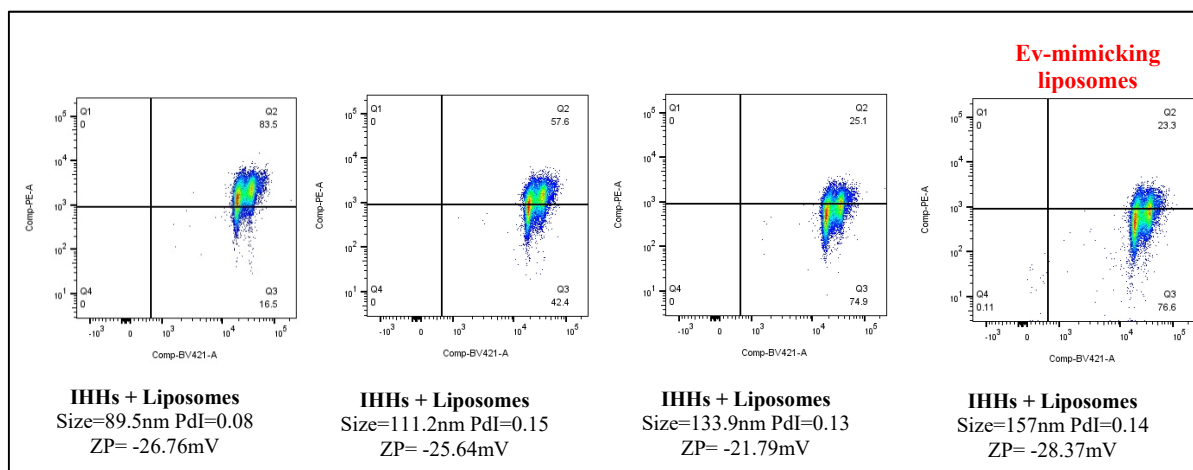


Figure 5.8 Flow cytometry results of IHH uptake of anionic liposomes
 Sizes are between 89.5nm to 157nm, and Zeta Potential is ~ -25 mV

With similar Zeta Potential, liposomes of smaller sizes (89.5nm and 111.2nm) were preferred by IHHs (Figure 5.8). The percentage of events detected in quadrant 2 (in Figure 5.8 both the red and blue channels' thresholds) was higher: 83.5% for 89nm liposomes and 57.6% for 111nm liposomes vs 23.3% for EV-like liposomes.

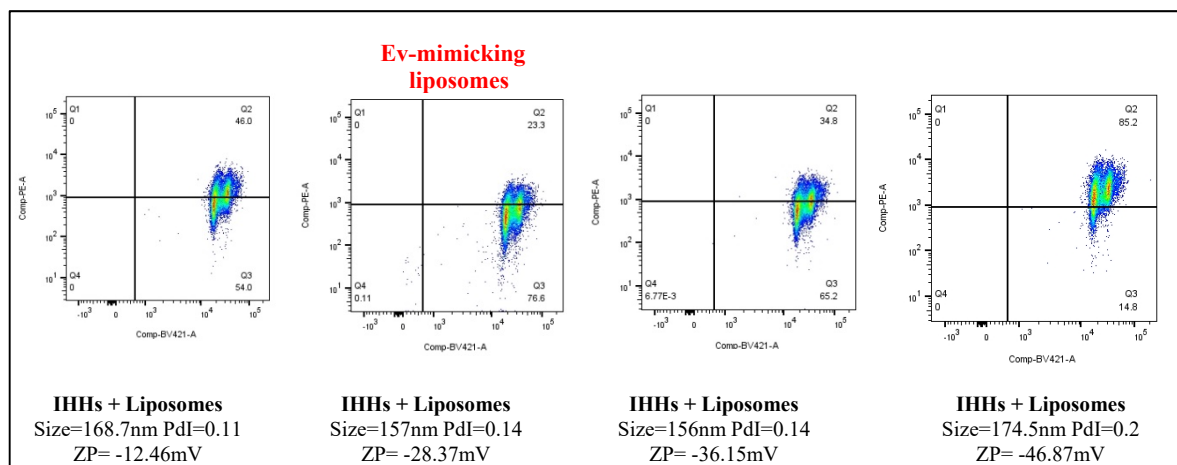


Figure 5.9 Flow cytometry results of IHH uptake of anionic liposomes
 Size is ~ 160 nm, and Zeta Potential ranges -12.46mV to -46.87mV

Among liposomes with a similar size of ~160nm, negatively charged liposomes with a Zeta Potential of -46.9mV were preferentially absorbed by IHHs, 85.2% of the events were detected in quadrant 2 (Figure 5.9). In second and third position, IHHs preferred liposomes with a Zeta Potential of -12.46mV and -36.15mV, respectively. Among liposomes with different Zeta Potentials, liposomes mimicking EVs (157nm in size and -28.37mV of Zeta Potential) were not effectively absorbed by IHHs in comparison with the more anionic liposomes (23.3%).

BJ fibroblast cells were exposed to the same liposomes. BJs were less responsive than IHHs and therefore have a very weak signal in quadrant 2 (<1% of the events, Figure 5.10).

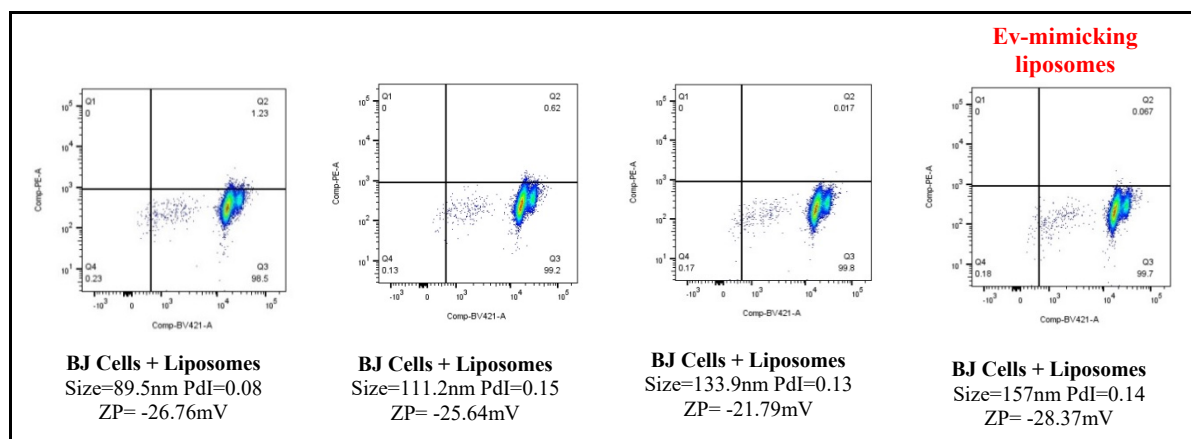


Figure 5.10 Flow cytometry results of BJs uptake of anionic liposomes. Sizes are between 89.5nm to 157nm, and Zeta Potential is ~ -25mV

Nonetheless, the same trend observed in IHHs was detected in BJ cells: fibroblasts prefer smaller liposomes.

When comparing the uptake of liposomes of ~160nm, BJs also preferred the more negatively charged liposomes of Zeta Potential=-46.87mV (26.9% events detected in quadrant 2). Liposomes of -12.46mV showed 3.86% events made it to quadrant 2. The uptake of the other liposomes with Zeta Potentials between -20mV and -30mV was below 1% (Figure 5.11).

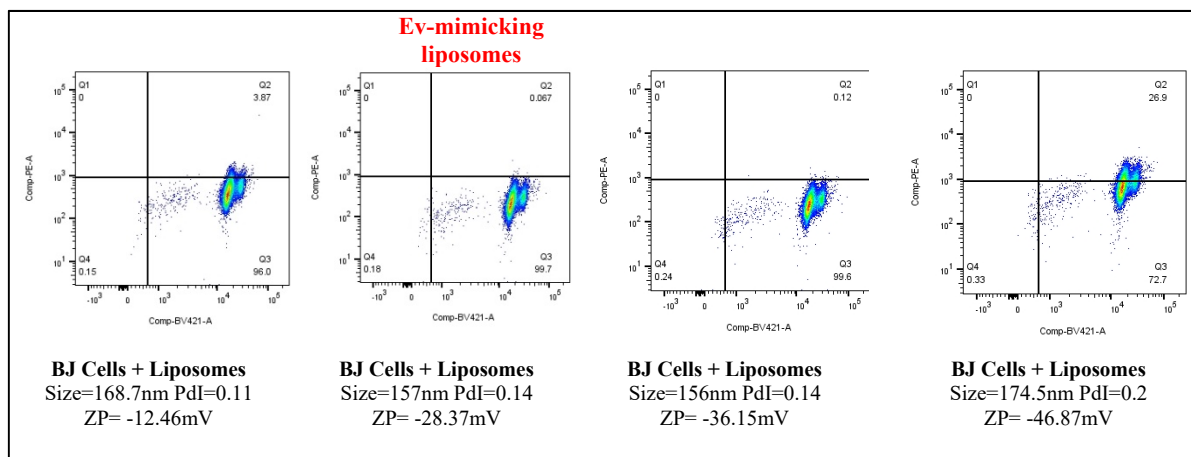


Figure 5.11 Flow cytometry results of BJ uptake of anionic liposomes
Size is ~160nm, and Zeta Potential ranges -12.46mV to -46.87mV

To summarize the results, the percentage of events detected for each type of cell is shown in Table 5.2, which values are represented in Figure 5.12 and Figure 5.13. IHH and BJ Events% (y-axis) are different: hepatocytes grow faster than BJs and inevitably become more numerous, which also explains why BJ have lower %Events. Nonetheless, the trend in cellular uptake are consistent in both cells.

Table 5.2 Percentage of events detected in quadrant 2 for IHH and BJ cells

Same Zeta Potential (~ -26mV) & different size	IHH	BJ	Same size (~ 160nm) & different Zeta Potential	IHH	BJ
Size=89.5nm PdI=0.08 ZP= -26.76mV	83.5%	1.23%	Size=168.7nm PdI=0.11 ZP= -12.46mV	46.0%	3.87%
Size=111.2nm PdI=0.15 ZP= -25.64mV	57.6%	0.62%	Size=157nm PdI=0.14 ZP= -28.37mV	23.3%	0.067%
Size=133.9nm PdI=0.13 ZP= -21.79mV	25.1%	0.017%	Size=156nm PdI=0.14 ZP= -36.15mV	34.8%	0.12%
Size=157nm PdI=0.14 ZP= -28.37mV	23.3%	0.067%	Size=174.5nm PdI=0.2 ZP= -46.87mV	85.2%	26.9%

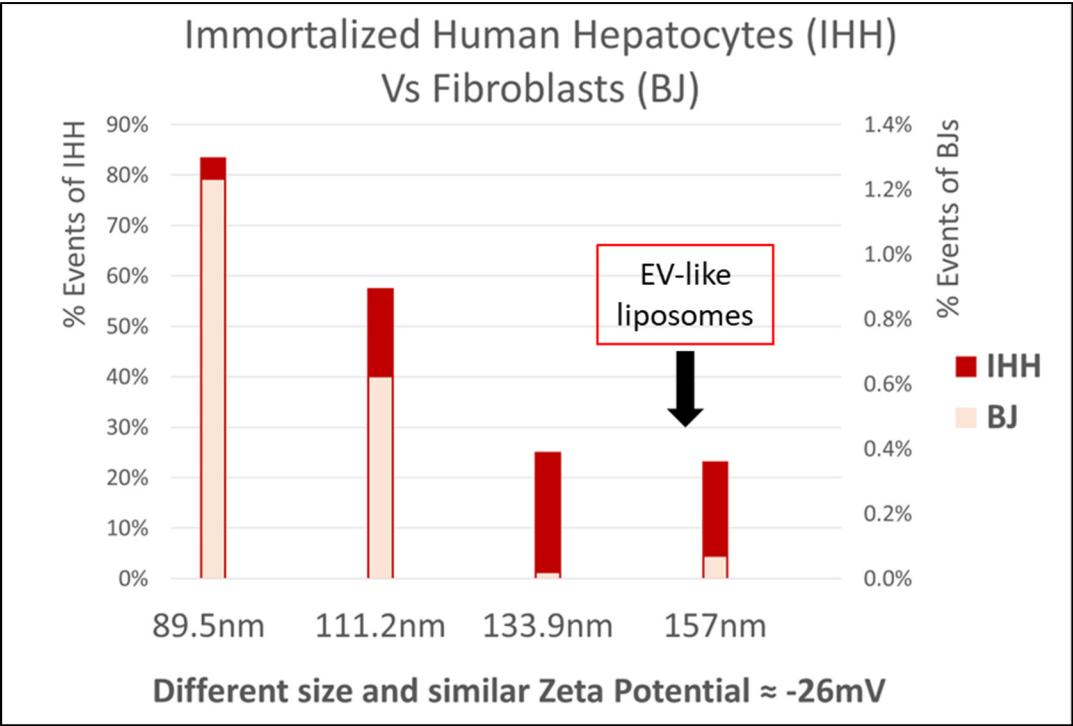


Figure 5.12 Quantitative uptake of liposomes of different sizes and similar Zeta Potential in IHH and BJ.

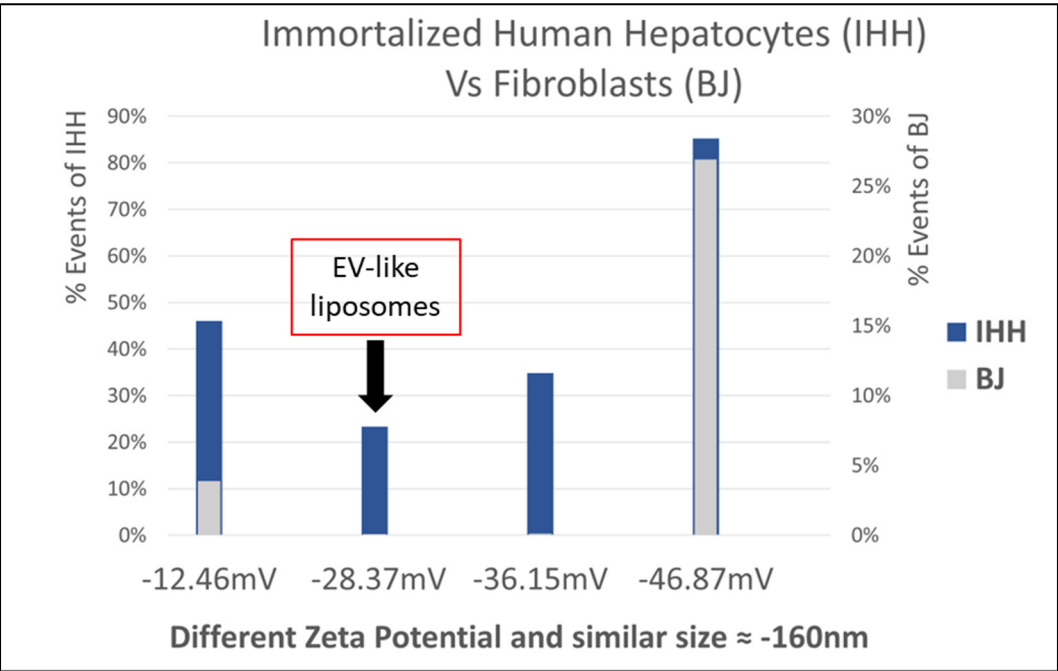


Figure 5.13 Quantitative uptake of liposomes of different Zeta Potentials and similar size in IHH and BJ.

5.4 Conclusion

The uptake of anionic liposomes has been evaluated qualitatively using confocal microscopy and quantitatively using flow cytometry. Given the importance of the Zeta Potential and the size for cellular uptake, these results have shown that anionic liposomes do interact with the cellular membrane. As expected, the electrostatic interaction between the negatively charged cell membranes of IHH and BJ cells and the liposomes were stronger for cationic liposomes than for anionic and neutral liposomes (Figure 5.5). However, anionic liposomes did have a significant interaction with the cell membrane, meaning that electrostatic interaction is not the only factor that influences the uptake of liposomes, otherwise the negatively charged cellular membranes would not have uptaken the negatively charge liposomes. It was already brought to attention that cellular uptake via endocytosis is influenced by many parameters on top of electrostatic interactions: for example, the structure of the cells' membrane is not homogenous and contains certain positively charged regions because of its surface moieties that could potentially be attracting the anionic liposomes (Nazareus et al., 2014; Verma et Stellacci, 2010).

Regarding the Zeta Potential of liposomes, when immersed in cellular media, the different ions, molecules, proteins, etc., play an important role: they cover the liposomes because they are electrostatically attracted to them and therefore might hinder the liposome-cell interaction. Several articles have discussed the protein corona that is formed on the liposomes (Forest et Pourchez, 2017) but further investigation of the changes in Zeta Potential and size of the liposomes must be undertaken.

CONCLUSION

This work has focused on the development of liposomes that resemble the naturally produced extracellular vesicles (EVs). Through a Design of Experiment (DoE) approach, we were able to synthesize liposomes in a periodic disturbance mixer that mimic the size (Z-average, nm) and charge (Zeta Potential, mV) of EVs released by uveal melanoma cancer cells (particularly MP41 cells). A response surface model exploring how the production conditions, the Total Flow Rate (TFR, mL/h), the Flow Rate Ratio and the lipid composition was used to fabricate tailored liposomes, with size and surface charge ranging from 80nm to >400nm and a -50mV to +50V, respectively. This model allowed us to successfully span a wide variety of liposomes to subsequently explore how these two physicochemical parameters affect the cellular uptake. Since Uveal Melanoma metastases to the liver, the EV-like liposomes were then exposed to Immortalized Human Hepatocytes (IHH), liver resident cells. As a control, BJ fibroblast cells were also exposed to the same liposomes. The cellular uptake was then observed via confocal microscopy and quantified via flow cytometry, yielding the following results:

- Among liposomes of the same charge, liposomes of a smaller size (~89nm) are uptaken the best.
- Among liposomes of the same size, liposomes of a more negative charge (~ -47mV) are uptaken the best.

This work has contributed to introducing the DoE approach as a valid methodology to control and predict the physicochemical parameters of liposomes. However, Response Surface Methodology is limited by the variables input in the system. This means that the model is only valid for the formulations and production conditions: CHOL, DMPC and DHP for the anionic liposomes; DOTAP, DOPE, DSPC and CHOL for the cationic liposomes; and a periodic disturbance mixer as microfluidic chip. Introducing more variables to create a bigger model may be useful to explore different combinations of lipids as well as different microfluidic chips.

Moreover, the models presented in this work have set the first step towards fabricating an efficient delivery system that will allow us to further study the influence of size and Zeta Potential on cellular uptake and explore how these two parameters translate on a physiological level. In fact, in the nano world, many variables come into play to dictate the fate of nanoparticles when entering the body. Among them is the protein corona, a collection of proteins and metabolites present in cellular media that adhere to the liposomes depending on their size and composition (Elechalawar et al., 2020). The protein corona plays a significant role in cellular uptake and also the distribution of liposomes in organs (biodistribution). A reliable and standardized production of nanoparticles will therefore be necessary to further refine this delivery system. The next step is therefore to functionalize the surface of liposomes and load them with different molecules of interest such as nucleic acids (DNA, RNA), proteins or anti-cancer drugs that will specifically target certain tissues. Finally, our recommendation is to use this model as a starting point to further study cell to cell communication, specifically cellular uptake.

ANNEX A

Z-AVERAGE OF ANIONIC AND CATIONIC LIPOSOMES

The Z-average (hydrodynamic diameter, nm) of the samples presented in section 3.1 are studied here. It is worth noticing that the liposomes have a size of ~300 nm. The liposomes made of CHOL: DMPC 1:1 was particularly big and polydisperse. This was troubleshooted by changing different elements of the set-up and it was ultimately solved by preserving the presence of ions in the set-up and not washing the system with ethanol and water when changing the formulation but ethanol and PBS. The role of PBS will be further explored in the following sections.

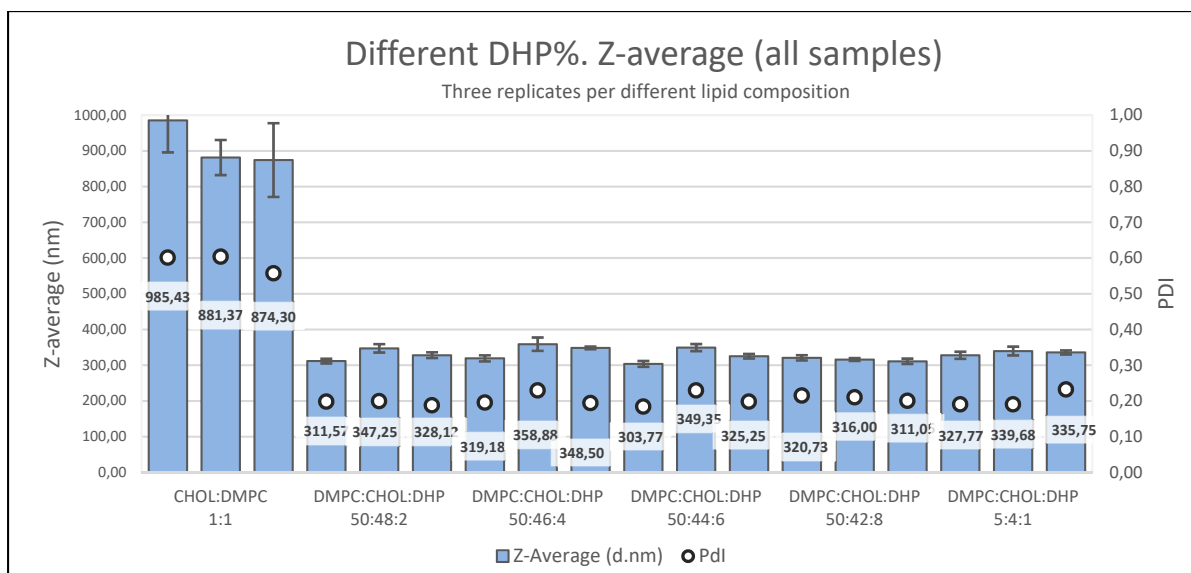


Figure-A I-1 Z-average and PDI measurement for all 18 samples, three replicates per lipid composition. The percentage of DHP is increased progressively in intervals of 2% molar ratio from 0% to 10%

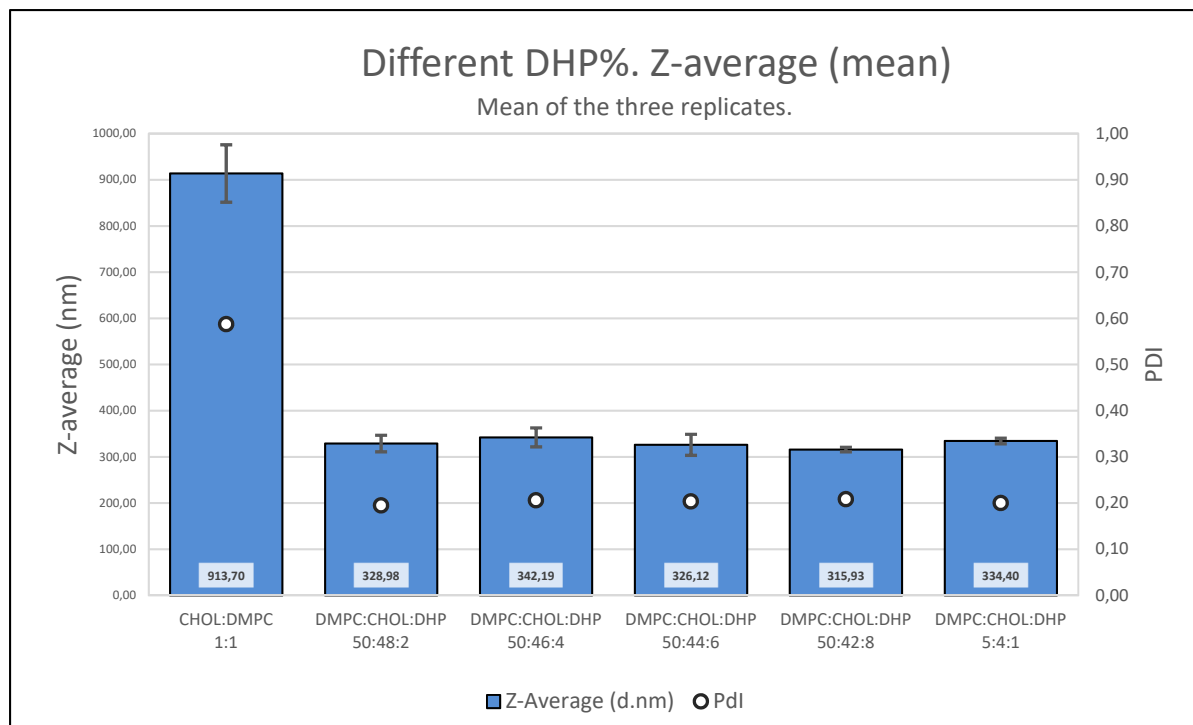


Figure-A I-2 Mean Z-average and PDI per increasing molar ratio of DHP
Average of three repeats per lipid formulation

As expected, the Zeta Potential highly depends on the formulation of liposomes. Changing the ratio of the negatively charge lipid DHP yielded a significant difference between the sample groups. Several parameters affect the Z-average and Zeta Potential of liposomes, this experiment fulfilled its role to provide a reliable factor to predict the Zeta Potential, but not the Z-average.

The Z-average of the cationic liposomes made of DMPC:DOPE:DOTAP in various ratios ranging from 50:50:0% molar to 50:25:25% molar first introduced in section 4.1 are shown below. Even though this formulation showed to be successful at proving that the Zeta Potential is truly affected by the DOTAP%, the liposomes seem to have suffered precipitation. The sizes shown in Figure-A I- and Figure are well above the μ meter with a PDI of more than 0.2, meaning they are highly polydisperse.

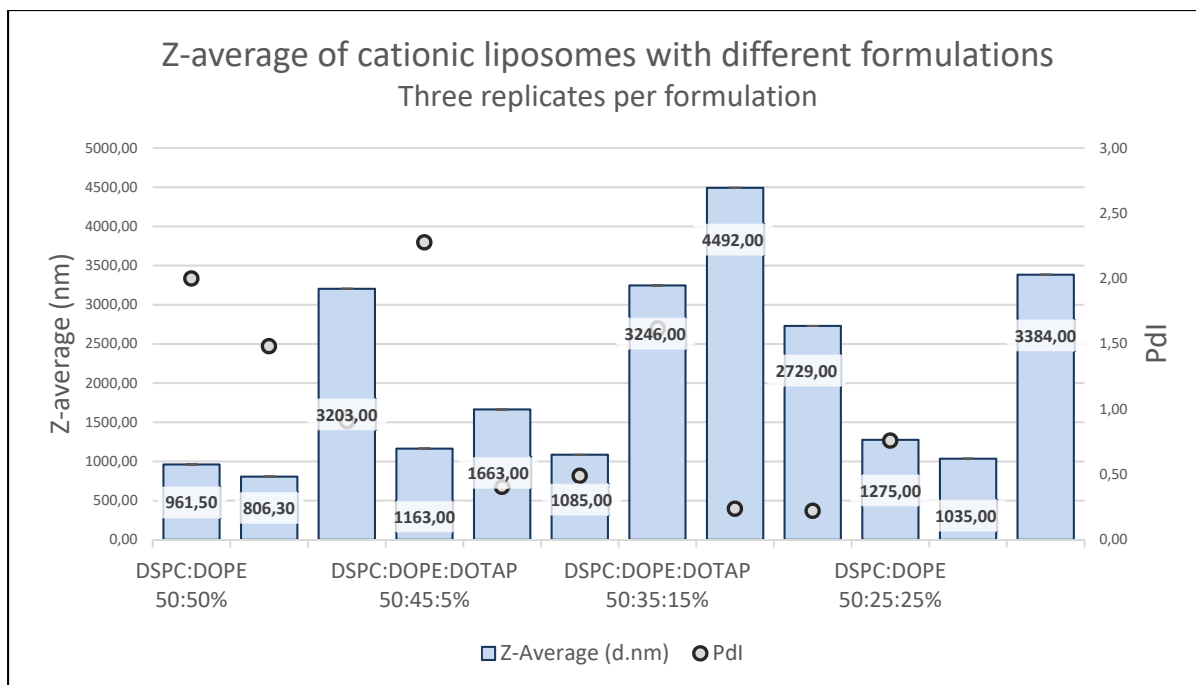


Figure-A I-3 Z-average of the liposomes produced with different cationic formulations (all replicates)

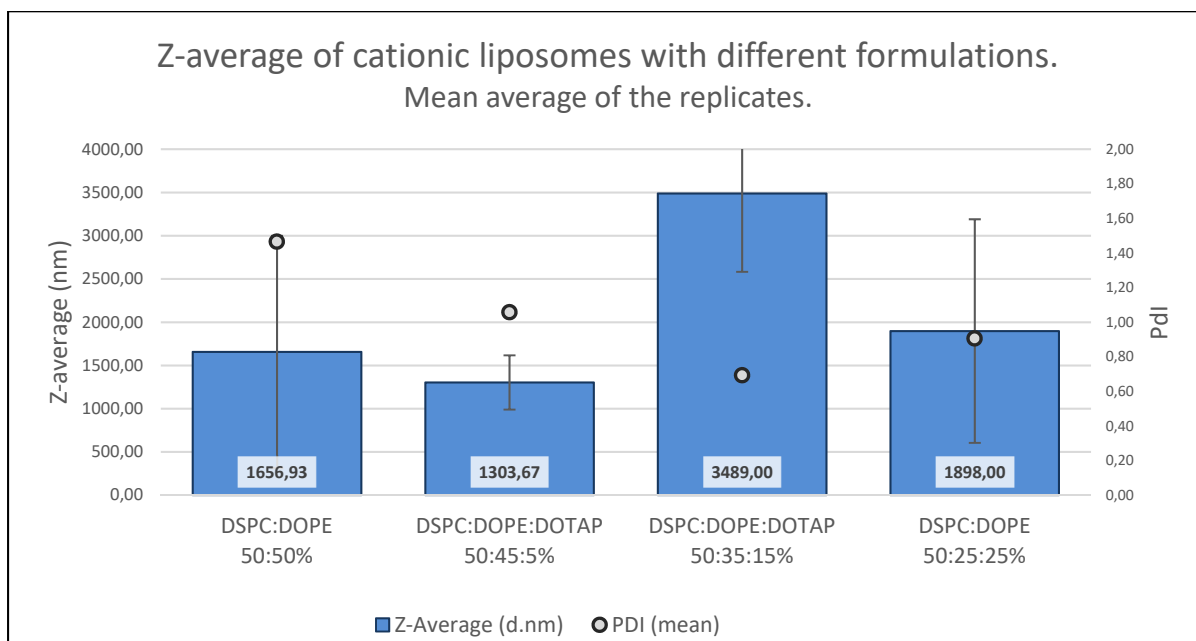


Figure-A I-4 Z-average of the liposomes produced with different cationic formulations (mean average)

LIST OF BIBLIOGRAPHICAL REFERENCES

- Akinc, Akin, Martin A Maier, Muthiah Manoharan, Kevin Fitzgerald, Muthusamy Jayaraman, Scott Barros, Steven Ansell, Xinyao Du, Michael J Hope et Thomas D Madden. 2019. « The Onpattro story and the clinical translation of nanomedicines containing nucleic acid-based drugs ». *Nature nanotechnology*, vol. 14, n° 12, p. 1084-1087.
- Ball, Rebecca L., Khalid A. Hajj, Jamie Vizelman, Palak Bajaj et Kathryn A. Whitehead. 2018. « Lipid Nanoparticle Formulations for Enhanced Co-delivery of siRNA and mRNA ». *Nano Letters*, vol. 18, n° 6, p. 3814-3822.
- Bangham, A. D., et R. W. Horne. 1962. « Action of Saponin on Biological Cell Membranes ». *Nature*, vol. 196, n° 4858, p. 952-953.
- Bangham, A. D., et R. W. Horne. 1964. « NEGATIVE STAINING OF PHOSPHOLIPIDS AND THEIR STRUCTURAL MODIFICATION BY SURFACE-ACTIVE AGENTS AS OBSERVED IN THE ELECTRON MICROSCOPE ». *J Mol Biol*, vol. 8, p. 660-8.
- Bangham, A. D., M. M. Standish et G. Weissmann. 1965. « The action of steroids and streptolysin S on the permeability of phospholipid structures to cations ». *Journal of Molecular Biology*, vol. 13, n° 1, p. 253-IN28.
- Batzri, S., et E. D. Korn. 1973. « Single bilayer liposomes prepared without sonication ». *Biochim Biophys Acta*, vol. 298, n° 4, p. 1015-9.
- Bhattacharjee, Sourav. 2016. « DLS and zeta potential – What they are and what they are not? ». *Journal of Controlled Release*, vol. 235, p. 337-351.
- Blanco, Elvin, Haifa Shen et Mauro Ferrari. 2015. « Principles of nanoparticle design for overcoming biological barriers to drug delivery ». *Nature Biotechnology*, vol. 33, n° 9, p. 941-951.
- Brown, Angela C., et Steven P. Wrenn. 2013. « Nanoscale Phase Separation in DSPC–Cholesterol Systems ». *Langmuir*, vol. 29, n° 31, p. 9832-9840.
- Chang, W. H., R. A. Cerione et M. A. Antonyak. 2021. « Extracellular Vesicles and Their Roles in Cancer Progression ». *Methods Mol Biol*, vol. 2174, p. 143-170.
- Charcosset, Catherine. 2016. « Electrophoretic Mobility ». In *Encyclopedia of Membranes*, sous la dir. de Drioli, Enrico, et Lidietta Giorno. Charcosset2016. p. 658-659. Berlin, Heidelberg: Springer Berlin Heidelberg. < https://doi.org/10.1007/978-3-662-44324-8_208 >.

- Cheng, Xinwei, et Robert J. Lee. 2016. « The role of helper lipids in lipid nanoparticles (LNPs) designed for oligonucleotide delivery ». *Advanced Drug Delivery Reviews*, vol. 99, p. 129-137.
- Chiesa, Enrica, Antonietta Greco, Federica Riva, Elena Maria Tosca, Rossella Dorati, Silvia Pisani, Tiziana Modena, Bice Conti et Ida Genta. 2019. « Staggered Herringbone Microfluid Device for the Manufacturing of Chitosan/TPP Nanoparticles: Systematic Optimization and Preliminary Biological Evaluation ». *International Journal of Molecular Sciences*, vol. 20, n° 24, p. 6212.
- Cugia, Francesca, Maura Monduzzi, Barry W. Ninham et Andrea Salis. 2013. « Interplay of ion specificity, pH and buffers: insights from electrophoretic mobility and pH measurements of lysozyme solutions ». *RSC Advances*, vol. 3, n° 17, p. 5882-5888.
- De Franceschi, Nicola, Hellyeh Hamidi, Jonna Alanko, Pranshu Sahgal et Johanna Ivaska. 2015. « Integrin traffic – the update ». *Journal of Cell Science*, vol. 128, n° 5, p. 839-852.
- Degors, Isabelle M. S., Cuifeng Wang, Zia Ur Rehman et Inge S. Zuhorn. 2019. « Carriers Break Barriers in Drug Delivery: Endocytosis and Endosomal Escape of Gene Delivery Vectors ». *Accounts of Chemical Research*, vol. 52, n° 7, p. 1750-1760.
- Du, Zixiu, Mustafa M. Munye, Aristides D. Tagalakis, Maria D. I. Manunta et Stephen L. Hart. 2014. « The Role of the Helper Lipid on the DNA Transfection Efficiency of Lipopolyplex Formulations ». *Scientific Reports*, vol. 4, n° 1, p. 7107.
- Elechalawar, Chandra Kumar, Md Nazir Hossen, Lacey McNally, Resham Bhattacharya et Priyabrata Mukherjee. 2020. « Analysing the nanoparticle-protein corona for potential molecular target identification ». *Journal of Controlled Release*, vol. 322, p. 122-136.
- Fessi, H., F. Puisieux, J. Ph Devissaguet, N. Ammoury et S. Benita. 1989. « Nanocapsule formation by interfacial polymer deposition following solvent displacement ». *International Journal of Pharmaceutics*, vol. 55, n° 1, p. R1-R4.
- Finsy, Robert. 1994. « Particle sizing by quasi-elastic light scattering ». *Advances in Colloid and Interface Science*, vol. 52, p. 79-143.
- Forest, Valérie, et Jérémie Pourchez. 2017. « Preferential binding of positive nanoparticles on cell membranes is due to electrostatic interactions: A too simplistic explanation that does not take into account the nanoparticle protein corona ». *Materials Science and Engineering: C*, vol. 70, p. 889-896.
- Foroozandeh, Parisa, et Azlan Abdul Aziz. 2018. « Insight into Cellular Uptake and Intracellular Trafficking of Nanoparticles ». *Nanoscale Research Letters*, vol. 13, n° 1, p. 339.

- Grossniklaus, H. E. 2013. « Progression of ocular melanoma metastasis to the liver: the 2012 Zimmerman lecture ». *JAMA Ophthalmol*, vol. 131, n° 4, p. 462-9.
- Hafez, I. M., N. Maurer et P. R. Cullis. 2001. « On the mechanism whereby cationic lipids promote intracellular delivery of polynucleic acids ». *Gene Ther*, vol. 8, n° 15, p. 1188-96.
- Han, Xuexiang, Hanwen Zhang, Kamila Butowska, Kelsey L. Swingle, Mohamad-Gabriel Alameh, Drew Weissman et Michael J. Mitchell. 2021. « An ionizable lipid toolbox for RNA delivery ». *Nature Communications*, vol. 12, n° 1, p. 7233.
- Harashima, Hideyoshi, Kazuya Sakata, Kouichi Funato et Hiroshi Kiwada. 1994. « Enhanced Hepatic Uptake of Liposomes Through Complement Activation Depending on the Size of Liposomes ». *Pharmaceutical Research*, vol. 11, n° 3, p. 402-406.
- Hou, Xucheng, Tal Zaks, Robert Langer et Yizhou Dong. 2021. « Lipid nanoparticles for mRNA delivery ». *Nature Reviews Materials*, vol. 6, n° 12, p. 1078-1094.
- Hyde, Alan M., Susan L. Zultanski, Jacob H. Waldman, Yong-Li Zhong, Michael Shevlin et Feng Peng. 2017. « General Principles and Strategies for Salting-Out Informed by the Hofmeister Series ». *Organic Process Research & Development*, vol. 21, n° 9, p. 1355-1370.
- Ikonen, E. 2008. « Cellular cholesterol trafficking and compartmentalization ». *Nat Rev Mol Cell Biol*, vol. 9, n° 2, p. 125-38.
- Jahn, Andreas, Wyatt N. Vreeland, Michael Gaitan et Laurie E. Locascio. 2004. « Controlled Vesicle Self-Assembly in Microfluidic Channels with Hydrodynamic Focusing ». *Journal of the American Chemical Society*, vol. 126, n° 9, p. 2674-2675.
- Koynova, Rumiana, Boris Tenchov et Gert Rapp. 1997. « Mixing behavior of saturated short-chain phosphatidylcholines and fatty acids: Eutectic points, liquid and solid phase immiscibility, non-lamellar phases ». *Chemistry and Physics of Lipids*, vol. 88, n° 1, p. 45-61.
- Lechanteur, A., V. Sanna, A. Duchemin, B. Evrard, D. Mottet et G. Piel. 2018. « Cationic Liposomes Carrying siRNA: Impact of Lipid Composition on Physicochemical Properties, Cytotoxicity and Endosomal Escape ». *Nanomaterials (Basel)*, vol. 8, n° 5.
- López, Rubén R., Ixchel Ocampo, Luz-María Sánchez, Anas Alazzam, Karl-F. Bergeron, Sergio Camacho-León, Catherine Mounier, Ion Stiharu et Vahé Nerguizian. 2020. « Surface Response Based Modeling of Liposome Characteristics in a Periodic Disturbance Mixer ». *Micromachines*, vol. 11, n° 3, p. 235.

- Meyer, Frédérick de, et Berend Smit. 2009. « Effect of cholesterol on the structure of a phospholipid bilayer ». *Proceedings of the National Academy of Sciences*, vol. 106, n° 10, p. 3654-3658.
- Milla, P., F. Dosio et L. Cattel. 2012. « PEGylation of proteins and liposomes: a powerful and flexible strategy to improve the drug delivery ». *Curr Drug Metab*, vol. 13, n° 1, p. 105-19.
- Mochizuki, Shinichi, Naho Kanegae, Koichi Nishina, Yumi Kamikawa, Kazunori Koiwai, Hiroyasu Masunaga et Kazuo Sakurai. 2013. « The role of the helper lipid dioleoylphosphatidylethanolamine (DOPE) for DNA transfection cooperating with a cationic lipid bearing ethylenediamine ». *Biochimica et Biophysica Acta (BBA) - Biomembranes*, vol. 1828, n° 2, p. 412-418.
- Nazarenus, Moritz, Qian Zhang, Mahmoud G. Soliman, Pablo del Pino, Beatriz Pelaz, Susana Carregal-Romero, Joanna Rejman, Barbara Rothen-Rutishauser, Martin J. D. Clift, Reinhard Zellner, G. Ulrich Nienhaus, James B. Delehanty, Igor L. Medintz et Wolfgang J. Parak. 2014. « In vitro interaction of colloidal nanoparticles with mammalian cells: What have we learned thus far? ». *Beilstein Journal of Nanotechnology*, vol. 5, p. 1477-1490.
- Ostróżka-Cieślik, Aneta, et Beata Sarecka-Hujar. 2017. « Chapter 7 - The Use of Nanotechnology in Modern Pharmacotherapy ». In *Multifunctional Systems for Combined Delivery, Biosensing and Diagnostics*, sous la dir. de Grumezescu, Alexandru Mihai. p. 139-158. Elsevier. <
<https://www.sciencedirect.com/science/article/pii/B9780323527255000071>>.
- Perli, G., Acsn Pessoa, T. A. Balbino et L. G. de la Torre. 2019. « Ionic strength for tailoring the synthesis of monomodal stealth cationic liposomes in microfluidic devices ». *Colloids Surf B Biointerfaces*, vol. 179, p. 233-241.
- Pons, Miquel, Mercè Foradada et Joan Estelrich. 1993. « Liposomes obtained by the ethanol injection method ». *International Journal of Pharmaceutics*, vol. 95, n° 1, p. 51-56.
- Rangamani, Padmini, et Ravi Iyengar. 2007. « Modelling spatio-temporal interactions within the cell ». *Journal of Biosciences*, vol. 32, n° 1, p. 157-167.
- Salvati, Anna, Inge Nelissen, Andrea Haase, Christoffer Åberg, Sergio Moya, An Jacobs, Fatima Alnasser, Tony Bewersdorff, Sarah Deville, Andreas Luch et Kenneth A. Dawson. 2018. « Quantitative measurement of nanoparticle uptake by flow cytometry illustrated by an interlaboratory comparison of the uptake of labelled polystyrene nanoparticles ». *NanoImpact*, vol. 9, p. 42-50.
- Schoenmaker, Linde, Dominik Witzigmann, Jayesh A. Kulkarni, Rein Verbeke, Gideon Kersten, Wim Jiskoot et Daan J. A. Crommelin. 2021. « mRNA-lipid nanoparticle

- COVID-19 vaccines: Structure and stability ». *International Journal of Pharmaceutics*, vol. 601, p. 120586.
- Smith, Mackensie C., Rachael M. Crist, Jeffrey D. Clogston et Scott E. McNeil. 2017. « Zeta potential: a case study of cationic, anionic, and neutral liposomes ». *Analytical and Bioanalytical Chemistry*, vol. 409, n° 24, p. 5779-5787.
- Soema, Peter C., Geert-Jan Willems, Wim Jiskoot, Jean-Pierre Amorij et Gideon F. Kersten. 2015. « Predicting the influence of liposomal lipid composition on liposome size, zeta potential and liposome-induced dendritic cell maturation using a design of experiments approach ». *European Journal of Pharmaceutics and Biopharmaceutics*, vol. 94, p. 427-435.
- Stano, Pasquale, Simone Bufali, Claudio Pisano, Federica Bucci, Marcella Barbarino, Mosè Santaniello, Paolo Carminati et Pier Luigi Luisi. 2004. « Novel camptothecin analogue (gimatecan)-containing liposomes prepared by the ethanol injection method ». *Journal of liposome research*, vol. 14, n° 1-2, p. 87-109.
- Sze, Alice, David Erickson, Liqing Ren et Dongqing Li. 2003. « Zeta-potential measurement using the Smoluchowski equation and the slope of the current–time relationship in electroosmotic flow ». *Journal of Colloid and Interface Science*, vol. 261, n° 2, p. 402-410.
- Thisted, Ronald A. 1998. « What is a P-value ». *Departments of Statistics and Health Studies*.
- Tsering, Thupten, Alexander Laskaris, Mohamed Abdouh, Prisca Bustamante, Sabrina Parent, Eva Jin, Sarah Tadhg Ferrier, Goffredo Arena et Julia V. Burnier. 2020. « Uveal Melanoma-Derived Extracellular Vesicles Display Transforming Potential and Carry Protein Cargo Involved in Metastatic Niche Preparation ». *Cancers*, vol. 12, n° 10, p. 2923.
- Valencia, Pedro M., Omid C. Farokhzad, Rohit Karnik et Robert S. Langer. 2012. « Microfluidic technologies for accelerating the clinical translation of nanoparticles ». *Nature nanotechnology*, vol. 7 10, p. 623-9.
- Verma, Ayush, et Francesco Stellacci. 2010. « Effect of surface properties on nanoparticle–cell interactions ». *small*, vol. 6, n° 1, p. 12-21.
- Zhao, Jiang, Jing Wu, Frederick A. Heberle, Thalia T. Mills, Paul Klawitter, Grace Huang, Greg Costanza et Gerald W. Feigenson. 2007. « Phase studies of model biomembranes: complex behavior of DSPC/DOPC/cholesterol ». *Biochimica et biophysica acta*, vol. 1768, n° 11, p. 2764-2776.